INFORMATION TO USERS

This manuscript has been reproduced from the microfilm master. UMI films the text directly from the original or copy submitted. Thus, some thesis and dissertation copies are in typewriter face, while others may be from any type of computer printer.

The quality of this reproduction is dependent upon the quality of the copy submitted. Broken or indistinct print, colored or poor quality illustrations and photographs, print bleedthrough, substandard margins, and improper alignment can adversely affect reproduction.

In the unlikely event that the author did not send UMI a complete manuscript and there are missing pages, these will be noted. Also, if unauthorized copyright material had to be removed, a note will indicate the deletion.

Oversize materials (e.g., maps, drawings, charts) are reproduced by sectioning the original, beginning at the upper left-hand corner and continuing from left to right in equal sections with small overlaps. Each original is also photographed in one exposure and is included in reduced form at the back of the book.

Photographs included in the original manuscript have been reproduced xerographically in this copy. Higher quality 6" x 9" black and white photographic prints are available for any photographs or illustrations appearing in this copy for an additional charge. Contact UMI directly to order.

UMI®

Bell & Howell Information and Learning
300 North Zeeb Road, Ann Arbor, MI 48106-1346 USA
800-521-0600

Phase Transitions Among Aqueous Soluble Surfactants at the Air-Water Interface and Its Effect on Dynamic Surface Tension and Spreading and Retention of Drops Impacting on a Hydrophobic Surface

by

Rajeev Subramanyam

A Dissertation submitted to the Graduate Faculty in Engineering in partial fulfillment of the requirements for the degree of Doctor of Philosophy, The City University of New York

1999

This manuscript has been read and accepted for the Graduate Faculty in Engineering in satisfaction of the dissertation requirements for the degree of Doctor of Philosophy.

9/21/99

Date

Charles Maldarelli

Chair of Examining Committee

9/22/1999

Date

Mumtaz K. Kassir

Executive Officer

Andreas Acrivos

Alexander Couzis

Joel Koplik

John Green

Supervisory Committee

THE CITY UNIVERSITY OF NEW YORK

Abstract

Phase Transitions Among Aqueous Soluble Surfactants at the Air-Water Interface and Its Effect on Dynamic Surface Tension and Spreading and Retention of Drops Impacting on a Hydrophobic Surface

by

Rajeev Subramanyam

Advisor: Professor Charles Maldarelli

The phase behavior of surfactant molecules adsorbed at an air/water interface describes their states of aggregation and molecular ordering. For insoluble surfactants, extended research has identified a varied polymorphism of gaseous (G), liquid expanded (LE) and condensed (LC) and solid states (S), and has demarcated phase boundaries and coexistence curves as a function of the surface pressure, area per molecule and temperature. Little attention has been devoted to the phase behavior of monolayers formed by self-assembly from solution at the air/water interface (Gibbs monolayers). The object of this thesis is to conclusively establish whether soluble surfactant monolayers form liquid and condensed phases, and if they do, map the phase behavior, determine the nature of the transitions and discover how the surfactant structure dictates which phases form. We study a homologous series of n-alkyl poly (ethylene glycol) ether nonionic surfactants C_iE_j (CH_3 $(CH_2)_{i-1}$ (OCH2CH2)$_j$-OH) with i=12 or 14 and j=0,1,2,4 and 6 in which the head group and chains can be systematically varied to cover a

range of surfactants from those that are nearly insoluble to those which are very soluble.

We visualize surface phases by exciting an insoluble dye dissolved in the monolayer which fluoresces in the liquid expanded state (and therefore illuminates this state), but is quenched in the gaseous state and is expelled from the condensed phases (which makes them appear dark). We will demonstrate that all the surfactants in the homologous series occupy gaseous and liquid expanded phases, and that the transition is first order and occurs at a tension close to the clean air/water tension.

Dynamic surface tension reductions measured for adsorption onto an initially clean interface exhibit induction periods in which the tension remains constant before decreasing rapidly. No definitive explanation for this induction period has been provided, but it plays a central role in designing surfactant systems to rapidly reduce tension in interfacial technological processes such as foaming and emulsion stabilization. Here we establish that the induction period is caused by a G/LE phase transition that the monolayer undergoes as adsorption from solution proceeds. The objective is to experimentally prove this hypothesis, and obtain from this interpretation of the induction period, an expression for the induction time in terms of the properties of the phase transition (i.e. the surface density of the nucleating LE phase).

Our studies of the monolayer phase behavior will also demonstrate that only the low solubility members of the series with zero or one ethoxy group can assemble into a liquid condensed or LC state. The close packing of this state

causes the maximum reduction in tension, and the development of a hydrocarbon phase which space fills with little free volume. This suggests that these LC forming surfactants may be useful in reducing the contact angle formed when an aqueous drop beads up on a hydrophobic surface because it can adsorb onto the hydrophobic surface of the solid, where it excludes water and presents to the aqueous phase only the polar groups of the molecule. The reduction in this contact angle has broad applications in optimizing many interfacial technological processes, including drop spraying of aqueous solutions of agrochemicals on waxy foliate surfaces. Here surfactants added to the aqueous solutions reduce the contact angle upon impact of the drops on the foliate surface and thereby allow the drops to spread rather than rebound. It is demonstrated that binary surfactant systems can form condensed phases rapidly and achieve equilibrium contact angles lower that that of the individual components. When drops laden with these surfactant mixtures impact on a hydrophobic surface, then the rapid lowering of the contact angle eliminates the rebound while conventional surfactants which do not achieve this large contact angle reduction, do not completely prevent droplet retraction and are not as effective.

Acknowledgements

First and foremost I would like to thank my advisor Charles Maldarelli for his constant support and help during my stay at City. He has been as much a friend as an advisor, helping me in ways beyond his advisory responsibilities. I could not have reached this stage without his assistance. He has always been behind me and his care and understanding has helped me get through unpleasant circumstances easily.

I also wish to thank Alex Couzis for his help, support and encouragement at every stage. He has helped me not only in research but in life as a whole. Working with him has made my stay at City a very pleasant and enjoyable one.

I would like to dedicate this thesis to my parents. Even though they are far away, their best wishes, understanding and encouragement has helped me complete every endeavor I have undertaken sincerely. They have always stood patiently by me and I could not have made where I stand today without them.

I would also like to thank my sister Radha Subramanyam and brother-in-law Joseph Walser for their patience with me especially in difficult times. They have always given priority to problems I face over theirs and their unwavering support has helped me reach this stage.

I would like to acknowledge the assistance of all the graduate students of our group especially Ravichandra Palaparthi, Jose Lorenzo and Nitin Kumar. I consider myself fortunate to be part of such a group.

Finally I am grateful to Andy Eng and Zhen Rong Xu for their help in making research so much easier.

Table of Contents

List of Tables

List of Figures

Chapter 1

Introduction

1.1 Background and Scope

Surfactants are amphiphilic molecules which contain a polar head group and a non-polar part comprised usually of an extended string of hydrocarbon methylene (-CH_2 -) groups. At an interface between an aqueous phase and water, surfactant molecules arrange themselves in a low free energy configuration in which the polar group remains immersed in the water where it can interact by dipolar forces (such as hydrogen bonding) with water, and the hydrocarbon chain is displaced from the water into the air. Displacing the chain from water is energetically favorable because when the chain is immersed in the water, it disrupts the low energy hydrogen bonding structure of the aqueous phase. The presence of amphiphiles at an air/water surface reduces the free energy and therefore the tension of the surface in proportion to the surface concentration of the surfactant.

The phase behavior of surfactant molecules at an air/water interface describes the state of aggregation of the molecules. The phase behavior is determined by the intermolecular interactions in the monolayer, namely the van der Waals attractive or cohesive forces between the hydrocarbon chains, and the repulsive interactions (e.g. dipolar, electrostatic and hydration) between the head groups. The phase behavior of insoluble surfactants spread at an air/water interface (Langmuir monolayers) and compressed (as on the surface of a

Langmuir trough) to a surface pressure π (defined as the difference in tension between a clean surface and the surface covered by the monolayer) has been studied extensively. Different monolayer phases have been identified and described in terms of the molecular configurations that the adsorbed molecules occupy. Phase boundaries have been mapped as a function of temperature, surface pressure and area per molecule (or surface concentration) for several amphiphiles, particularly fatty acids, alcohols and phospholipids. This literature is reviewed below in Sec. 1.2. The major conclusion from these studies is that at and around room temperature, insoluble amphiphiles exist generally in three phases. At low surface pressure, they occupy a gaseous (G) state in which adsorbed molecules are widely separated and do not interact. At higher pressure, the molecules exist in an amorphous liquid state (called a liquid expanded or LE state) in which the hydrocarbon chains of the surfactant molecule are loosely cohered. Finally, at elevated pressures the monolayer exists in a series of condensed states in which order in the chains and then (at the highest pressures) the head groups appears. These are the liquid condensed (LC) and liquid solid (LS) states. At the phase boundaries, transitions between phases have been found to be generally of first order between the G and LE phases, and the LE and LC phases, and second order between the LC and LS phases. During the first order transitions, the two phases co-exist as the monolayer is compressed, and the surface pressure remains constant.

Little attention has been devoted to the phase behavior of monolayers formed by self-assembly from solution at the air/water interface (Gibbs

monolayers). Soluble surfactants achieve their solubility in water by a balance between head group size and chain length. The larger the headgroup and the smaller the chain, the more soluble the surfactant is in water. This is for two reasons. First, larger head groups interact more strongly with water through dipolar interactions such as hydrogen bonding. Second, the smaller the hydrocarbon chain, the less is the disruption of the low free energy hydrogen bonding structure of water (the hydrophobic effect). Thus soluble surfactants tend to have smaller chains and larger headgroups relative to their insoluble analogues. The fact that monolayers assembled from solution generally consist of amphiphiles with reduced cohesion (due to smaller chain lengths) and greater dipolar repulsion and steric hindrance to packing (due to larger head groups) means that they are less able to cohere into the liquid and condensed phases which the insolubles are able to occupy. Recognize also that aggregation in soluble monolayers can only be driven by the combined driving forces of adsorption from the bulk and van der Waals cohesion between the adsorbed molecules. The insolubles are compressed into the liquid and condensed phases, and hence the driving force for aggregation is the chain cohesion and the externally applied compression force. As the latter tends to be stronger than the purely chemical driving force for adsorption, at the very least, condensed phases may possibly only exist in insoluble monolayers. To date, which phases form in Gibbs monolayers, and how the structure affects the phase behavior, is not resolved.

The focus of this thesis is to study the phase behavior of monolayers formed by self-assembly from solution. The scope of the study contains three objectives:

(i) The first is to establish whether soluble surfactant monolayers form liquid and condensed phases, and if they do, map the phase behavior, determine the nature of the transitions and discover how the surfactant structure determines which phases form. We will study a homologous series of n-alkyl poly (ethylene glycol) ether nonionic surfactants C_iE_j ($CH_3(CH_2)_{i-1}$ (OCH2CH2)$_j$-OH) with i=12 or 14 and j=0,1,2,4 and 6. We use this nonionic series because the surfactants can be obtained in high purity, and because the head group and chains can be systematically varied to cover a range of surfactants from those that are nearly insoluble to those which are very soluble.

(ii) Our monolayer phase studies will show that all the surfactants in the homologous series occupy gaseous and liquid expanded phases, and that the transition is first order and occurs at a negligible surface pressure (i.e. a tension close to the clean air/water tension). This discovery suggested a possible explanation for the induction period which is observed in the reduction in dynamic tension as surfactant adsorbs from solution onto an initially clean interface. When a fresh interface is created in a surfactant solution, the adsorption of surfactant onto the surface is not accompanied by an immediate reduction in tension. Instead, the tension remains constant at (or near) the clean value for a period of time before precipitously dropping to the equilibrium value. The reason for this induction period has not been explained, but it plays a central role in designing

surfactant systems to rapidly reduce tension in interfacial technological processes such as foaming and emulsion, where rapid reduction is necessary for the process, and surfactants are used to facilitate rapid reduction. Design formulations seek to minimize this induction time. Here we hypothesize that the induction period is caused by a G/LE phase transition that the monolayer undergoes as adsorption from solution proceeds. The induction period arises from the first order nature of the transition: Surfactant first adsorbs into the gaseous/dilute state (G) onto the interface causing a small drop in tension from the clean interface value. With the passage of time, the increased adsorption at a critical gaseous concentration causes surface condensation leading to the nucleation of a liquid expanded (LE) state in equilibrium with the gaseous phase. In time, the liquid expanded state grows at the expense of the gaseous state, leading to two-phase equilibrium coexistence at the interface with the surface tension remaining constant and thereby creating the induction period. Finally when the monolayer is completely in the liquid expanded state, further adsorption causes a rapid decrease in tension. The second objective is to experimentally prove this hypothesis, and obtain from this interpretation of the induction period, an expression for the induction time in terms of the properties of the phase transition (i.e. the concentration of the liquid phase on nucleation). This expression will allow surfactant formulators to estimate induction times given the surfactant structure, and will allow for optimizing for a reduction in tension in that time.

(iii) Our studies of the monolayer phase behavior will demonstrate that only the low solubility members of the series with zero or one ethoxy group (in particular $C_{12}E_0$ or dodecanol) and $C_{12}E_1$ and $C_{14}E_1$ can condense from the LE state into a liquid condensed or LC state. The close packing of this state affords the maximum reduction in tension, and the development of a hydrocarbon phase which space fills with little free volume. This reduced tension and hydrocarbon space filling suggested that these LC forming surfactants may be useful in reducing the contact angle formed when an aqueous drop beads up on a hydrophobic surface. The contact angle is determined by the Young-Duprè equation:

$$\gamma_{S/A} - \gamma_{S/L} = \gamma_{L/A} \cos\theta_e \qquad [1.1]$$

where $\gamma_{S/A}$, $\gamma_{S/L}$ and $\gamma_{L/A}$ are the tensions of the solid/air, solid/water and air/water surfaces, respectively. The solid/water tension is high (since it is a polar/non-polar interface), and the solid/air tension is low (since it is a non-polar/non-polar interface); the air/water interface orients itself with an obtuse angle so that the $\gamma_{L/A}$ tension acts in concert with the tension $\gamma_{S/A}$ to balance the solid/water tension. The LC phase forming surfactant, because it forms a dense hydrophobic surface, can adsorb onto the hydrophobic surface of the solid, where it excludes water and presents to the aqueous phase only the polar groups of the molecule. This arrangement should be of low energy, thereby reducing the solid/water tension and from (1) decreasing the contact angle. The reduction in this contact angle has broad applications in optimizing many interfacial technological processes, including:

(i) Drop spraying of aqueous solutions of agrochemicals on waxy foliate surfaces; surfactants added to the aqueous solutions reduce the contact angle upon impact of the drops on the foliate surface and thereby allow the drops to spread rather than rebound[1].

(ii) The impregnation by capillary action of aqueous solutions containing conditioners into hydrophobic fabrics; surfactants added to the conditioner reduce the contact angle, increase the capillary pressure and force the conditioning solution more completely into the fabric pores giving a more complete treatment.

(iii) The liquefaction and removal of aggregated hydrophobic soils deposited on surfaces by coaxing cleaning solutions through the soil pores; surfactants are added to reduce the contact angle and increase the capillary pressure so the pores of the soil can be filled with the cleaning solution, thereby liquefying the soil and making it much more amenable to removal by abrasion[2].

Our third objective will be to use these LC forming surfactants as a base for designing surfactant systems that optimally and rapidly reduce the contact angle. With a view towards improving agrochemical delivery by drop spraying, we will demonstrate that these LC forming surfactant systems enable spreading of impacting drops on model hydrophobic surfaces.

This thesis is organized into the following chapters: Chapter 2 examines the existence of gaseous and liquid expanded phases and their coexistence in the homologous series of aqueous soluble surfactants. Chapter 3 examines the

effect of the G/LE phase transition on dynamic tension reduction accompanying surfactant adsorption onto an initially clean interface. Chapter 4 identifies members of the homologous series which assemble from solution into liquid condensed phases with a detailed analysis of one such surfactant dodecanol. Chapter 5 studies how the transport rates of these sparingly soluble surfactants to interfaces can be accelerated by either dispersing the surfactant finely or by using a second surfactant which allows the mixed adsorbed monolayer to form a condensed state. Chapter 6 studies how surfactants which form liquid condensed states at the air/water interface can be used to lower the contact angle of an aqueous drop on a hydrophobic surface, and how this angle can be reduced further by using a co-surfactant which preserves the condensed state. This chapter also demonstrates how the mixed surfactant systems which form condensed states and significantly lower the contact angle can be used to dramatically facilitate the retention of impacting aqueous drops on model hydrophobic surfaces.

1.2 A Literature Review on Polymorphism in Langmuir Monolayers

As mentioned above, the current state of understanding of the phase behavior of surfactants at interfaces has been reached from studies on monolayers of insoluble surfactants. It was first pointed out by Henri Devaux[3] at the turn of the century, that insoluble surfactant molecules in monolayers at interfaces could exist in different states, analogous to the three-dimensional liquids, solids or gas states. Based on molecular proximity, interactions and orientation, these states are typically classified as either condensed (solid or

liquid) films, expanded films (also termed liquid or liquid expanded) and gaseous films.

As in the case of three-dimensional matter, the simplest state of a monolayer is the gaseous state. The molecules in such films are floating at the interfaces relatively far apart, effectively unaware of the presence of other molecules at the interface and consequently exerting little or no force on the other molecules. They are experimentally characterized by a surface pressure (which is the difference in surface tension between the clean interface and the surfactant covered interface) which asymptotically approaches zero as the mean area occupied by a molecule increases. The conventional approach in analyzing these monolayers is a two dimensional kinetic analysis, similar to the three dimensional ideal gas theory in which it is assumed that molecules move about with an average translational kinetic energy of 1/2kT for each degree of freedom. The two dimensions in the plane of the surface lead to a total energy of kT, which causes the surface pressure, and consequently a simple equation similar to the ideal gas equation is obtained. Mathematically

$$\pi A = kT \qquad [1.2]$$

where π is the surface pressure and A the mean molecular area. Typical inverse surface concentrations are of the order of a few thousand $Å^2$/molecule, and the surface pressure a few tenths of a mN/m.

Molecules at interfaces in much higher surface concentrations exist in what is a loosely cohered expanded state. This state is usually termed liquid or liquid expanded, and is characterized by random orientations of the hydrophobic

portions with only the polar functional groups constrained to be in contact with the sub-phase. The viscosity and compressibility of this phase are what might be expected for such structures. There is no ordering among either the polar groups or the hydrocarbon tails.

The opposite extreme of the gaseous state are the condensed states in which molecules are arranged in nearly their closest packing configuration. In the liquid condensed (LC) state there is tilt ordering among the hydrophobic chains, but no long range positional ordering, the molecular density being close to the crystalline state. In the liquid solid (LS) state, molecules are arranged similar to a two dimensional crystalline structure with the molecular distances comparable to lattice spacing with complete short range positional ordering in the structure. In both these states the surface pressure-area plots are nearly vertical indicating very low compressibility, which reflects the strong interchain attractive forces which hold the molecules in their closest packed structure with little or no dependence on the surface pressure. Despite the apparent simplicity of these film, there are many minor variations in the structure and this has led various authors to postulate a number of surface states or phases. Some states are experimentally well characterized while others have the backing of limited experimental evidence. These include the CS (close-packed solid) and Ov phases. The surface concentrations are close to 20 $Å^2$/molecule in this tightly packed configuration for long chain fatty acids and alcohols.

Phase transitions among surfactant molecules at interfaces may occur, where the monolayer may go from one state to another through a coexistence

regime in which two phases coexist in equilibrium at the interface e.g. from gaseous to liquid expanded. They are usually first order transitions in which, analogous to a three dimensional gas to liquid phase change where the pressure stays constant, the surface pressure or tension stays constant. First order phase changes from liquid expanded to condensed states may also occur (similar to the liquid to solid phase change) but at much higher constant surface pressures. Higher order transitions from a liquid condensed to a liquid solid state may also occur at even higher surface pressures. These phase changes are accompanied by changes in film properties, most notably the compressibility and the viscosity.

The experimental evidence for the above picture of different phases of insoluble monolayers spread and compressed at the air/water interface has been obtained by surface pressure/area[3], fluorescence[4-6] and Brewster angle microscopy[7-9], x-ray[10] and electron diffraction[11], and neutron reflectivity[12-14]. The microscopy techniques allow for the visual distinguishing of these phases, and have been the most useful in understanding the monolayer phase behavior. In fluorescence an insoluble dye consisting of a hydrocarbon chain and a fluorescing fluorophore is placed on the surface. The dye dissolves in the gaseous and liquid expanded phases, but is expelled from the condensed phase. Upon illumination, the dye does not fluoresce in the gaseous state because the fluorophore is in contact with water, which quenches the fluorescence, while in the LE state it does fluoresce as the fluorophore is removed from the water surface. Thus the dye illuminates the liquid state and makes the condensed and gaseous states appear dark. In Brewster angle microscopy, the reflectivity of the

monolayer along the surface is recorded onto a camera. The incident light impinges at the Brewster angle of the clean surface, so that there is no reflected light. The gaseous state also reflects little light so also appears dark, while the liquid and solid states change the refractive index so that these phases appear bright, with the condensed phase brighter than the expanded phase. Using the microscopy techniques, the G/LE and LE/LC transitions have been shown to be first order, since co-existing phases were visualized, and this confirms the plateaus in surface pressure recorded during the transitions.

Quantitative studies of insoluble monolayers began with simple surface pressure measurements[3] (i.e. plots of the surface pressure against inverse surface concentration). To illustrate quantitatively the phase behavior of an insoluble surfactant we discuss the well-studied alkanoic acid PDA (Pentadecanoic acid), which can exist in up-to four different phases at room temperature. This phase behavior of PDA has been classified by many researchers using a broad range of techniques e.g. by Pallas and Pethica[15] and Winch and Earnshaw[16] by surface pressure measurements. At extremely low surface coverages, PDA exists in a gaseous state with surface pressures close to zero indicating that this state is very expanded. As the area/molecule (Γ^{-1}) is reduced from 1500 to 42 $Å^2$/mol, a plateau in surface pressure at π=0.132 mN/m is found at 20 ^{0}C indicating coexistence of the gaseous phase with a disordered liquid expanded (LE or L_1) phase through a first order transition [15]. On further reducing the area/molecule the entire interface goes into the LE state, and on even further increasing the surface coverage, it undergoes a second phase

transition (LE-LC) evident in the form of a plateau in surface pressure at 2 mN/m. Eventually a transition from a LC to an even more compact LS state is observable in the form of a kink in the surface pressure isotherm. Fig. 1.1 is a schematic of the surface pressure isotherm for PDA.

Visual confirmation of two-phase coexistence, both the gaseous-liquid expanded (G/LE or L_1) and the liquid expanded-liquid condensed (LE/LC or L_2) has been obtained by fluorescence microscopy for myristic[17], pentadecanoic[18] and stearic acid[19]. In the PDA LE/LC phase transition, the ratio of light to dark areas gave pure phase densities consistent with surface pressure measurements[18]. Further visual verification of two-phase coexistence has been obtained for the G-LE and LE-L_2 states of PDA[18] and Myristic[17] acid, and the G-LC transition for stearic acid[19] using Brewster angle microscopy (BAM), thus confirming the fluorescence results. In addition, efforts have been made to hypothesize the phase behavior in terms of demarcating phase coexistence regimes[5] and to locate boundaries of these regions. Similar polymorphism exists for other insoluble surfactants when they are at an interface, which is well documented.

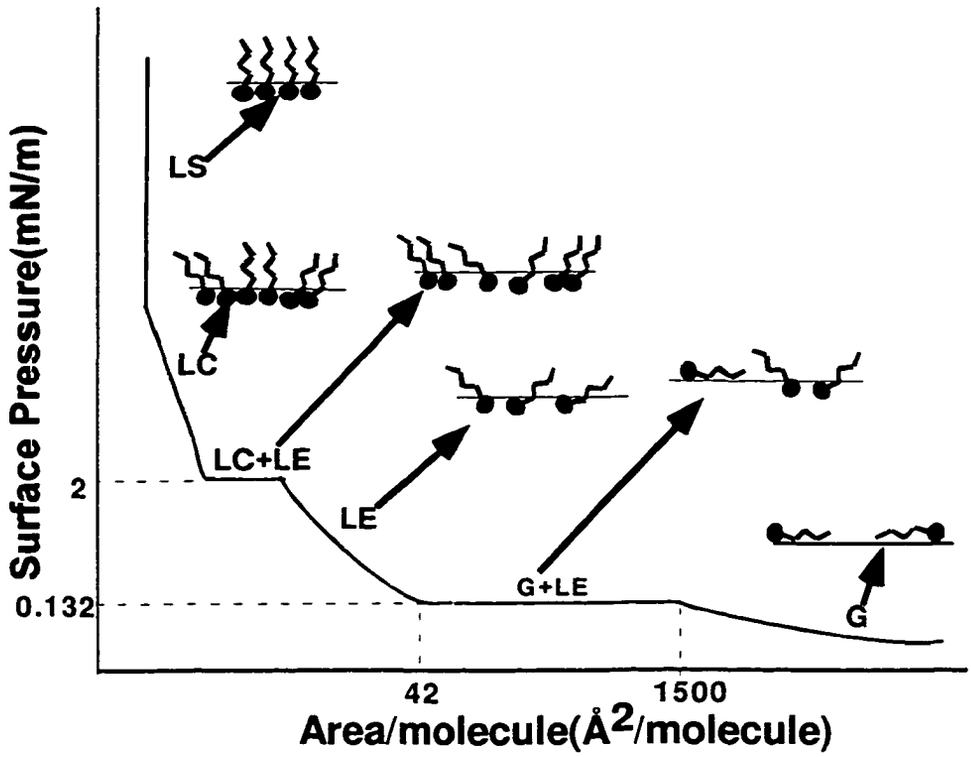

Fig 1.1: Schematic for the Phase Behavior of Insoluble Surfactants at an Air/Liquid Interface: Illustration for Pentadecanoic Acid (PDA).

References

1)Reichard, D. L.; Cooper, J. A.; Bukovac, M. J.; Fox, R. D. *Pesticide Science* **1998**, *53*, 291-299.

2)Cox, M. F. *Journal of the American Oil Chemists Society* **1990**, *63*, 559-565.

3)Gaines, G. L. *Insoluble monolayers at liquid-gas interfaces*; Wiley-Interscience: New York, 1966.

4)McConnell, H. M.; Tamm, L. K.; Weis, R. M. *Proc. Natl. Acad. Sci. USA* **1984**, *81*, 3249-3253.

5)Knobler, C. M. *Science* **1990**, *249*, 870-874.

6)Stine, K. J. *Micros. Res. Tech.* **1994**, *27*, 439-450.

7)Hénon, S.; Meunier, J. *J. Chem. Phys.* **1991**, *68*, 936-939.

8)Hönig, D.; Möbius, D. *J. Phys. Chem.* **1991**, *95*, 4590-4592.

9)Vollhardt, D. *Adv. Coll. Int. Sci.* **1996**, *64*, 143-171.

10)Jacquemain, D.; Wolf, S. G.; Leveiller, F.; Deutsch, M.; Kjaer, K.; Als-Nielsen, J.; Lahav, M.; Leiserowitz, L. *Angew. Chem. Int. Ed. Engl.* **1992**, *31*, 130-152.

11)Kajiyama, T.; Oishi, Y.; Hirose, F.; Shuto, K.; Kuri, T. *Lang.* **1994**, *10*, 1297-1299.

12)Thomas, R. K.; Penfold, J. *Current Opinion in Colloid and Interface Science* **1996**, *1*, 23.

13)Als-Nielsen, J.; Jacquemain, D.; Kjaer, K.; Leveiller, F.; Lahav, M.; Leiserowitz, L. *Phys. Rep.* **1994**, *246*, 252-313.

14)Crowley, T. L.; Lee, E. M.; Simister, E. A.; Thomas, R. K.; Penfold, J.; Rennie, A. R. *Coll. Surf.* **1990**, *52*, 85-106.

15)Pallas, N. R.; Pethica, B. A. *J. Chem. Soc. Farad. Trans. I* **1987**, *83*, 585-590.

16)Winch, P. J.; Earnshaw, J. C. *J. Phys.: Condens. Matter* **1989**, *1*, 7187-7205.

17)Suresh, K. A.; Nittmann, J.; Rondelez, F. *Europhys. Lett.* **1988**, *6*.

18)Moore, B. G.; Knobler, C. M.; Akamatsu, S.; Rondelez, F. *J. Phys. Chem.* **1990**, *94*, 4588-4595.

19)Moore, B.; Knobler, C. M. *J. Chem. Soc., Faraday Trans. 2* **1986**, *82*, 1753-1761.

Chapter 2

Existence of Gaseous and Liquid Expanded Phases Among Aqueous Soluble Polyethoxylated Surfactants

2.1 Introduction

As discussed in Chapter 1, the phase behavior of insoluble surfactants spread and compressed at an air/water interface has been well studied and classified using a wide array of analytical techniques. However, the phase behavior of the more important aqueous soluble surfactants has not been given much attention, nor has its effect on film properties as well as dynamic processes been understood. From the generalized isotherm described for an archetype PDA in the introduction, one would intuitively expect that as films of aqueous soluble surfactants assemble from solution, they undergo some or all of the phase changes described, and consequently there would be a pronounced effect on the interfacial properties. One might expect the phase behavior of sparingly soluble surfactants to be similar to the insoluble surfactants as they have comparative structures as insoluble surfactants. However the normal industrial surfactants have extremely high solubility owing to different structure, especially a much larger polar group. The presence of the large polar group induces other forces in the delicate balances in phase coexistence, much higher dipolar interactions and large steric hindrance. In addition the additional degree of freedom of the possibility of bulk exchange influences the overall equilibrium. Thus one might expect soluble surfactants to exhibit limited phase behavior, for instance an inability to assemble into condensed phases.

By analogy with the medium chain length insoluble amphiphiles mentioned in the introduction, Lin *et al.*[1] expected that for bulk soluble amphiphiles with polar groups larger than hydroxyls or carboxylates, or with smaller chains (as for example decanol), the monolayer, although unable to condense into the LC and LS states, should exist in the G and LE phases.

There is increasing evidence in the literature that suggests that bulk soluble surfactants can undergo the G/LE phase transition as they adsorb from solution. Gas-Liquid phase transitions in soluble surfactants have been inferred by cusps in the equilibrium surface tension-bulk concentration (γ-ln c_b) curves. The slope of the γ-ln c_b curve is proportional to the surface excess Γ, hence a true cusp in the γ-ln c_b curve would be indicative of a phase transition. Extensive work carried out by Matuura [2,3] and coworkers obtained evidence of phase transitions from cusps in the γ-ln c_b curve. They studied a series of n-octyl (octanol, octanoic acid, sodium octanoate), n-dodecyl (sodium dodecylsulfate, dodecylammonium chloride[4] and dodecyltrimethylammonium chloride[5]) adducts and decylammonium chloride. The cusps occurred at surface tensions between 67 and 70 mN/m and at bulk concentrations well below their critical micellar concentrations. The slopes of the γ-ln c_b curves gave surface coverages of 160-282 $Å^2$/molecule at the lower density end and 88-260 $Å^2$/molecule at the higher density end depending on the polar group size and the ionization. Since these films are fairly expanded and the tensions close to the clean interface value, the transition was classified as gaseous to liquid expanded. Cusps in γ-ln c_b curves have also been observed by different authors for n-octanol[6] and n-decanol[1].

Direct visual evidence of phase coexistence, in which the surface phases assemble from solution was first observed by Bergé *et al.*[7] using fluorescence for a film of SDS, which when subjected to changes in temperature, displayed a discontinuity in surface pressure suggesting the transition to a condensed state. However as first pointed by Hénon *et al.*[8], this evidence was inconclusive as SDS strongly hydrolyzes to the relatively insoluble/extremely surface-active dodecanol which is present on the interface in a high proportion and it is the condensation of dodecanol which is being actually observed. Hénon *et al.* studied the self-assembly of a film of hexadecanoic acid[8] at a pH of 6.5 (where the surfactant was sparingly soluble) onto an initially surfactant free interface. BAM monitoring of the interface with concomitant surface pressure measurements displayed bright domains in a mainly dark background. The relative percentage of dark regions (high reflectivity) decreased with time indicating a phase transition from a dilute, low reflectivity gaseous state to a phase of higher reflectivity. Further polarization analysis of the reflected light indicated tilt ordering among the domains, hence the transition was classified as gaseous to liquid condensed.

Recently, direct visual evidence for a transition from a gaseous to a liquid state has been provided by Pollard *et al.*[9] These authors studied the n-alkyl poly (ethylene glycol) ether or poly ethylene-oxide $C_{14}E_1$ (CH_3 $(CH_2)_{13}(OCH_2CH_2)_1OH$) which is slightly soluble in water. The polar group is however large enough so that, as verified by fluorescence microscopy in their study, directly spread monolayers exist in G, LE and LC states rather than just G and LC states as was

the case with hexadecanoic acid. Pollard *et al*[9] used an open channel flow cell in which surfactant adsorbed from a flowing solution onto an initially clean surface of the channel in which the fluorescing dye was previously spread. Illumination at the excitation wavelength allowed for the study of the evolution of the phases. Initially, with just the dye existing on the interface, there was no fluorescence and the interface was completely dark. During the initial adsorption, a bright LE phase was found to nucleate in a (dark) gaseous background, and grow at nearly the constant tension of the clean surface. Eventually, the entire interface was occupied by the LE phase on subsequent adsorption. Once again as the tension was close to the clean interface value during this transition, it was verified that sparingly soluble surfactants do undergo a gaseous to liquid expanded phase transition as they adsorb onto an interface from solution.

In related work, G/LE phase transitions have been observed by Riegler[10] using Brewster angle microscopy and ellipsometry for alkane vapors at the air/water interface saturated with the alkane vapor. The estimated surface densities of the two phases were similar to that of PDA. Tension measurements as a function of surfactant concentration and temperature for fluoroalkanols at the hydrocarbon/water interface have shown the presence of a G/LC transition for CF_3 $(CF_2)_9(CH_2)_2OH$ and a G/LE transition for a similar but smaller chain amphiphile CF_3 $(CF_2)_7(CH_2)_2$ OH[11].

As mentioned above, more and more evidence has been cropping up in the literature about the existence of phase transitions among aqueous soluble surfactants. While the majority of studies have been carried out for sparingly

soluble surfactants, the few studies on truly soluble surfactants have used techniques which provide only indirect evidence for the existence of phase transitions e.g. cusps in the γ-ln c_b curves. In the first section of this work we intend to map out the phase behavior (the gaseous-liquid expanded phase transition) of a homologous series of surfactants, namely C_mE_n ($CH_3(CH_2)_{13}(OCH_2CH_2)_nOH$ m=14,n=1,2,4 and 6). As the number of ethoxy groups increases the solubility shows a corresponding rise; $C_{14}E_1$ is sparingly soluble while $C_{14}E_6$ is very soluble and is a commonly used industrial surfactant. We choose this surfactant series because of their technological importance, high purity and non-polydispersity, and to study the effect of increasing hydrophilicity on the phase behavior. In the first part of the research we intend to establish using fluorescence microscopy, whether or not each homologue undergoes the gaseous-liquid expanded phase transition as its film assembles from solution, in effect prove if or not that similar to the insoluble surfactants, the gaseous-liquid expanded transition is universal to these class of surfactants. Further using fluorescence microscopy and carrying out compression/expansion on a mini Langmuir trough we intend to find the surface coverage Γ_{LE}^c, at which the gaseous-liquid expanded transition ends (if they undergo the transition), as films assemble from solution for each of these homologues, and correlate these values to the polar group size. Before presenting the results, we provide a brief description of the materials utilized and experimental techniques used and a synopsis of the actual kinds of experiments conducted.

2.2: Experimental

Materials: N-alkyl poly (ethylene glycol) ether surfactants (C_mE_n=$CH_3(CH_2)_{m-1}(OCH_2CH_2)_nOH$, m=14, n=1,2,4,6), >99.9% purity, were obtained from Nikko Chemicals, Japan. Pentadecanoic Acid (PDA) >99 % purity was obtained from Fluka. HPLC grade chloroform, stabilized with 0.5-1% ethanol, obtained from Sigma, MO or Fluka, was used as the spreading solvent. For fluorescence studies, the surfactant solutions were doped with ~0.5-1 mol % of a fluorophore NBD-HDA (4-(hexadecylamino)-7-nitrobenz-2-oxa-1,3-diazole) supplied by Molecular Probes, OR. All chemicals were used as received without any further purification. The sub-phase in all experiments was deionized water purified by a Milli-Q filter system fitted with an Organex-Q column to remove trace contaminants (Millipore, MA). The resistivity of the deionized water was at least 15 MΩ cm.

Langmuir Trough Method: A commercial Langmuir Trough (Lauda Model D, Lauda-Konigshofen, Germany) or mini-Langmuir Trough (Nima Technology (type 601 M), UK) was used to measure the surface pressure isotherms as well as to test the purity of the solvent. In the Lauda trough, the surface pressure was measured with the help of a pressure transducer which was connected to a teflon float which separates the clean interface from the monolayer covered interface and lateral forces acting on the float are transmitted to the transducer. The resolution of the transducer was ±0.1 mN/m. The Nima trough utilized a paper Wilhelmy plate to measure the surface tension (this technique is described in detail in Chapter 3). In either case, the trough was first wiped with a dry kimwipe,

filled with deionized water following which the surface was aspirated both manually and later after compression to the minimum area, automatically, through suction nozzles. The clean interface was then checked for surface active contaminants by compression to note change in surface pressure, if any. Once the surface was clean, a few microlitres of a chloroform solution of each surfactant was spread on it. After waiting a minute for the chloroform to evaporate, the movable barrier was rapidly compressed to minimize dissolution and the isotherm recorded.

Fluorescence Microscopy Experiments: Details of the experimental setup have been described in a previous paper[9]. While the fundamental principles involved in these techniques have been described in the first chapter, a brief description of the setup utilized is described below. In brief, the main components of this setup were a laser to excite the fluorophore, a high sensitivity silicon intensified target (SIT) camera to view and record the dye partitioning at the interface and a mini-Langmuir Trough (Nima Technology (type 601 M), UK). The trough consisted of a teflon trough with two movable barriers used to expand/compress a monolayer spread at the air-fluid interface. The area between the barriers at its most expanded position was 91 cm^2 and at the most compressed position at which observations could still be made, without interfering with the laser beam was 12-15 cm^2. Thus a monolayer on the interface between the barriers could be compressed to a surface coverage as much as seven times the minimum value. The mini-trough was connected to an interface unit, which in turn was connected to the serial port of a 486 PC that was used to

control all trough operations such as barrier motion etc. The barriers could be moved at variable speeds and moved symmetrically about the centerline of the rectangular trough. A plexiglas cover with openings for the objective and for spreading solutions was used to reduce surface convection due to air currents. The fluorescence dye NBD-HDA used in this study has its absorption and emission band maxima at 468 nm and 523 nm respectively. A 10 mW argon ion laser, λ=488 nm (Ion Laser Technology, UT) used to fluoresce the dye, impinged on the interface between the two movable barriers and directly under the microscope objective (Leitz Wetzlar NPL 10x/0.2N.A; focal length=2.03 cm). The emission passed through the objective and an emission filter (Omega, VT) with a cutoff wavelength of 515 nm, to the high sensitivity SIT video camera (Hamamatsu model C2741-08, Japan) which were all mounted on the microscope. The fluorescence images were simultaneously observed on a monitor and captured/digitized with the help of a frame-grabber card (Data Translation DT 2861, MA or Scion LG-3, Scion co., MD) on a 486 or a 200 MHz PC. The digitized images were further processed to enhance contrast with LViewPro and Adobe Photoshop software.

The fluorescence experiments consisted of deposition experiments in which the surfactant molecules were physically spread onto an interface (as if they were insoluble surfactants). These involved spreading a small amount (~15 μl) of a chloroform solution of each surfactant containing the dye (~1 mol %) onto the clean interface of either a petridish or a Langmuir mini-trough filled with deionized water. The first experiments were 'single shot' experiments done at

constant monolayer surface density in a fixed area petridish, just to verify the co-existence of the gaseous and liquid phases. The amount usually spread on the petridish interface corresponded to a surface coverage of about 1000 $Å^2$/molecule, where, based on data for insoluble surfactants[12], we expected the monolayer to be in the two-phase coexistence region. The bulk of the experiments were done in the mini Langmuir trough to study phase behavior at different surface coverages. Before spreading surfactant solutions, the trough was thoroughly cleaned, first with a 0.1M solution of NaOH at 50° C, and then by rinsing it with deionized water repeatedly. In either case, the water surface was further cleaned by manual aspiration and viewed under the microscope to verify that it was contaminant and dust free. The solution was then spread using a microsyringe with the barriers at its most expanded position, so that the monolayer was at its most expanded state, and in the phase transition region, usually around 1000 $Å^2$/molecule. After waiting about a minute to allow the chloroform to evaporate, the monolayer was then compressed using the movable barriers, the initial barrier speed being kept high to minimize desorption. Once we approached the end of the phase coexistence region, as was evident visually, the barrier speed was reduced to get an accurate estimate of the surface coverage at that state. After compressing the monolayer into the single-phase regime, the barriers were re-expanded to check for any hysteresis effects on the measurement of Γ_{LE}^c due to desorption. All fluorescence deposition experiments on the trough were thermostatted to 23^0 C. The entire compression and re-expansion cycle was completed within 15 min for the most bulk soluble

surfactant. The typical barrier speeds used varied from 20 cm^2/min at the most expanded state to 2 cm^2/min near the end of the phase coexistence region. As the monolayer was compressed fluorescence images were digitized at different surface coverages, the barriers being stopped momentarily during image digitization to prevent flow effects on domain shapes. The barrier spacing at which gaseous (dark) domains completely disappeared, and the interface turned completely bright was carefully noted both in the compression and re-expansion mode. The experiments in the gaseous-liquid expanded region, were at extremely low surface pressure, lower than the resolution of the pressure transducer, hence no surface pressure measurements were made on the mini-trough just fluorescence observations. Fig. 2.1 illustrates the fluorescence microscopy apparatus with the mini-Langmuir trough being replaced by the petridish for single shot experiments.

2.3 Fluorescence Results

The first fluorescence images presented in Fig. 2.2, are 'single shot' images (as described in sec 2.2 (b)) of a monolayer at fixed surface density, for each of the surfactants $C_{14}E_1$ (a), $C_{14}E_2$ (b), $C_{14}E_4$(c) and $C_{14}E_6$ (d). One clearly sees the dye demarcation into two phases, the bright regions representing the liquid expanded phase and the dark regions the gaseous state. Thus visual confirmation that the gaseous-liquid phase transition is prevalent in each of these surfactant homologues was obtained. The domains were typically 10-100 μm in diameter and very much like those observed for the insoluble monolayers. On leaving the monolayer overnight, the overall intensity of the bright regions seemed

to have reduced, but the domain distribution seemed to be unaltered. The monolayer was completely stagnant as the petridish was well covered and the domains were round. It must be emphasized that the surface densities given alongside the images are those assuming no desorption into the bulk, based on the amount actually spread onto the interface. However, there was no noticeable desorption even over a period of days as evidenced by the fact that the relative areas remain unchanged. The sublayer concentration at these low surface coverages is extremely low, and hence the diffusive driving force into the bulk is negligible, causing negligible desorption. So the assumptions of the apparent area/molecule, though an upper bound on the surface coverage, are probably quite accurate.

In the second kind of experiments, surfactant was dissolved (along with the dye) in chloroform, and spread on the surface of the mini-trough with the barriers initially at the most expanded state and the inverse surface coverage approximately 1000 $Å^2$/molecule. The G and LE phases at this overall surface concentration were immediately noticeable, confirming again the fact that this transition occurs for each homologue. As one compressed the barriers, thus increasing the surface coverage, the proportion of bright regions increased at the expense of dark regions implying an increasing LE fraction in the monolayer. The background started going from mainly a dark gaseous one to a bright LE one. On further compression as the surface coverage approached the end of the phase transition this trend continued until there were very few gaseous domains, visible as dark spots in the mainly LE background. Finally on further compression the

gaseous domains completely disappeared and the monolayer was in its liquid expanded (bright) state. The area between the barriers at the point at which the gaseous domains completely disappeared was carefully noted as this gives Γ_{LE}^{c}, and we record a value of 235-250 $Å^2$/molecule for instance for $C_{14}E_6$. Once the monolayer was in its LE state the barriers were expanded to once again determine the surface coverage at which gaseous domains would re-nucleate. A slight difference in surface coverages at which domains disappeared on compression and re-nucleated on expansion was found. Digitized images at different surface coverages are presented in Fig. 2.3 for $C_{14}E_1$, Fig. 2.4 for $C_{14}E_2$ and Fig. 2.5 for $C_{14}E_6$. The gaseous domains are not perfectly round but appear to be sheared, the reason for which is that we were unable to completely cutoff air currents causing surface convection. It must be emphasized that the surface densities given alongside the images are those assuming no desorption into the bulk, based on the amount actually spread onto the interface. However, the trough had a small volume to area ratio (~$3*10^{-3}$ m) so that even at equilibrium the amount depleted from the surface is negligible. So the assumptions of the apparent area/molecule, though an upper bound on the surface coverage, are probably quite accurate. A quantitative analyses to justify our assumption of negligible desorption will also be presented in Chapter 3 (see Appendix A) for one homologue.

An attempt was also made to measure the density of the gaseous state at the point of liquid nucleation (Γ_G^{c}). Instead of compression, monolayers of $C_{14}E_6$ were expanded from 1000 to 4000 $Å^2$/molecule in an effort to observe the

disappearance of the bright LE state. However, although the field was nearly completely dark, a few tiny (<10 μm in diameter) bright islands remained. Although this could imply that $1/\Gamma_G^c$ is larger than a few thousand Å^2/molecule, it seems more likely that these persistent tiny islands are due to the presence of surface impurities aggregated in a LE state. Thus the gaseous end of the phase transition can not accurately be determined by these fluorescence experiments.

To verify that the dye concentration is low enough so that it does not affect the transition, Γ_{LE}^c for PDA on an acidified sub-phase (pH=2) at 25° C was determined. We choose PDA because we have an independent measurement of Γ_{LE}^c by direct surface pressure measurements without dye (see Pethica and coworkers[8]). In addition we carried out our own surface pressure/ area isotherm measurement for PDA. Pethica *et al.'s* value for Γ_{LE}^c for PDA was 43.5 Å^2/molecule and from our isotherm shown in Fig. 2.6, the pressure starts rising rapidly at an area/molecule of 41-42 Å^2/molecule which is in very good agreement with their data. Having obtained this independent estimate of Γ_{LE}^c for PDA, we made a chloroform solution of PDA with the dye, spread the solution on the interface of the mini trough and carried out a compression to see if we could visually determine Γ_{LE}^c and compare it to the available value. Figs. 2.7 (a)-(d) show images for PDA at increasing surface concentrations upon compression of the monolayer. We once again see two phase coexistence at low surface concentrations, and there is an increasing LE (bright) fraction of the monolayer upon compression. The area of the trough and hence the surface concentration at which the monolayer turned completely bright was carefully noted and this

value is 45-56 $Å^2$/molecule which is in good agreement with the independent estimate of 43 $Å^2$/molecule. Such a test of the effect of the dye on Γ_{LE}^c for PDA has also been carried out by Knobler *et al*[13]. He observed gaseous domains at 50 $Å^2$/molecule and the interface was bright and in the LE state at 36.5 $Å^2$/molecule, which is again in good agreement with the isotherm data. Hence the visual technique of obtaining Γ_{LE}^c is justified.

2.4 Discussion and Conclusions

In this study a homologous series of n-alkyl poly (ethylene glycol) ethers was analyzed for its phase behavior. Fluorescence microscopy was used to establish that each of the homologues can exist in (at-least) two phases: the gaseous and liquid expanded states. Fluorescence microscopy experiments by compressing a monolayer on a mini-Langmuir trough, were successfully used to determine the critical surface density of the nucleating LE phase (Γ_{LE}^c) in a two phase coexistence regime. Impurities preclude the corresponding measurement for the density of the gaseous state.

It was found that for a fixed hydrocarbon tail length the liquid phase density (Γ_{LE}^c) decreases with increasing number of ethoxy groups. Thus there exists a phase envelope for the G/LE transition for the homologous series with increasing ethoxy number and the LE boundary of the envelope (Fig. 2.8) has been constructed. The inability to measure the gaseous phase density (Γ_G^c) prevents the quantification of this density and subsequent construction of the right side of the phase envelope. This phase envelope is very similar to that obtained by

increasing the temperature as has been demonstrated by many authors for insoluble surfactants (for instance for the LE/LC transition for PDA by Winch and Earnshaw[14]) and for sparingly soluble surfactants by Pollard *et al.* for the LE/LC phase transition of $C_{14}E_1$[9] and by Aveyard *et al.* for the LE/LC transition of $C_{12}E_1$[15]. The bigger polar groups on the more soluble surfactants act so as to expand the monolayer and reduce the critical density of the liquid phase.

The values of these surface coverages measured using fluorescence are once again we emphasize, the upper bound as there could be some desorption. We expect desorption to be minimal however as shall be demonstrated for one homologue $C_{14}E_6$ in Chapter 3. The measured density of the liquid phase for the most insoluble homologue studied ($C_{14}E_1$) is small when compared to insoluble surfactants of comparable structure, i.e. 130 $Å^2$/molecule when compared to the PDA measurements (43 $Å^2$/molecule) of Pethica and co-workers. It is also small when compared to the inferred value of 36 $Å^2$/molecule for decanol by Lin and co-workers. This could be due to the additional presence of the bulky ethoxy group in $C_{14}E_1$. When compared to the cusp measurements of this density by Matuura and co-workers, the densities for all the homologues are in reasonable agreement their estimates. This is because the surfactants they studied are more soluble and have a bigger polar group.

Although it was found difficult to measure the critical density of the gaseous phase, a lower bound estimate was obtained for this density for $C_{14}E_6$. Even monolayers expanded to over 2000 $Å^2$/molecule were found to be in two-phase co-existence. When compared to similar measurements on insoluble monolayers,

this density is comparable to that obtained by Pethica and co-workers for PDA using surface pressure measurements, but is smaller than that estimated by Kim and Cannell for Pentadecyclic acid[16]. As compared to soluble surfactants, this measurement is much too low when compared to much larger values of this density estimated by Matuura and co-workers for a series of amphiphiles and Lin and co-workers for decanol using cusps in the γ-ln c_b curves. Cusp estimates of this density (especially the gas phase density) are somewhat questionable due to inaccuracies in the very dilute concentrations and sparse data points in that region. The extremely small values for this density also suggests that intermolecular attractive forces are much longer in range than previously presumed. Therefore these forces exist at densities much smaller than that corresponding to a density where each molecule would just touch each other when lying completely flat on the interface[17].

It has not been established if highly soluble surfactants with extremely large polar groups exhibit similar polymorphism i.e. does the phase envelope depicted in Fig. 2.8 have an upper critical point such that once the polar group size is exceeded beyond a certain limit for a give chain length, the monolayer will always exist in a single phase. It is difficult to obtain surfactants with a large polar group in a mono-disperse form (with the exception of the betaine surfactants) and consequently difficult to study their phase behavior. So no definitive conclusions can be drawn about these homologues. This is one open question which needs to be addressed in future work.

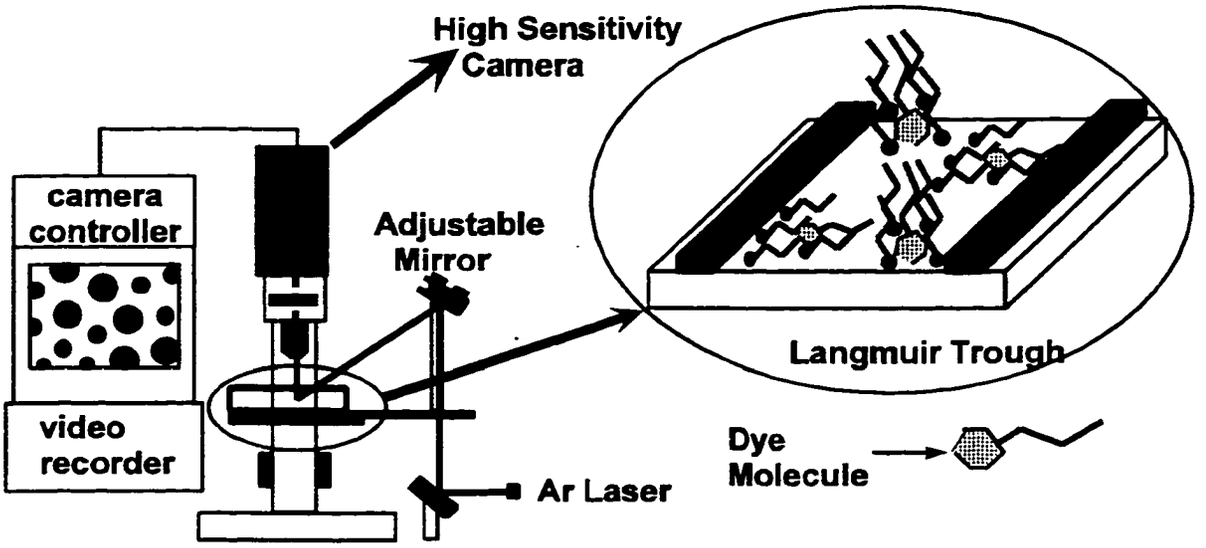

(a)

Under Microscopy:

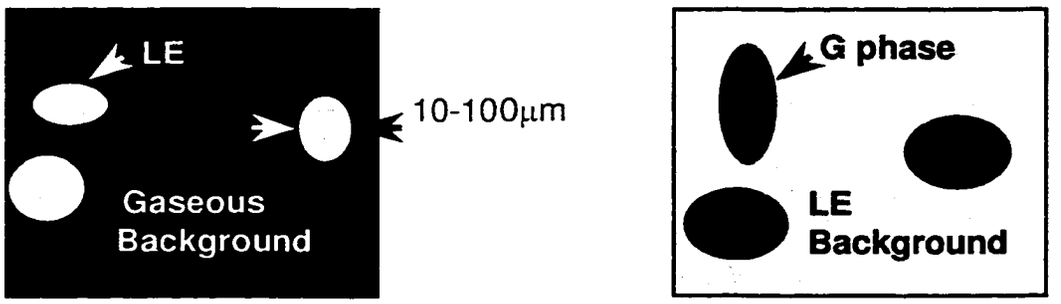

G end of G/LE

LE end of G/LE

(b)

Fig. 2.1: Illustration of the Fluorescence Microscopy Setup (a) Microscope, Excitation Laser and mini-Langmuir trough and (b) Direct Visualization of Surface Phases.

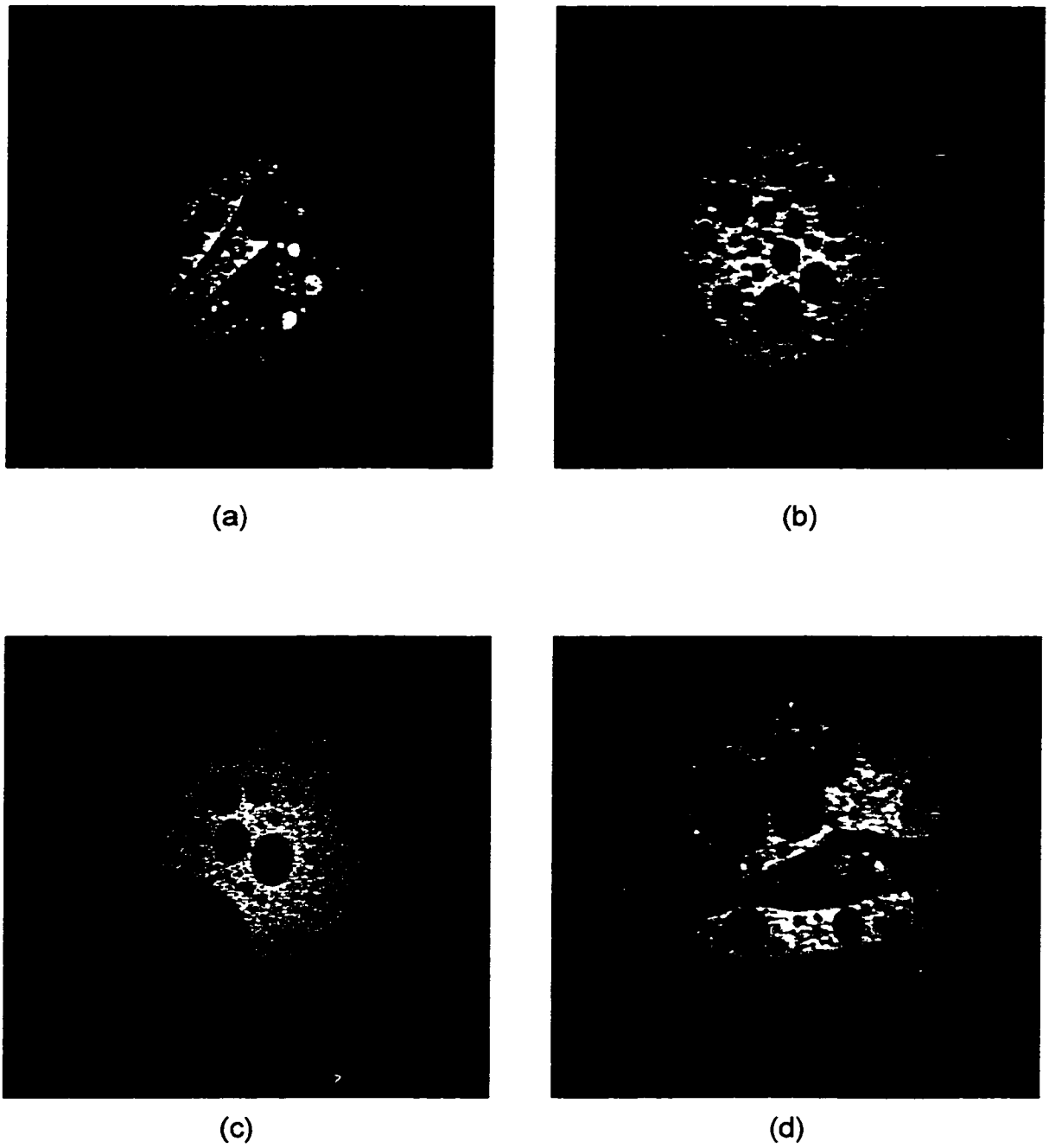

Fig. 2.2: Single Shot Images Demonstrating Two-Phase Coexistence For (a) $C_{14}E_1$ at 530Å^2/molecule (b) $C_{14}E_2$ at 1060 Å^2/molecule (c) $C_{14}E_4$ at 1500 Å^2/molecule and (d) $C_{14}E_6$ at 1460 Å^2/molecule.

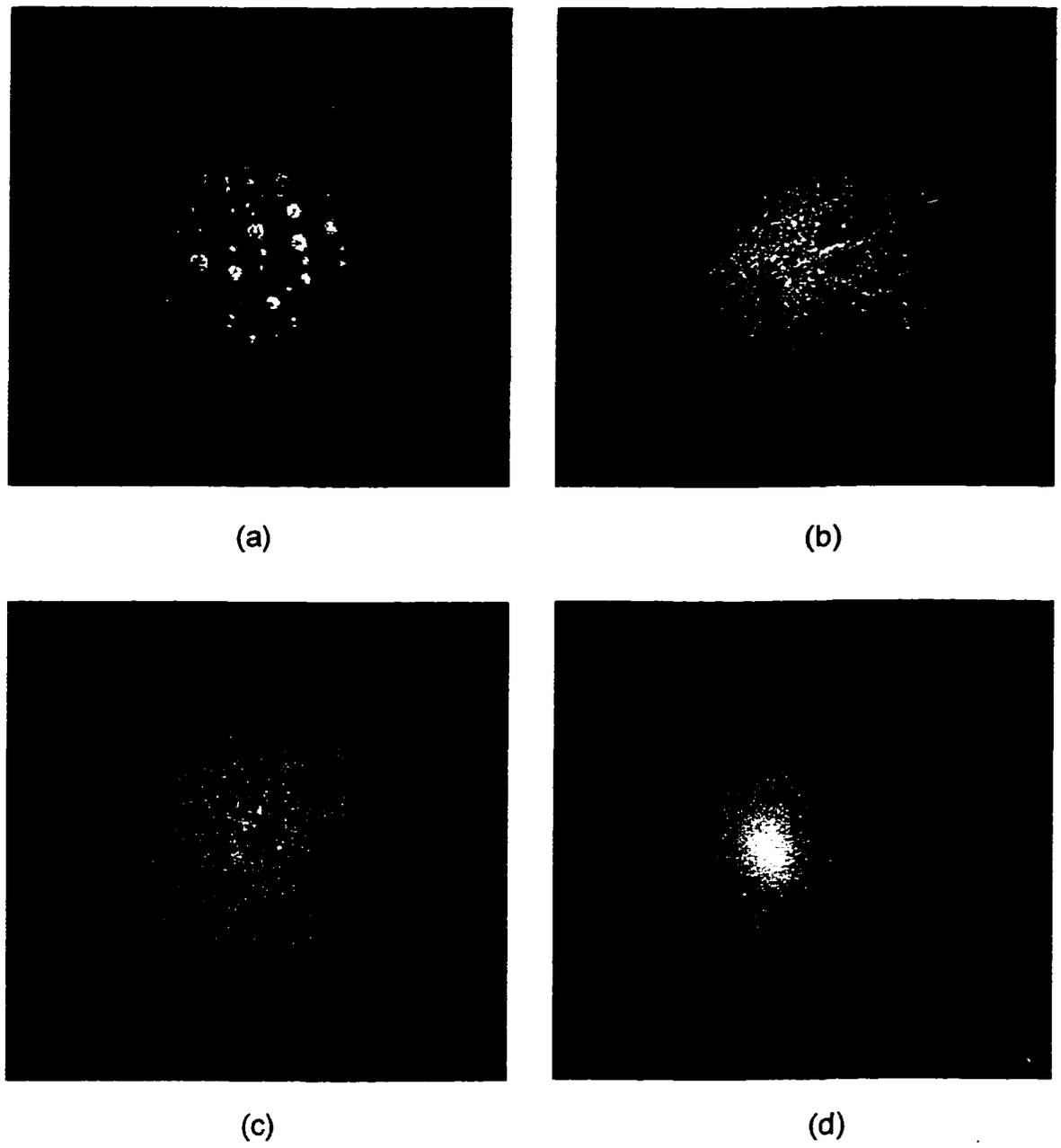

Fig. 2.3: Sequence of Fluorescence Images For $C_{14}E_1$ on the mini-Langmuir trough as the Surface Concentration is Increased by Compression to Determine Γ_{LE}^{c}: (a) 657 $Å^2$/molecule (b) 254 $Å^2$/molecule (c) 183 $Å^2$/molecule and (d) 133 $Å^2$/molecule.

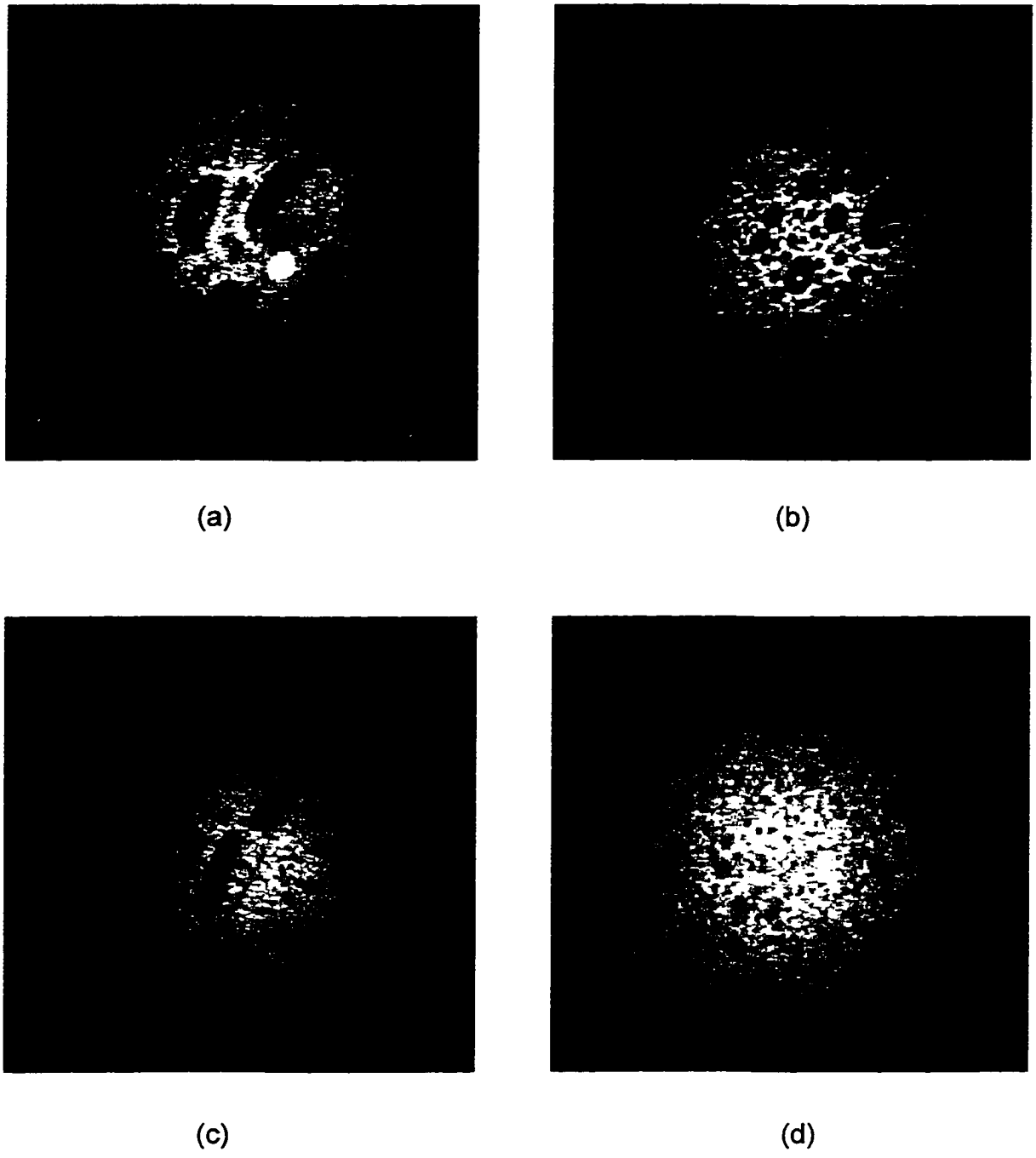

Fig. 2.4: Sequence of Fluorescence Images For $C_{14}E_2$ on the mini-Langmuir trough as the Surface Concentration is Increased by Compression to Determine Γ_{LE}^{c}: (a) 1407 $Å^2$/molecule (b) 807 $Å^2$/molecule (c) 515 $Å^2$/molecule and (d) 230 $Å^2$/molecule.

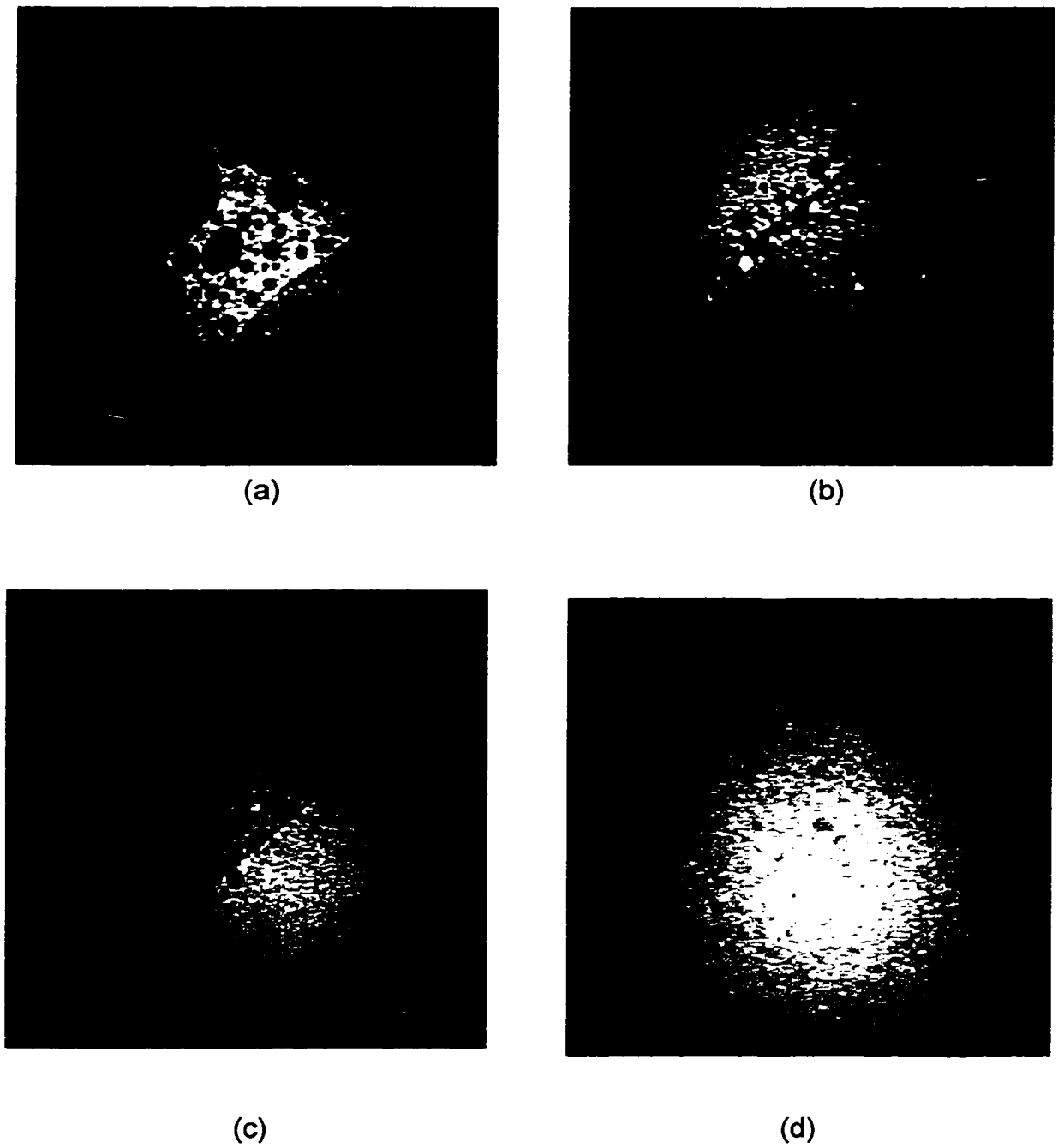

Fig. 2.5: Sequence of Fluorescence Images For $C_{14}E_6$ on the mini-Langmuir trough as the Surface Concentration is Increased by Compression to Determine Γ_{LE}^{c}: (a) 990 $Å^2$/molecule (b) 495 $Å^2$/molecule (c) 330 $Å^2$/molecule and (d) 282 $Å^2$/molecule.

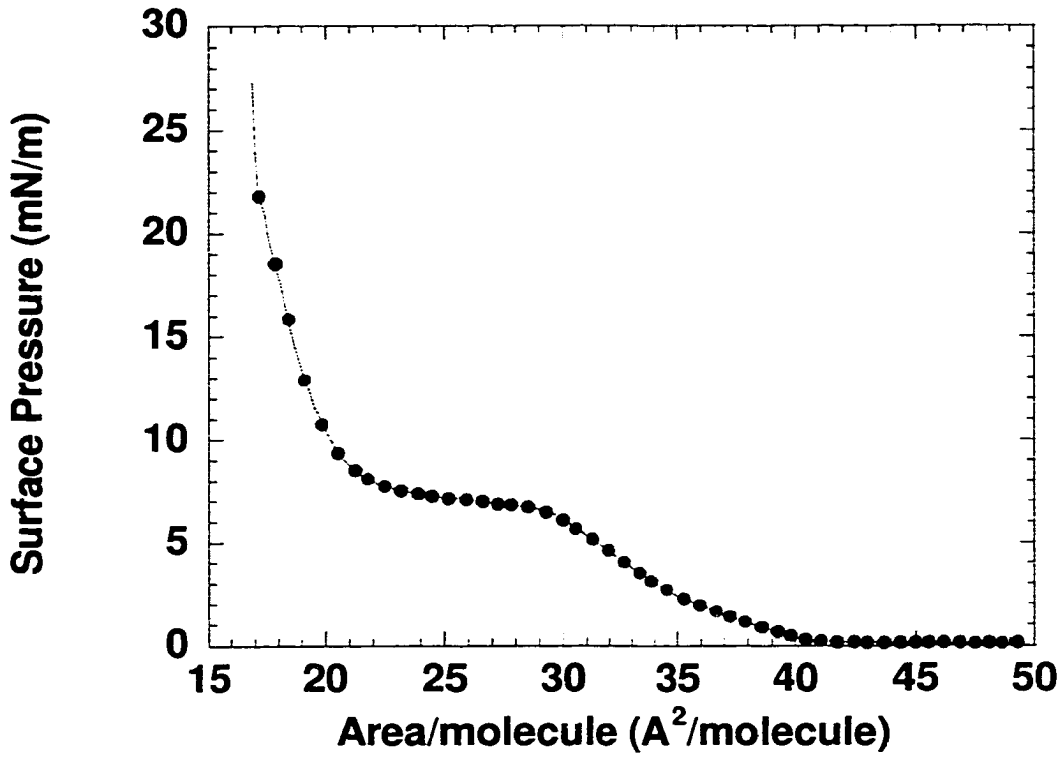

Fig. 2.6: Surface Pressure Isotherm For PDA on an Acidified Sub-Phase (pH=2) and at 25^0 C.

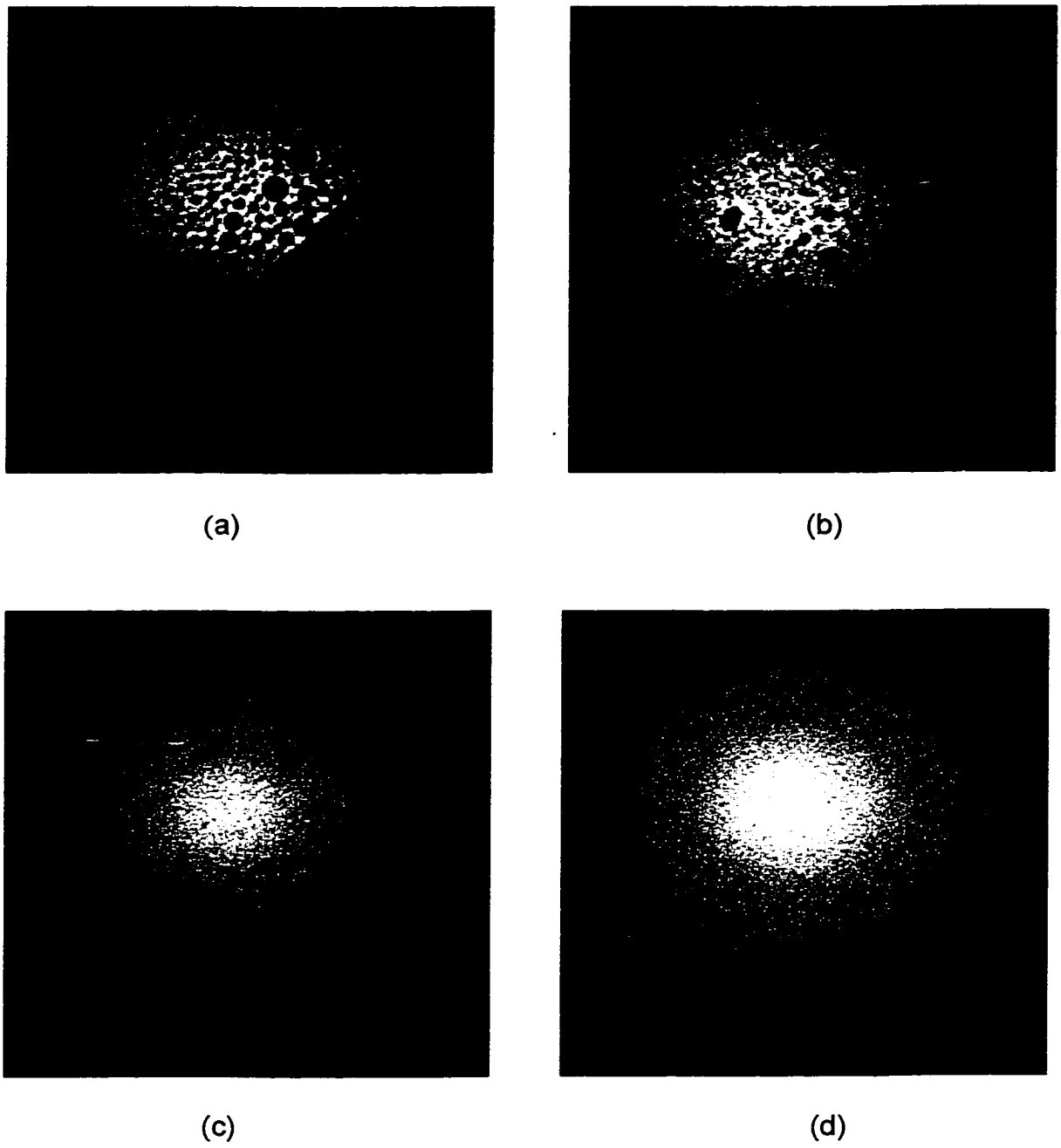

Fig. 2.7: Sequence of Fluorescence Images For PDA on an acidified sub-phase (pH=2) on the mini-Langmuir trough as the Surface Concentration is Increased by Compression to Determine Γ_{LE}^{c} (Fluorescence) and Compare it with Γ_{LE}^{c} From Surface Pressure Measurements to Verify that the Dye has no Effect on this Measurement: (a) 91Å^2/molecule (b) 76 Å^2/molecule (c) 66 Å^2/molecule and (d) 46 Å^2/molecule

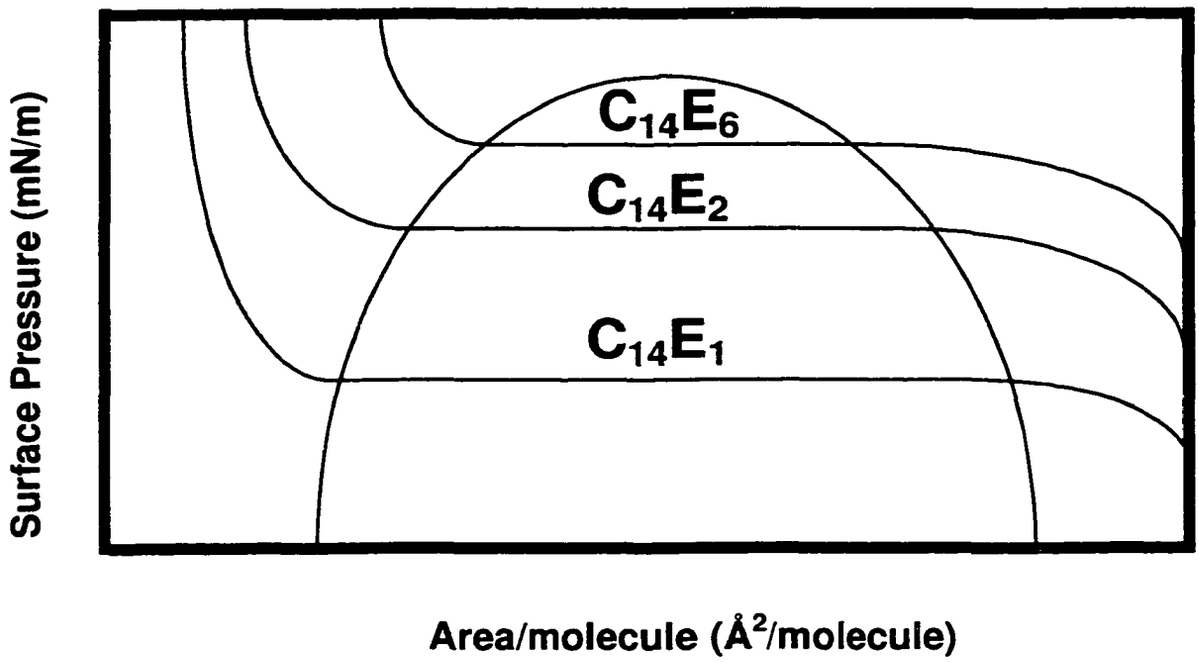

Fig. 2.8: Phase Envelope Demarcating the Two-Phase (G/LE) Coexistence Regime For the Homologous Series of Poly-(EthyleneOxide) Surfactants C_mE_n (m=14;n=1,2,6).

	$C_{14}E_1$	$C_{14}E_2$	$C_{14}E_6$
Γ^{-1} (Å^2/molecule)	130-150	190-210	235-250

Table 2.1: Inverse Surface Concentration Corresponding to the Density of the Nucleating Liquid-Expanded Phase For the Homologous Series of Poly-(EthyleneOxide) Surfactants C_mE_n (m=14;n=1,2,6).

References

1)Lin, S.-Y.; McKeigue, K.; Maldarelli, C. *Langmuir* **1991**, *7*, 1055-1066.

2)Motomura, K.; Matuura, R. *J. Coll. Int. Sci.* **1969**, *29*, 617-622.

3)Motomura, K.; Matuura, R. *J. Coll. Int. Sci.* **1969**, *29*, 623-628.

4)Aratono, M.; Uryu, S.; Hayami, Y.; Motomura, K.; Matuura, R. *J. Coll. Int. Sci.* **1983**, *93*, 162-168.

5)Aratono, M.; Uryu, S.; Hayami, Y.; Motomura, K.; Matuura, R. *J. Coll. Int. Sci.* **1984**, *98*, 33-38.

6)Lunkenheimer, K.; Serrien, G.; Joos, P. *J. Coll. Int. Sci.* **1990**, *134*, 407.

7)Berge, B.; Simon, A. J.; Libchaber, A. *Phys. Rev. A* **1990**, *41*, 6893-6900.

8)Hénon, S.; Meunier, J. *J. Chem. Phys.* **1993**, *98*, 9148-9154.

9)Pollard, M.; Pan, R.; Steiner, C.; Maldarelli, C. *Langmuir* **1998**, *14*, 7222-7234.

10)Pfohl, T.; Möhwald, H.; Riegler, H. *Langmuir* **1998**, *14*, 5285-5291.

11)Takiue, T.; Uemura, A.; Ikeda, N.; Motomura, K.; Aratono, M. *Journal of Physical Chemistry B* **1998**, *102*, 3724-3729.

12)Pallas, N. R.; Pethica, B. A. *J. Chem. Soc. Farad. Trans. I* **1987**, *83*, 585-590.

13)Moore, B. G.; Knobler, C. M.; Akamatsu, S.; Rondelez, F. *J. Phys. Chem.* **1990**, *94*, 4588-4595.

14)Winch, P. J.; Earnshaw, J. C. *J. Phys.: Condens. Matter* **1989**, *1*, 7187-7205.

15)Aveyard, R.; Carr, N.; Slezok, H. *Can. J. Chem.* **1985**, *63*, 2742-2746.

16)Kim, M. W.; Cannell, D. S. *Phys. Rev. A* **1976**, *14*, 1299-1300.

17)Lin, S.-Y.; McKeigue, K.; Maldarelli, C. *AIChE J.* **1990**, *36*, 1785-1795.

Chapter 3

The G/LE Phase Transition and its Effect on the Induction Period in Dynamic Tension Relaxation

3.1 Introduction

How the phase behavior of aqueous soluble surfactants studied in Chapter 2, affects interfacial processes such as tension reduction accompanying adsorption onto clean interfaces is extremely important in many industrial applications especially those which require a rapid and significant reduction in interfacial tension. For instance it has been shown by Rosen *et al.*[1] that the wetting out time for fabrics correlates with the reduction in dynamic surface tension at a time of one second i.e. t_{1s} and does not correlate with the equilibrium tension. It is clearly evident from the general plot of surface pressure vs surface concentration for insoluble surfactants (Fig. 1.1) that the phase aggregation of surfactant molecules strongly influences the tension (pressure). The gaseous state is highly compressible with little change in tension with surface concentration of surfactant, the liquid expanded phase is less compressible with larger changes in tension with surface concentration. The condensed states are highly incompressible with large changes in tension with minute variations in the surface concentration. Phase transitions are evident from the isotherm as plateaus for first order and kinks for higher order transitions. Soluble surfactants may undergo similar phase transitions as they adsorb from solution onto an interface and it is crucial to study its effect on dynamic tension reduction. For

instance does the G/LE transition manifest itself as a plateau or an induction period in tension reduction as was suggested and observed by Lin[2].

Aqueous soluble surfactants adsorb from solution onto freshly created surfaces where they lower the surface tension γ from the clean value γ_c. The surfactant transport which underlies and determines the rate of reduction in surface tension $\gamma(t)$ is now fairly well understood. When the surface is first created, surfactant in the sublayer adjacent to the surface kinetically adsorbs onto the surface, depleting the sublayer concentration (c_s). This initial kinetic step increases the surface concentration Γ from zero and reduces the tension γ from γ_c. The reduction in the sublayer concentration creates a diffusive flux of surfactant from the bulk to the surface to replenish the sublayer. The driving force for this flux is the difference between the bulk and sublayer concentration (i.e. $c_b - c_s$). As adsorption onto the surface proceeds, the surface concentration continues to increase and the tension decreases. With increasing surface concentration, the rate of desorption off of the surface begins to increase. This reduces the net adsorption to the surface, and the sublayer concentration eventually increases due to the diffusive flux. As desorption matches adsorption, equilibrium is achieved with the equilibrium-adsorbed amount (Γ_{eq}) and tension (γ_{eq}) a function of the bulk concentration c_b. The higher the bulk concentration, the greater is the diffusive flux to the interface and the more rapid is the reduction in tension.

Contrary to a monotonic tension reduction however, a characteristic dynamic tension relaxation curve (γ vs time) usually shows an initial induction or

shouldering behavior during which there is negligible decrease in surface tension before it finally starts falling rapidly. This induction period is more prominent in the relaxation of tension for low concentration solutions of surfactants, and in surfactants with long unbranched hydrophobic chains/small polar groups. However it is very much present in the dynamic relaxation in tension of a whole broad range of fairly aqueous soluble surfactants, from cationic and anionic surfactants to even surfactant mixtures. The induction period was first observed by Lucassen *et al.*[3,4] in the adsorption of hexadecyl dimethylamino propanesulfonate. It has also been noted in the observations of Hua and Rosen for Aerosol OT-100 and N-dodecyl-N-bezyl-N methylglycine[5], Joos *et al.*[6] for the lower chain alcohols(C_7-C_8) , Svitova[7] for HTAB and SDS, Zhang *et al.*[8] for an anionic/cationic mixture (C_8PyBr-C_{10}Sna), Lin *et al.*[2] for 1-decanol and by Gao and Rosen[9] for over 20 surfactant systems, spanning anionic, nonionic and zwitterionic surfactants.

No definitive explanation has been established for this induction period. Lin *et al.*[2] suggested two possible explanations. In the first, the initial period of constant tension is due to a gaseous/liquid phase transition in the monolayer that occurs during adsorption. By analogy with these medium chain length amphiphiles, Lin *et al.* expected that for bulk soluble amphiphiles with polar groups larger than hydroxyls or carboxylates, or with smaller chains (as for example decanol), the monolayer, although unable to condense into the LC and LS states, should exist in the G and LE phases. This hypothesis was based on

the existing cusp evidence for the existence of phase transitions among aqueous soluble surfactants.

How the G/LE phase transition gives rise to an induction period during adsorption onto an initially clean surface was explained by Lin *et al.* as follows (Fig. 3.1; see also Svitova[7]): Surfactant first adsorbs into the gaseous/dilute state (G) onto the interface causing a small drop in tension from the clean interface value. With the passage of time, the increased adsorption at a critical gaseous concentration (Γ_G^c) causes surface condensation leading to the nucleation of a liquid expanded (LE) state with surface concentration (Γ_{LE}^c) in equilibrium with the gaseous phase. In time, the liquid expanded state grows (at the density Γ_{LE}^c) at the expense of the gaseous state, leading to two phase equilibrium coexistence at the interface with the surface tension remaining constant and thereby creating the induction period. Finally when the monolayer is completely in the liquid expanded state, further adsorption causes a rapid decrease in tension. In the context of this model, the higher the bulk concentration, the greater the diffusive flux and the shorter the induction time required to completely fill the surface with the LE phase. At sufficiently high enough concentrations the induction period would not be evident at all, and the tension would appear to decrease monotonically as the observed tension reduction is for the LE state alone.

Lin *et al.* also detail a model to describe the surfactant transport when a phase transition takes place, and use this model to predict induction times for the example amphiphile decanol which (as we remarked in chapter 2) exhibits a cusp

in its γ-ln c_b curve. In this phase transition model, surfactant first diffuses and kinetically adsorbs into the gaseous state. Kinetic exchange was assumed to be rapid, so the sublayer and surface were in equilibrium and this was described by a Langmuir equation. Numerical solutions were obtained for the surface concentration as a function of time by solving the unsteady diffusion and surface/sublayer equilibrium equations (fluid convection was neglected). These solutions were continued until the (gaseous) surface concentration reached Γ_G^c. At this point, the liquid expanded phase emerges in equilibrium with the gaseous state and grows in co-existence with the surface concentrations in each phase remaining constant. Kinetic exchange between the LE phase and the sublayer is assumed to be rapid (and given by a separate Langmuir equation with different model constants from the gaseous phase). During co-existence, with the kinetic rates assumed rapid, the sublayer is in equilibrium with both surface phases, and therefore at the unique concentration (c_b^c) at which both phases exist on the surface. Numerical solutions for the diffusion rate to the surface with this stipulation on the sublayer concentration were obtained and continued until the amount of surfactant adsorbed on the surface equaled Γ_{LE}^c, at which point the surface is entirely in the LE phase. Further solutions for adsorption into the LE phase were obtained by solving the diffusion and surface/sublayer (LE) equilibrium conditions until equilibrium was reached. The model constants for the Langmuir adsorption isotherms and the state equations for each phase were obtained by modeling the (γ -ln c_b) data for decanol. By fitting only the diffusion coefficient, Lin *et al.* calculated induction periods that agreed well with

measurements for decanol using the pendant bubble technique in which surfactant adsorbs onto an impulsively formed pendant bubble, and the tension is measured by imaging the bubble shape.

The cusp evidence for a G/LE phase transition for bulk soluble surfactants from which Lin *et al.* inferred the phase transition model is suggestive but not conclusive evidence for this transition because of the difficulty in unambiguously distinguishing a cusp from the data. In the absence of definitive evidence, Lin *et al.* (see also Gao *et al.*) suggested alternatively a single phase model in which the induction period could be caused by chain cohesion alone, without the cohesion being strong enough to cause a phase transition. In this view, cohesion diminishes the reduction in tension normally accompanying the increase in concentration as surfactant adsorbs. This gives rise to the induction time in which the tension reduces slowly. As adsorption proceeds, and the surface concentration increases further, repulsive forces between the headgroups, which acts to increase the surface pressure and reduce the tension, begin to dominate over the cohesive forces. This accelerates the reduction in tension. Lin *et al.* undertook numerical calculations of the tension reduction using this single-phase model, again assuming sublayer/surface equilibrium. To account for the effect of cohesion on the tension, Frumkin adsorption in which the interaction is linear in the surface concentration was assumed. By modeling the equilibrium tension - bulk concentration data (γ -ln c_b) for decanol assuming Frumkin adsorption, the equation of state, and surface/sublayer equilibrium were obtained. Diffusion

limited calculations also agreed well with the measurements of the reduction in dynamic tension

Since Lin *et al.*'s publication, several recent studies on the phase behavior and dynamic tension of *slightly soluble* amphiphiles, suggest that a G/LE phase transition is the more likely explanation for the induction period observed in the reduction in dynamic tension for soluble surfactants. Recent studies have more conclusively shown that a first order phase transition during adsorption creates a plateau in dynamic tension reduction. Henon and Meunier studied the self-assembly of a film of hexadecanoic acid[10] at a pH of 6.5 (where the surfactant was sparingly soluble) onto an initially surfactant free interface in a static cell. Brewster angle microscopy (BAM) monitoring of the interface displayed bright domains in a mainly dark background. Further polarization analysis of the reflected light indicated tilt ordering among the domains, hence the transition was classified as G/LC. During adsorption, concomitant measurements of the tension were obtained with a Wilhelmy plate. The relative percentage of dark regions decreased with time at constant though near zero surface pressure indicating a first order phase transition from a dilute, low reflectivity gaseous state to the condensed state of higher reflectivity. The adsorbing surfactant is taken up mainly by the condensed state domains (causing no change in tension) at the expense of the gaseous state. This study was the first providing direct evidence of self-assembly from solution of an LC state from a gaseous state, and the induction period in dynamic tension which accompanies this phase transition. The transition is not G/LE because the long (16) chain of hexadecanoic acid

gives a condensation directly to the condensed state. In a recent article, Melzer *et al.*[11,12] presented a study on formation and growth kinetics of condensed phases in adsorbed films of the slightly soluble N-dodecyl-hydroxybutric acidamide (DHBAA) in a static cell. Their BAM observations demonstrated a transition from a LE to a LC state during adsorption, and simultaneous tension measurements indicated that during the transition the surface pressure was constant (although the plateau in tension lagged the appearance of the condensed phase). They also carried out dynamic adsorption studies for similar amphiphiles: N-Dodecyl-γ–hydroxy-butyric acidamide (DHBA), N-tetradecyl--γ–hydroxy-butyric acidamide (THBA) and N-(γ-hydroxypropyl) tridecanoic (and tetradecanoic) acid amide (HTRAA and HTEAA)[13,14] and found plateaus in surface pressure at intermediate times demonstrating transitions from liquid to condensed states. These authors did not study the phase behavior and induction period during initial adsorption where a G/LE phase transition may have occurred.

The study of Pollard *et al.*[15] provides more direct evidence that the initial induction period in dynamic tension reduction of soluble surfactants is due to a G/LE phase transition. These authors studied the poly (ethylene glycol) n-alkyl ether or poly ethylene-oxide $C_{14}E_1$ ($CH_3(CH_2)_{13}(OCH_2CH_2)_1$ OH) which is slightly soluble in water. The polar group is however large enough so that, as verified by fluorescence microscopy in their study, directly spread monolayers exist in G, LE and LC states rather than just G and LC states as was the case with hexadecanoic acid. To demonstrate the connection between the phase behavior

and the dynamic tension, Pollard *et al*[15] used an open channel flow cell in which surfactant adsorbed from a flowing solution onto an initially clean surface of the channel in which the fluorescing dye was previously spread. Illumination at the excitation wavelength allowed for the study of the evolution of the phases, and the positioning of a Wilhelmy plate into the surface allowed for the measurement of dynamic tension. During the initial adsorption the LE phase was found to nucleate in a gaseous background, and grow at nearly the constant tension of the clean surface. When the surface was completely occupied by the LE state, further adsorption caused a decrease in tension with the monolayer remaining in the LE state. At extended times nucleation of a liquid condensed stated was observed, accompanied by a second plateau in tension. Further in Chapter 2, it has been confirmed that the G/LE phase transition is not restricted to the insoluble and sparingly soluble surfactants. Fairly soluble surfactants also undergo this transition as was demonstrated for candidates such as $C_{14}E_4$ and $C_{14}E_6$. This is the most convincing evidence for the phase transition hypothesis.

In light of the dynamic tension/phase behavior studies of Henon and Meunier, Volhardt and coworkers, Pollard *et al.* using slightly soluble amphiphiles and the more convincing evidence obtained in Chapter 2 for truly soluble surfactants, the G/LE phase transition explanation for the induction period for soluble surfactants appears likely. The purpose of this chapter is to demonstrate the direct connection between the G/LE phase transition and the induction period for a soluble surfactant. We choose the poly-ethylene-oxide $C_{14}E_6$ ($CH_3(CH_2)_{13}(OCH_2CH_2)_6$ OH) as a model, fairly bulk soluble surfactant. We

choose this surfactant because of its availability in relatively high purity (relative non-polydispersity), solubility and because its tension relaxation process displays long induction times which we intend to analyze. As was done by Pollard *et al.*, we use fluorescence microscopy to image the monolayer phase behavior and the Wilhelmy plate technique to measure the tension as surfactant adsorbs onto the air/water surface of a solution flowing in an open channel. For purposes of modeling, we also measure dynamic tensions in the static pendant bubble configuration in which surfactant adsorbs onto a bubble. In Sec. 3.2 we provide details of these techniques. In Sec. 3.3 we detail fluorescence results establishing conclusively that for this soluble surfactant the induction period is caused by the G/LE phase transition. In Sec. 3.4, we first present (in 3.4.1) a model for the induction period which accounts for kinetic exchange as well as diffusion, and thereby generalizes the model of Lin *et al.* To use this model to predict tension reductions we need the equation of state, diffusion coefficient and kinetic coefficients. In separate Appendices (A and B), we determine an accurate empirical equation by using the pendant bubble as a Langmuir trough, and the kinetic coefficients and the bulk diffusion constant by undertaking dynamic tension experiments at high bulk concentration where the induction period is not evident and the adsorption is to a single (LE) phase. Using these coefficients and the density of the LE state at nucleation, we present simulations (3.4.2) of the induction period and subsequent rapid tension reduction with no adjustable constants, and demonstrate very good agreement with tension relaxation measurements and induction periods using the pendant bubble technique. Finally

in Sec 3.5. we present a simple analysis to predict induction times in a diffusion-limited case and 3.6 gives the conclusions of the research.

3.2 Experimental

Materials: The polyethoxylated surfactants ($C_{14}E_6$=$CH_3(CH_2)_{13}(OCH_2CH_2)_6OH$), >98% purity, was obtained from Nikko Chemicals, Japan. For fluorescence studies, a fluorophore NBD-HDA (4-(hexadecylamino)-7-nitrobenz-2-oxa-1,3-diazole) supplied by Molecular Probes, OR was used. All chemicals were used as received without any further purification. The sub-phase in all experiments was deionized water purified by a Milli-Q filter system fitted with an Organex-Q column to remove trace contaminants (Millipore, MA). The resistivity of the deionized water was at least 15-MΩ cm.

Fluorescence Experiments: Here only in-situ adsorption experiments were carried out with the simultaneous surface tension measurements, to study the effect of a G/LE phase transition on the dynamic tension reduction accompanying surfactant adsorption. In these experiments, a flow cell was initially filled with deionized water and its surface was aspirated thoroughly. After viewing the interface under the microscope to ensure that it was contaminant and dust free, an insoluble dye NBD-HDA was deposited from a chloroform solution in an expanded state at a surface concentration of 10000 $Å^2$/molecule, so that the dye was in a gaseous state and appeared completely dark. The surfactant solution flow was then started with the inlet under the interface. The surfactant was allowed to adsorb onto the interface which was continuously monitored using the camera, and images were digitized at periodic intervals of time. In certain

experiments the surface tension was continually monitored using a Wilhelmy plate electrobalance. This technique is described in the measurement of surface pressure section.

Dynamic Surface Tension Measurements: Pendant bubble tensiometry is now a well established and accurate technique for measuring and modeling dynamic surfactant transport to interfaces. The details of this method are given elsewhere[16]. In brief this procedure consists of quickly forming a pendant bubble at the tip of an inverted needle immersed in surfactant solution of known concentration. As surfactant adsorbs onto the interface the shape of the bubble, which is a balance between surface tension and gravitational forces, changes. The profile of the silhouette of the bubble is digitized at periodic intervals of time. The shape of the bubble at any time is governed by the static Young-Laplace equation that relates the pressure drop across the interface to the two radii of curvature. The digitized images are then subjected to an optimization program in which the theoretical Young-Laplace shape is compared to the experimentally determined profile to determine the surface tension. In this study only dilute solutions were used and there was significant depletion of the surfactant from the bulk solution at the cuvette air-water interface, and hence equilibration at this interface was allowed before proceeding with the experiment. In each experiment, a small air bubble (V~15 μl) was formed at the end of a teflon tube passing through an inverted needle. The shape change was monitored until equilibrium between the bulk and the interface was established, and then the dynamic tension relaxation was established. Initial values were always close to

the clean air-water tension of 72 mN/m. Since dilute solutions were used these experiments typically ran for upto an hour.

Wilhelmy Plate Electrobalance for Surface Tension Measurements: The Wilhelmy Plate technique is among the oldest and most conventional method to measure surface tension. As opposed to the differential principle of the Langmuir trough, this relies on the absolute measurement of the force on a plate immersed in water. The calibration of the balance is carried out on a set of weights, giving a calibration plot of the weight (force) vs the voltage. The Wilhelmy plate is of known dimensions and as is described below, the surface tension can be inferred from the voltage measured by the balance. The forces acting on the plate are gravity, surface tension and buoyancy and hence a simple force balance yields the following expression:

$$F = \rho_p g l w t - \rho_l g h w t + 2\gamma\,(t + w)\cos\theta \qquad [3.1]$$

Here l is the total length and h the immersed length. The usual procedure involves using a completely wetted plate (θ=0, $\cos\theta$=1) and using a very thin plate (t<<w) and in addition neglecting buoyancy effects ($\rho_p >> \rho_l$ and h<<l). In this case the equation simplifies to

$$F = \rho_p g l w t + 2\gamma\,(w) \qquad [3.2]$$

So a change in tension is measured by a change in force on the plate, which in turn is converted to a voltage, from which the tension change can be inferred using the calibration plot. Mathematically

$$\Delta\gamma = \frac{\Delta F\,(or\,\Delta V)}{2(w)} \qquad [3.3]$$

The plate is usually of flame blasted platinum to ensure complete wetting. In our case we used a KSV electrobalance (KSV Ltd., Helsinki, Finland). This apparatus was used to concomitantly measure the surface tension during the adsorption fluorescence experiments.

3.3 Fluorescence Results

The fluorescence results presented in Fig. 3.3(a)[I-VI] are those for clean interface adsorption of $C_{14}E_6$ onto the open channel surface. With just the dye present on the otherwise initially clean interface, there is no fluorescence and it appears completely dark. Immediately after the flow was started the evolution of large bright LE pockets with round dark (gaseous) domains in a mainly dark background was evident. On continuation of the flow, the LE regions increased at the expense of the dark gaseous regions until the background went from dark to bright, with dark domains now existing in the bright background. With the continued adsorption of surfactant, the monolayer turned completely bright as the monolayer was in the LE state. Note that during the sequence (I)-(VI), the flow was stopped intermittently to capture the images. This experiment therefore provides direct visual evidence of the self-assembly of films of $C_{14}E_6$ into a LE state through a G/LE phase transition. Fig. 3.3 (b) shows the trace of the surface tension with time during the adsorption fluorescence experiment. It is clear that adsorption through the G/LE phase transition takes place at a tension close to the clean interface value. Also once the monolayer is in a completely liquid

expanded state (uniformly bright 3.3 (a)[VI]), the tension does indeed drop. The only drawback of this experiment is that the surface concentration at any time is unknown, and it is therefore not possible to determine the surface concentration of the LE state in equilibrium with the gaseous state (Γ_{LE}^{c}). However as described in Chapter 2 we had determined this value by resorting to rapid compression on a Langmuir trough which was monitored by fluorescence. In Chapter 2 we obtained a value of 235-250 $Å^2$/molecule for Γ_{LE}^{c} for $C_{14}E_6$.

3.4 Model of the Surfactant Mass Transfer, Simulations of Induction Periods and Comparisons with Experiments

The fluorescence evidence verifies visually the hypothesis that the induction time in the dynamic tension relaxation is due to a gaseous to liquid expanded phase transition and measures directly a value for Γ_{LE}^{c}. In order to predict induction times, a surfactant transport model should be constructed and solved. As mentioned in the Introduction, Lin *et al.*[2] developed a diffusion limited transport model which we extend here (3.4.1) to include kinetic effects and compare to measured induction times (3.4.2).

3.4.1 Surfactant Transport Model

In the phase transition model for the induction, there are three regimes of surfactant transport: In the first, which extends from the time of creation of the clean interface, surfactant adsorbs into a gaseous state. The density as a function of time is denoted as $\Gamma_G(t)$. We use the Arrhenius rate law equation to provide a general description of the kinetic adsorption into this state:

$$\frac{d\Gamma_G}{dt} = \beta_G c_s(t) e^{-E_{A(G)}(\Gamma_G(t))/RT} - \alpha_G \Gamma_G(t) e^{-E_{D(G)}(\Gamma_G(t))/RT} \quad [3.4]$$

In the above, β_G and α_G are the kinetic coefficients for adsorption and desorption, respectively, RT is the thermal energy and $E_{A(G)}$ and $E_{D(G)}$ are, respectively, the activation energies for adsorption and desorption in the gaseous phase and are a function of the surface concentration in that phase (i.e. Γ_G). When the concentration in the gaseous state reaches a critical value, a liquid phase nucleates and begins to grow with additional adsorption. This is the second regime. We assume that when the two phases are present in this regime, they are in thermodynamic equilibrium on the surface, i.e. the concentrations of the phases are the values during equilibrium coexistence Γ_G^c and Γ_{LE}^c. Finally when the surface is completely covered with the LE state, we enter the third and final regime of adsorption into the liquid expanded state. For this state, kinetic adsorption is described by

$$\frac{d\Gamma_{LE}}{dt} = \beta_{LE} c_s(t) e^{-E_{A(LE)}(\Gamma_{LE}(t))/RT} - \alpha_{LE} \Gamma_{LE}(t) e^{-E_{D(LE)}(\Gamma_{LE}(t))/RT} \quad [3.5]$$

where the subscript LE references the liquid expanded phase.

To make further progress, explicit equations are necessary for the activation energies in each of the phases. The simplest approach is to posit a mechanistic model for the activation energy for adsorption. The desorption barrier then follows from equilibrium considerations as we discuss below. Consider adsorption into a single phase. In a picture first described by MacRitchie[17], molecules adsorb into a monolayer with surface concentration Γ by

sweeping an area ΔA clean of surfactant. The contribution to the activation energy for adsorption is the work done against the surface pressure to form this clean area, or $\pi(\Gamma)\Delta A$. In addition to this contribution, as pointed out by Joos and coworkers[18], at zero coverage, there is a contribution arising from the energy required to disrupt the surface water molecules as surfactant adsorbs onto the clean (or cleared) surface (less the entropic "hydrophobic" energy gained by removing the surfactant hydrophobe from the bulk). This contribution, independent of the coverage is denoted by $E_A(0)$ so that the activation energy for adsorption is taken to be

$$E_A(\Gamma)=E_A(0)+\pi(\Gamma)\Delta A \qquad [3.6]$$

We note that this decomposition is valid for either the G or LE phases. We assume further that the area swept out is the same for both phases, and can be taken as the limiting area (i.e. the surface concentration at the CMC). Since the contributions to the activation energies at zero coverage are independent of the phase, $E_A(0)$ is the same and we may use (3.6) for both phases.

To formulate kinetic equations for the second regime in which the two phases are in equilibrium, we assume that the adsorption rate constants into both phases are the same ($\beta_G = \beta_{LE} = \beta'$). The bulk is in equilibrium with the two surface phases at a concentration c_b^c. This concentration can be obtained by equating either eq. (3.4) (for the gaseous phase) or eq. (3.5) (for the LE phase) to zero. Thus:

$$c_b^c = \frac{\alpha_G}{\beta'}\Gamma_G^c e^{-(E_{D(G)}(\Gamma_G^c)-E_{A(G)}(\Gamma_G^c))/RT} = \frac{\alpha_{LE}}{\beta'}\Gamma_{LE}^c e^{-(E_{D(LE)}(\Gamma_{LE}^c)-E_{A(LE)}(\Gamma_{LE}^c))/RT} \qquad [3.7]$$

At co-existence, the surface pressure is equal in both phases and from (3.6):

$$\alpha_{LE}\Gamma_{LE}^{c}e^{-E_{D(LE)}(\Gamma_{LE}^{c})/RT} = \alpha_{G}\Gamma_{G}^{c}e^{-E_{D(G)}(\Gamma_{G}^{c})/RT} \qquad [3.8]$$

From (3.8) and the equality of the adsorption rates it is clear that when the two phases coexist, the kinetic exchange rates are equal into both phases and the rate can be represented by a single equation, which we choose to be the LE equation as Γ_{LE}^{c} has already been determined independently from fluorescence experiments. Thus

$$\frac{d\Gamma^{*}}{dt} = \beta c_s(t)e^{-\pi_c\Delta A/RT} - \alpha_{LE}\Gamma_{LE}^{c}e^{-E_D(\Gamma_{LE}^{c})/RT} \qquad [3.9]$$

where $\beta=\beta'\exp(-E_A(0)/RT)$, $\pi_c= \pi(\Gamma_{LE}^{c})= \pi(\Gamma_{G}^{c})$ and Γ^{*} is $x_{LE}\Gamma_{LE}^{c}+ x_G\Gamma_G^{c}$ where x denotes the area fraction of the G or LE phase.

In principle, our simulation starts at zero gaseous surface concentration ($\Gamma_G(t=0)=0$)) and uniform bulk concentration. For comparison to our pendant bubble dynamic tensions, we obtain simulations for a spherical geometry with radius b ($=10^{-3}$ m). At time t=0, the bulk concentration is uniform; the surface concentration can be expressed in terms of the sublayer concentration $c_s(t)$ by the Ward and Tordai equation (extended here to spherical geometry[16]):

$$\Gamma(t) = \frac{D}{b}[c_0 t - \int_0^t c_s(\tau)d\tau] + 2(\frac{D}{\pi})^{1/2}[c_0\sqrt{t} - \int_0^{\sqrt{t}} c_s(t-\tau)d\sqrt{\tau}] \qquad [3.10]$$

where D is the bulk diffusion coefficient. Eq. (3.10) (with Γ replaced by Γ_G) along with the kinetic adsorption eq. (3.4) are solved to obtain $\Gamma_G(t)$ until Γ_G reaches Γ_G^{C}. During co-existence, the Ward and Tordai expression (with Γ replaced by

Γ^*) along with eq. (3.9) is solved until the area average surface coverage Γ^* reaches $\Gamma_{LE}{}^c$. Finally for later times the Ward and Tordai expression (with Γ replaced by Γ_{LE}) along with eq. (3.5) is solved to obtain $\Gamma_{LE}(t)$. Lastly, dynamic tensions follow from the equations of state for the two phases.

3.4.2 Comparison of the Phase Transition Model Simulation and Experimental Dynamic Tension Data

In this section, we use the phase transition model to simulate dynamic tension reduction, and compare these simulations to experiments using $C_{14}E_6$. To carry out such a comparison, we need kinetic rate constants, activation energies and the equation of state for this surfactant for the two phases and the bulk diffusion coefficient. For the LE phase, the equation of state can accurately be measured by using the pendant bubble as a Langmuir trough. These measurements are given in Appendix A. The state equation is modeled using an empirical correlation rather than either the Langmuir or Frumkin equations of state because the correlation demonstrates the best agreement with the data. From the correlation, a numerical representation of the activation energy for desorption as a function of the surface coverage is obtained. To obtain the kinetic constants for the LE phase, we undertake (see Appendix B) measurements of the dynamic tension reduction for adsorption onto a clean interface at high bulk concentrations for which the induction period is negligible. By varying β and D, we fit these relaxations to solutions of eqs. (3.5) and (3.10) with $\Gamma_{LE}(0)=0$, thus ignoring the gaseous region and the two phase coexistence.

With regard to the parameters of the gaseous state, we have stated (Sec. 2.3) that the density of the gaseous state at the nucleation of the LE state (Γ_G^c) was not determined during the fluorescence experiments. However monolayers expanded to inverse surface concentrations of 2000 Å^2/molecule were clearly still in two-phase coexistence, suggesting that $1/\Gamma_G^c$ > 2000 Å^2/molecule. If we assume a lower bound for $1/\Gamma_G^c$ of 2000 Å^2/molecule, we can estimate the time for nucleation of the LE state assuming diffusion control by using the Ward and Tordai expression (eq. (3.10)) and neglecting the integral terms which are negligible in this approximation. Thus $\Gamma_G(t) \approx 2c_b(Dt/\pi)^{1/2}$ and the time to reach $1//\Gamma_G^c$ is equal to $\frac{\pi\Gamma_G^{c^2}}{4Dc_b^2}$ or 5s at the lowest bulk concentration (even shorter time if we include terms due to spherical geometry) and for $1/\Gamma_G^c$ = 2000 Å^2/molecule and D=6*10^{-10} m^2/sec (the value obtained in Appendix B). As we will see below, induction times at the lowest concentration are of the order of 500s so the time required to nucleate the LE phase is a negligible part of the induction time. Consequently in our modeling, we can ignore the initial adsorption into the gaseous state and directly proceed to adsorption into the two-phase coexistence region. As we discussed above, to describe adsorption into the two-phase region, we only require the kinetic expression of the LE state (see (3.9)). Our actual simulation starts with $\Gamma^* = 0$ and $\gamma = \gamma(\Gamma_{LE}^c)$ (known from the LE equation of state) and proceeds as was mentioned in the previous section with the simultaneous solution of eqs (3.9) and (3.10) to determine the surface concentration Γ^* as a function of time until it reaches the value Γ_{LE}^c with the surface tension being kept

constant at the value $\gamma=\gamma$ (Γ_{LE}^{c}). Once this value of the coverage is attained the simulation further proceeds with the simultaneous solution of eqs. (3.5) and (3.10) for the surface concentration and the corresponding tension reduction given by the absolute equation of state for the LE phase.

In principle the tension relaxations recorded with the Wilhelmy plate in the open channel flow can be simulated by solving the phase transition adsorption equations together with the convective diffusion equation. However because the flow in these experiments was intermittent and therefore difficult to model, we focus on modeling the simpler, static adsorption of surfactant onto a impulsively formed pendant bubble, with the tension measured by shape analysis (see Fig. 3.4). Dynamic tension relaxation profiles for a range of apparent concentrations, varying from $8.37*10^{-4}$-$8.37*10^{-3}$ mol/m^3 $C_{14}E_6$ [1] solutions were measured. The profiles at low concentrations (see Fig. 3.5) in this range show a prominent induction period in tension relaxation, the induction time for this range of concentrations varying from 50-500 s. The higher the concentration, the faster was the relaxation, the shorter and less visible was the induction time and the lower was the equilibrium tension as expected.

The theoretical simulations and experimental data are shown for the dynamic relaxation at four different concentrations (Figs. 3.6-3.9: $8.77*10^{-4}$ mol/m^3, $1.25*10^{-3}$ mol/m^3, $1.88*10^{-3}$ mol/m^3 and $2.65*10^{-3}$ mol/m^3). The agreement at all concentrations is very good, and given the fact that there are no

[1] The CMC for $C_{14}E_6$ is $9.19*10^{-3}$ mol/m^3

fitted parameters in these simulations, supports the phase transition model we have constructed.

3.5 A Simple Analysis Based on a Diffusion Limited Interpretation

It has already been demonstrated that the induction times predicted by the complete model accounting for both diffusion and kinetics match the experimental data very well. Here we develop a simple, analytical, diffusion limited expression for the induction time, and by comparing to the exact kinetic-diffusive model simulations, check the range of bulk concentrations for which the diffusion limited model is valid. Previous studies have demonstrated that the dynamic tension relaxation process shifts from diffusive to mixed kinetic-diffusive control, as the bulk concentration is increased [19-21]. To verify this for our system, simulations using the kinetic parameters obtained earlier and the phase transition model were carried out for low ($8.77*10^{-4}$ mol/m^3) and moderate ($2.65*10^{-3}$ mol/m^3) bulk concentrations, for a diffusion controlled as well as mixed kinetic-diffusive control case. The diffusion-controlled simulation is obtained in the following way. Again, the adsorption into the gaseous region is neglected, and the simulation begins with the beginning of the two-phase coexistence. During the coexistence, the sublayer concentration is a constant, and equal to c_b^c ($=1.2785*10^{-6}$ mol/m^3) as given by eq. 3.7. The Ward and Tordai expression is then used directly to calculate $\Gamma^*(t)$ until $\Gamma^*(t)$ reaches Γ_{LE}^c. This is the end of the induction period. For longer times, the Ward and Tordai expression is solved with the equilibrium condition to obtain $\Gamma_{LE}(t)$. The results are shown in Fig. 3.10 (for the lowest concentration that an induction period was measured) and Fig. 3.11

(for the highest concentration an induction period was measured). It is clear that at the low concentrations the process is diffusion controlled, and the mixed curve deviates further from the diffusion controlled curve as the concentration is increased. But, the deviation is not dramatically large even for the highest concentration for which we measured an induction period (i.e. $2.65*10^{-3}$ mol/m^3, see Fig. 3.11) and therefore a diffusion-limited interpretation is certainly justified.

For the diffusion-limited case, an analytical expression can be derived for the induction period. We note in this case, during the induction period the sublayer concentration in constant and equal to c_b^c. From eq. 3.10, we then obtain the induction period by setting $c_s(t)= c_b^c$.

$$\Gamma(t) = (c_b - c_b^c)[2 * \sqrt{\frac{Dt}{\pi}} + \frac{D}{b}t] \qquad [3.11]$$

For all bulk concentrations whose induction times were measured, $c_b^c << c_b$, so

$$\Gamma_{LE}^c = \text{const} = 2c_b\sqrt{\frac{Dt_{ind}(c_0)}{\pi}} + \frac{D}{b}c_b t_{ind} \qquad [3.12]$$

To see if this simple formulation is sufficient to predict induction times when compared to the calculations based on the complete model, we solve eq. (3.12) using the fluorescence value of Γ_{LE}^c to predict the induction time at a given bulk concentration. We also know the corresponding value using the diffusive kinetic phase transition model. Plotted in Fig. 3.12 is the difference between these two predictions normalized by the diffusive-kinetic model prediction and expressed as a percentage, against the bulk concentration. From Fig. 3.12 it is clear that that only

at the relatively larger concentrations is there any deviation between the predicted induction times of both cases (and is only 6% for the highest concentration for which the simulations were compared with experimental data). So for this case the simple diffusion limited expression is sufficient to estimate the induction time; however, for more aqueous bulk soluble surfactants (higher CMC's), the concentrations considered will be much higher and so the framework established for the complete model is necessary to predict induction times in those cases.

3.6 Conclusions

The shoulder period in the reduction in surface tension as surfactant adsorbs from aqueous solution onto an initially clean surface has long been observed, especially at low bulk concentrations. In this chapter, utilizing the n-alkyl poly (ethylene glycol) ether surfactant $C_{14}E_6$ as a model aqueous soluble surfactant, we have used fluorescence microscopy on the surface of an open channel flow, together with simultaneous measurements of dynamic tension, to provide conclusive evidence that this shoulder behavior is caused by a gaseous (G) to liquid expanded (LE) phase transition. Investigation of the phase behavior of $C_{14}E_6$ was undertaken by rapid compression of spread monolayers of this amphiphile on a Langmuir mini-trough in Chapter 2. These experiments confirmed that the amphiphile at low density exists in a gaseous state, then undergoes a G/LE first order phase transition, and finally exists in a LE state. The density of the LE phase in equilibrium with the G phase (Γ_{LE}^{c}) was measured to be 235-250 A^2/molecule. This G/LE phase transition is of course common in medium (12-16) hydrocarbon chain insoluble alcohols and carboxylic acids,

whose structures this ethoxylate resembles. This fact, taken together with the widespread observation of the occurrence of induction periods, indicates that the G/LE phase transition is common to many aqueous soluble surfactants.

A surfactant transport model was also developed to model the adsorption onto a clean interface when a phase transition occurs. In this model, surfactant first diffuses and kinetically adsorbs onto the surface in a gaseous state, and then onto a surface in which both G and LE phases co-exist in equilibrium (with constant surface concentrations (Γ_{LE}^{c} and Γ_{G}^{c})). The kinetic exchange into either the G or LE phases was modeled by Arrhenius equations, and bulk diffusion was described (in the absence of convection) by the Ward and Tordai expression. We showed that the time the monolayer exists in the initial, purely gaseous state, was very short compared to the induction time when the two phases co-exist, and was therefore neglected. When surfactant adsorbs onto the surface with co-existing phases, we assumed that the kinetic adsorption rates into both phases were identical, and we showed that the desorption rates were equal. One kinetic expression can therefore be used to describe kinetic exchange to the co-existing monolayer. We used the LE phase kinetic Arrhenius equation whose constants (along with the bulk diffusion coefficient) we measured separately by modeling dynamic tension relaxations at high bulk concentrations where no induction period exists. The kinetic-diffusive adsorption persists until the surface concentration becomes everywhere Γ_{LE}^{c} (as measured by the mini-trough compression experiments), at which point the induction period ends. The equation of state in the LE phase is measured separately by using the pendant

bubble technique as a Langmuir trough, and from this state equation we are able to simulate the tension relaxation accompanying the surfactant adsorption. We compare our simulations to induction periods in tension relaxation as measured for clean interface adsorption of surfactant on the surface of a pendant bubble, and we found good agreement with no adjustable constants. We also compared our kinetic diffusive simulations to diffusion controlled simulations (i.e. the circumstance where the sublayer and surface are in equilibrium), and we found that the kinetic effect is only marginally influential at the higher concentrations where the induction time is the shortest. We developed a simple, approximate, analytical expression for the induction time for the diffusion limited case, $\Gamma_{LE}^{c} = 2c_b(Dt_{ind}/\pi)^{1/2}+(D/b)c_bt_{ind}$, and we demonstrated that this relation predicts very well the induction period. Hence independent measurements of Γ_{LE}^{c} from fluorescence provides a technique for exactly quantifying, in particular, how the induction time depends on the bulk concentration.

APPENDIX A

Measurement of the LE Phase Equation of State and Adsorption Isotherm for $C_{14}E_6$

Literature measurements of the equation of state for soluble surfactants usually treat the monolayer as existing in one phase, disregarding any distinction between gaseous and liquid expanded phases. In the usual indirect approach to measure the state equation for this one phase, $\gamma(c_b)$ is first measured. An Arrhenius rate equation (as eq. (3.4) or (3.5)) is assumed for the kinetic adsorption, and set equal to zero to obtain the adsorption isotherm ($\Gamma(c_b)$). The activation energy difference (E_A-E_D) appearing in the Arrhenius equation is in general dependent on the surface coverage, and this dependence accounts for interactions between the adsorbed molecules. In the Langmuir scheme, the activation energies are assumed to be independent of surface concentration and in the Frumkin scheme they are assumed to be linear in Γ. Integrating the Gibbs - Duhem equation along with the adsorption isotherm then yields an equation of state ($\gamma(\Gamma)$) and the dependence of the tension on the bulk concentration ($\gamma(c_b)$). The relation for $\gamma(c_b)$) is compared to the data to obtain the model constants with usually fairly good agreement, and the equation of state then follows. In light of the discussions in this paper, the equation of state which is determined in this way is for the LE phase, since the measured tensions from which the state equation is constructed are several mN/m below the clean tension value.

Recently the pendant bubble technique has been used as a Langmuir trough to measure directly the tension as a function of the surface concentration

for the soluble surfactant $C_{12}E_6$[21-23]. These studies showed that the direct measurements do not match the predictions of the Langmuir equation of state which was obtained indirectly from $\gamma(c_b)$ data as outlined above. Although the predictions of the Frumkin equation of state (also obtained indirectly) provided a better match to the direct measurements, the agreement was not uniform over the entire surface concentration range. As explained by Pan *et al.*, the origin of this discrepancy is the fact that as the monolayer density increases from Γ_{LE}^{C}, the nature of the interactions between the adsorbed molecules changes from cohesive to repulsive, and this change is not accounted for at all in the Langmuir description (which assumes no interaction between the molecules), and cannot be modeled as linear in the surface concentration as in the Frumkin equation. These comparisons also point to the fact that the indirect approach of determining the equation of state $\gamma(\Gamma)$ by fitting $\gamma(c_b)$ data is not necessarily accurate because equations which can fit the $\gamma(c_b)$ data do not, when there are a limited number of points, necessarily fit the slope of the data which is the surface concentration.

In this study, to formulate accurately the equation of state of the LE phase, without recourse to Langmuir or Frumkin equations, we use a different approach that is described in detail in a separate paper[24] and outlined briefly here. As we have already described in 3.4.1, the dependence of the activation energy for adsorption on the surface concentration is formulated as the work required to create a hole in the monolayer (eq. (3.6)). Instead of formulating an equation for the activation energy for desorption, we obtain the functional

dependence numerically from the available data and thereby describe accurately the monolayer interactions. We begin by measuring the tension as a function of the relative surface concentration as Pan *et al.*: A pendant bubble is formed at the tip of an inverted needle in a surfactant solution of reasonably low concentration and allowed to come to equilibrium. The bubble is then either rapidly expanded and then compressed (or shrunk and then expanded); to minimize exchange with the bulk, the expansion/contraction or contraction/expansion cycle was undertaken in less than 10 to 15 seconds. During the area change, the image is digitized and the tension $\gamma(t)$ as a function of the pendant bubble area $A(t)$ is obtained. If the amount of surfactant on the surface is conserved, then the surface concentration at some time t during the area change can be written as $A(t)\Gamma(t) = \nu$, where ν is a constant. For a single experiment, this constant can be written in terms of a reference surface concentration and the area at that concentration which are both achieved during the area change. Assuming the tension is a unique function of the surface concentration (no surface relaxation effects), we choose for a reference surface concentration the value when the tension is 65×10^{-3} N/m (each area change experiment is designed to pass through this tension). This reference tension is achieved at a certain area ($A(\gamma=65\times10^{-3}\text{N/m})$), and thus $\Gamma(t)/\ \Gamma(\gamma=65\times10^{-3}\ \text{N/m}) = A(\gamma=65\times10^{-3}\ \text{N/m})/A(t)$. We plot the tension during the area change as a function of $A\ (\gamma=65\times10^{-3}\ \text{N/m})/A(t) = \Gamma(t)/\Gamma(\gamma=65\times10^{-3}\ \text{N/m})$. For a given bulk concentration, the experiment was repeated several times, obtaining the tension as a function of $\Gamma(t)/\ \Gamma(\gamma=65\times10^{-3}\ \text{N/m})$. Finally the process was repeated at different bulk

concentrations, and the data of the tension as a function of $\Gamma(t)/\Gamma(\gamma=65x10^{-3}$ N/m) for all experiments at a particular concentration, and for all concentrations, was plotted on the same graph (Fig. 3.A1). If the amount of surfactant is conserved during the area change, and the tension is a unique function of the surface concentration, then the data for all the experiments should correlate to a single line which is the surface equation of state (referenced to a particular surface concentration). The assemblage of data does in fact correlate to one line verifying our assumptions. Note that most of the data is for $\Gamma/\Gamma(\gamma=65$ mN/m)>0.5 which is exclusively in the LE phase.

The equation of state data in Fig.3.A1 is fit to a correlation whose form is suggested by Pan[23].

$$\gamma = \gamma_c - q_1 \ln(1+\frac{e^{q_3 x}-1}{q_2}) \qquad [3.A1]$$

where $x= \Gamma/\Gamma(\gamma=65$ mN/m). This is an empirical equation whose form is chosen to enable one to write the surface concentration as an explicit function of the tension, as will be needed later. Furthermore, as is evident in Fig. 3.A1, this correlating form fits the experimental data extremely well through the entire surface concentration range. The parameter values obtained were q_1= 5.6991, q_2=31.962 and q_3=4.447. Expressing Γ as a function of γ from (A1), we have

$$\Gamma = \frac{\Gamma(\gamma = 65mN/m)}{q_3}\ln(1+q_2(e^{\frac{\gamma_c-\gamma}{q_1}}-1)) \qquad [3.A2]$$

At this point $\Gamma(\gamma=65$ mN/m) is still unknown and we substitute the above equation into the Gibbs equation to yield

$$d\gamma = -\frac{\Gamma(\gamma = 65mN/m)}{q_3}\ln(1+q_2(e^{\frac{\gamma_c-\gamma}{q_1}}-1))RTd\ln c_b \qquad [3.A3]$$

With the q1, q2, q3 known, a numerical solution of the above using the Runge-Kutta scheme is calculated and fitted to the experimental surface tension/bulk concentration data to optimize for $\Gamma(\gamma=65$ mN/m) (see Fig. 3.A2). To start the Runge-Kutta iteration a Henry's law type form is assumed for the surface concentration vs the bulk concentration i.e. $\Gamma=kc$ and $\gamma_c-\gamma= kcRT^2$. The value of $\Gamma(\gamma=65$ mN/m) obtained by this technique is $1.33*10^{-6}$ mol/m^2 which is in very good agreement with the value of $1.36*10^{-6}$ mol/m^2 obtained directly from compression of spread monolayers on a Langmuir trough by Pollard[15]. The results of the fitting procedure for the corrected along with the experimental data are shown in Fig. 3.A2.

---

[2] We also simultaneously have to make a correction for the bulk concentration as the adsorption at the cuvette air-water interface can cause significant depletion of the bulk surfactant concentration[21] and hence the actual concentration in the bulk is lower than the apparent solution concentration. The appropriate correction to the bulk concentration is

$$c_{BULK} = c_{APP} - \frac{A_{Cuvette}}{V_{Cuvette}}\Gamma(\gamma_{eq})$$

where Γ is the surface excess corresponding to each equilibrium tension value γ_{eq} and this correction is embedded in the fitting procedure. Thus each of the apparent concentrations was corrected appropriately, the correction at worst being 6% for the lowest concentration.

Using the value of $\Gamma(\gamma=65$ mN/m) and the correlation, we now know the surface tension vs absolute surface concentration. In particular, the tension at the LE end of the phase transition (Γ_{LE}^{c}) is 71.37 mN/m, using the value of 240 $Å^2$ /molecule as was obtained by fluorescence. As expected, this is close to the clean interface value. From the integration of (A3), we also now know numerically $\gamma(c_b)$; from the correlation and the numerical values of $\gamma(c_b)$ we obtain numerically the adsorption isotherm Γ_{LE} (c_b). Using the fluorescence value of 240 $Å^2$ /molecule for Γ_{LE}^{c}, the critical concentration c_b^c for which G and LE phases are in equilibrium is found from the adsorption isotherm to be $1.28*10^{-6}$ mol/m^3. Finally, from the isotherm, the dependence of the activation energy for desorption as a function of the coverage follows from the Arrhenius expression at equilibrium, i.e

$$\frac{c_b}{\Gamma_{LE}} = \frac{\alpha_{LE}}{\beta}\exp\left(\frac{\pi\Delta A - E_{D(LE)}(\Gamma_{LE})}{RT}\right) \qquad [3.A4]$$

Having determined the adsorption isotherm for $C_{14}E_6$, we can now provide a quantitative justification of the assumption of negligible desorption into the bulk of spread surfactant in the mini-trough compression experiments to measure Γ_{LE}^{c}. In the trough experiments, G and LE phases are in equilibrium. To estimate the maximum amount of desorption, we assume that the subphase reaches equilibrium with the surface at a concentration which at co-existence is equal to c_b^c or $1.28*10^{-6}$ mol/m^3. Therefore the amount lost to the sub-phase assuming we start the compression at Γ^{-1}=1000 $Å^2$/molecule, is simply $(Vc_b/\Gamma_{initial}A)$, which for a V/A ratio of $3*10^{-3}$ m is 0.022. Hence the assumption of negligible desorption into the bulk is justified.

As a final observation, we note that for $C_{14}E_6$, there is no obvious cusp in the surface tension-bulk concentration equilibrium data (Fig. 3.A2) at low concentration which would be suggestive of the G/LE phase transition, while for the alcohols octanol and decanol, as mentioned in the introduction, a cusp is more discernible. This may be attributed to the fact that the Γ_{LE}^{c}'s for the alcohols, because of their smaller head group, are larger than that for $C_{14}E_6$, and therefore the slope change at the bulk concentration of the phase co-existence (c_b^c) is greater for the alcohols. This would make the cusp more noticeable. In general, these cusps are experimentally nearly inaccessible because the bulk concentration at which the slope change occurs is relatively low, and usually below the range for which accurate solution concentrations can be prepared.

APPENDIX B

Determination of the Kinetic Rate Constants for the LE Phase by Fitting Relaxations in Tension as Surfactant Adsorbs onto a Clean Interface

In Appendix A, the equation of state and adsorption isotherm for $C_{14}E_6$ was obtained, and a ratio of the kinetic adsorption to desorption (including the activation energy) rate constants was determined numerically as a function of the surface concentration. To determine the rate constants themselves, the conventional technique of matching simulations to measurements of the reduction in tension as surfactant adsorbs onto a clean interface is employed. Dynamic tensions were measured by the pendant bubble technique at higher concentrations than were used for the measurement of induction periods in Sec. 3.4.2, but still less than the CMC. The concentrations used were $8.27*10^{-3}$ mol/m^3, $6.62*10^{-3}$ mol/m^3, $5.60*10^{-3}$ mol/m^3, and $3.74*10^{-3}$ mol/m^3; and the tension relaxations are given in Figs. 3.B1-3.B4. At these higher bulk concentrations, the adsorption rates are faster and induction times as evident in B1 are minimal. We therefore avoid fitting data with a long induction period, and restrict ourselves to fitting experimental measurements of the LE phase and its kinetic parameters. Furthermore the relaxation at the higher concentrations is mixed diffusive-kinetic[19-21] allowing accurate determination of rate constants. We could also fit data of an experiment in which a bubble at equilibrium is suddenly compressed and its tension re-equilibration monitored with time[21] which would avoid the co-existence region entirely.

To model the theoretical tension relaxation, eq. (3.10) has to be solved simultaneously with the kinetic adsorption step for the LE phase alone (eq. (3.5)) to determine the sublayer as well as surface concentration with time. For this, the activation energy for adsorption as mentioned earlier is assumed to be of the form $E_A(\Gamma)= E_A(0)+\pi(\Gamma)\Delta A$, where π is the surface pressure corresponding to a surface concentration in the LE phase and ΔA the limiting area/ molecule at the CMC (found to be 50.3 $Å^2$/molecule for $C_{14}E_6$ from the numerically determined adsorption isotherm, see Appendix A). Assuming a value of β, we know the value of $\alpha_{LE}\exp(-E_{D(LE)}(\Gamma_{LE})/RT)$ for the LE phase as a function of surface concentration and therefore we can carry out the simulation to predict the surface concentration with time. We then use the empirical relation to determine the tension against time (even if the adsorbed amount corresponds to a surface concentration in the two-phase region) and fit the experimental data of tension relaxations at high concentrations. We optimize for the assumed value of β and linearly interpolate the data for the alpha term in between surface concentration grid points. The best-fit value of β is $1.25*10^{-4}$ m/s and the fits are shown in Figs. 3.B1-3.B4. The diffusion coefficient obtained is $6*10^{-10}$ m^2/s which is in excellent agreement with that obtained by Pan [21] for $C_{12}E_6$ and Lin[20] for $C_{12}E_8$.

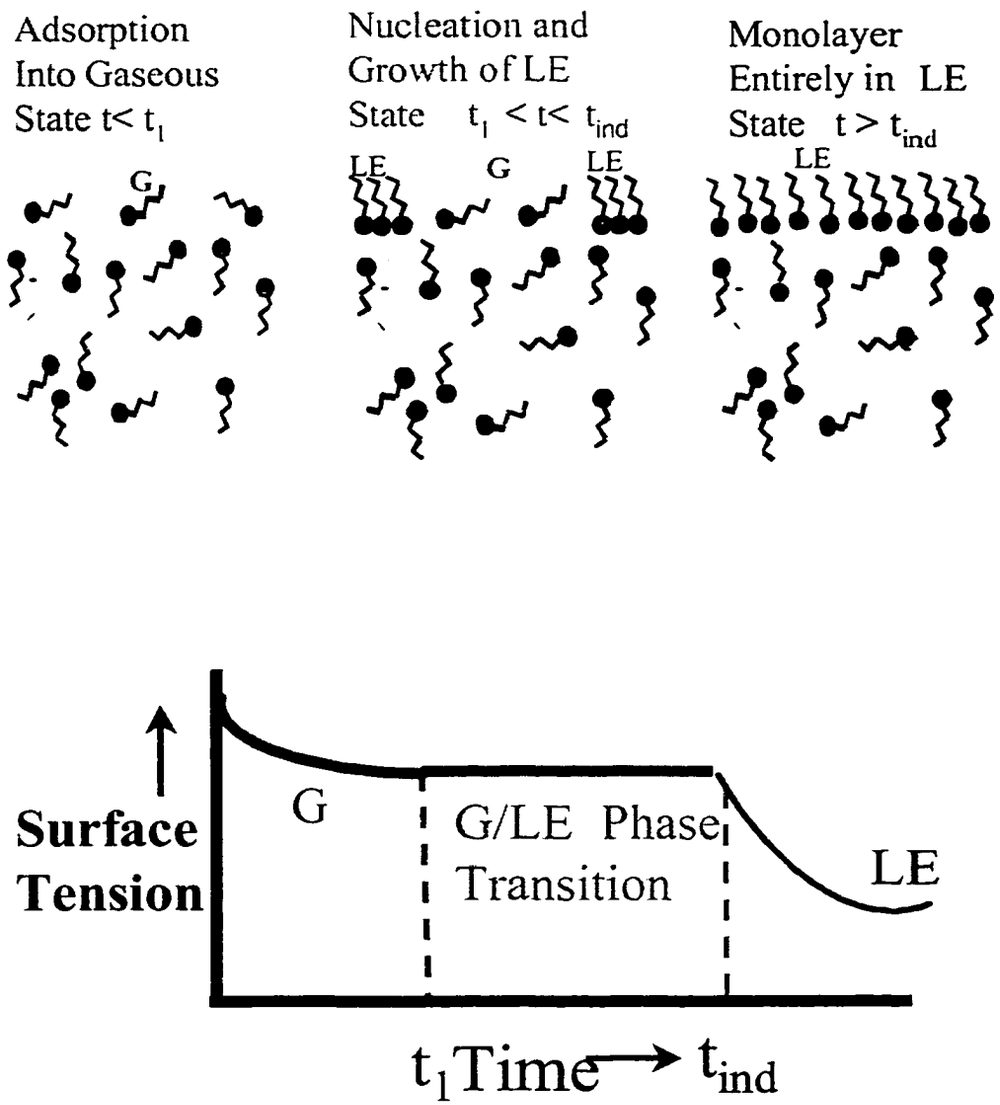

Fig. 3.1: Schematic of Adsorption and Accompanying Surface Tension Reduction through a G/LE Phase Transition.

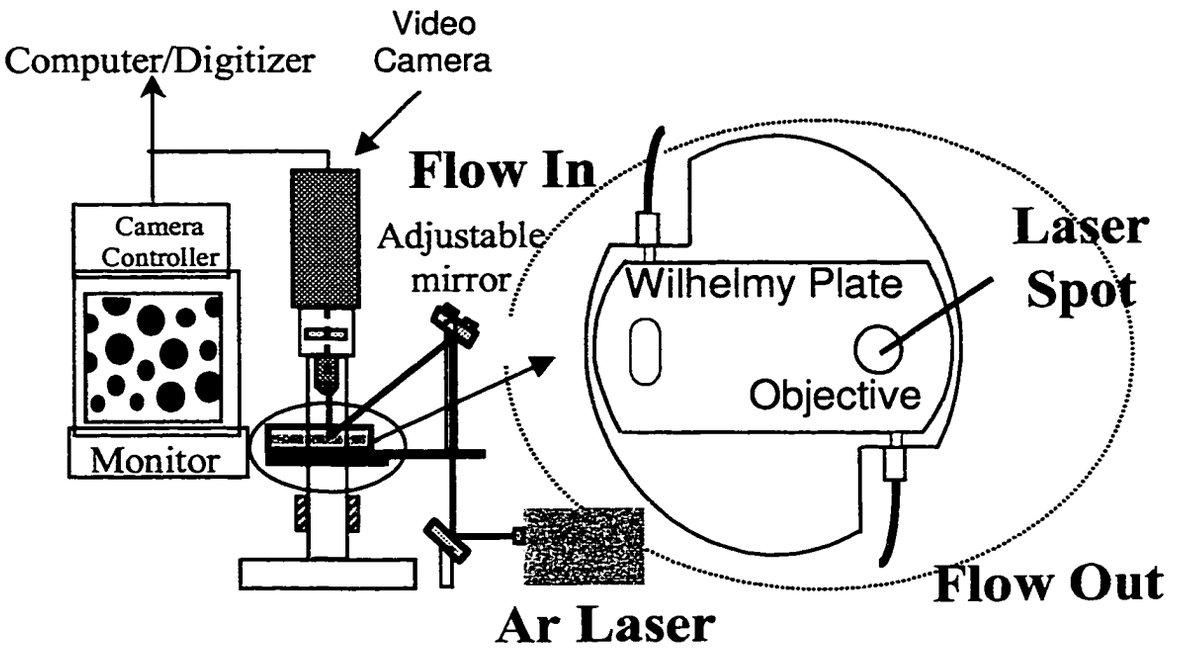

Fig. 3.2: Schematic of the Fluorescence Microscopy Apparatus For the In-Situ Flow-Adsorption Experiments.

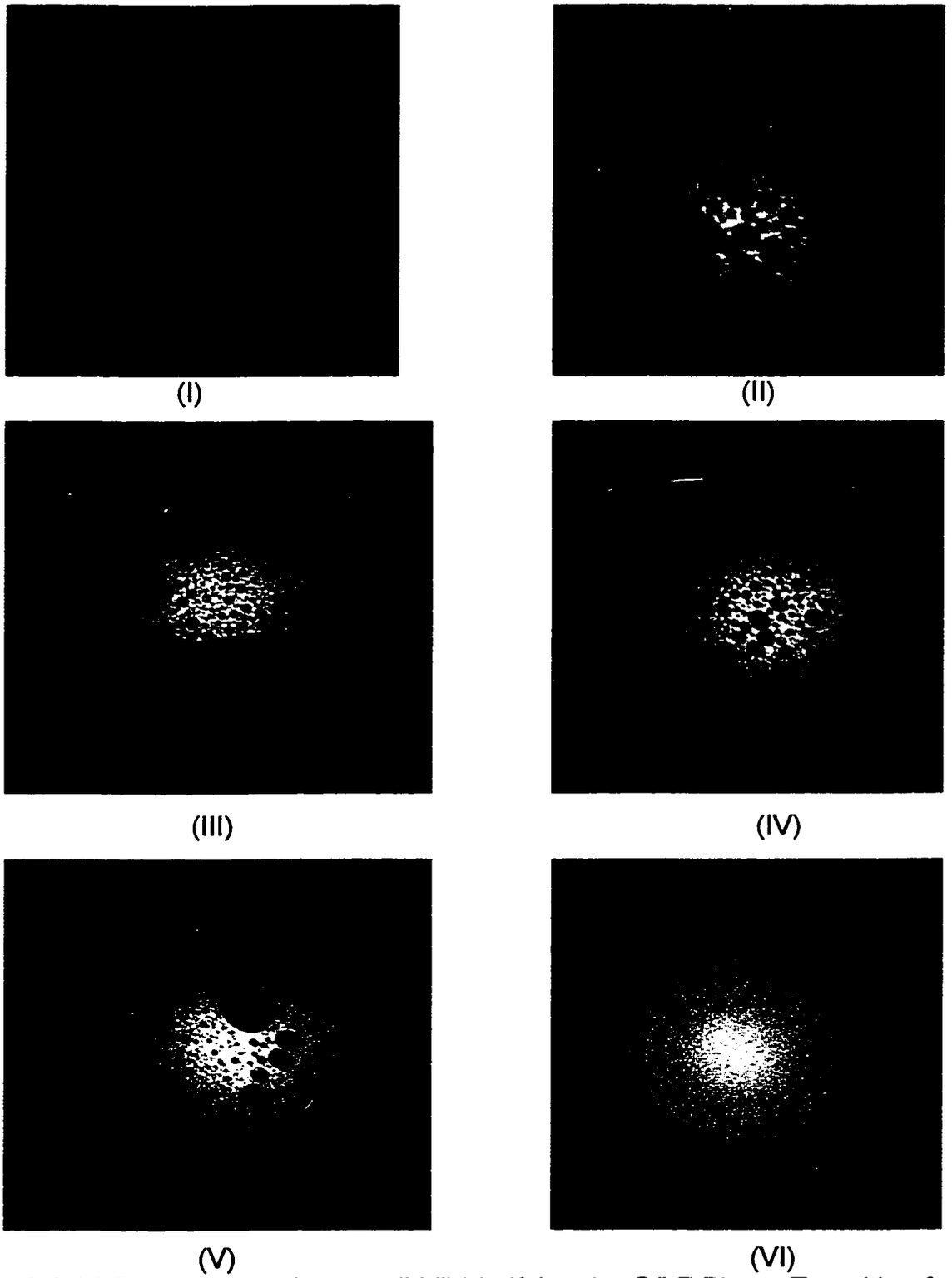

Fig. 3.3 (a) Fluorescence images (I-VI) Verifying the G/LE Phase Transition for $C_{14}E_6$ During Clean Interface Adsorption.

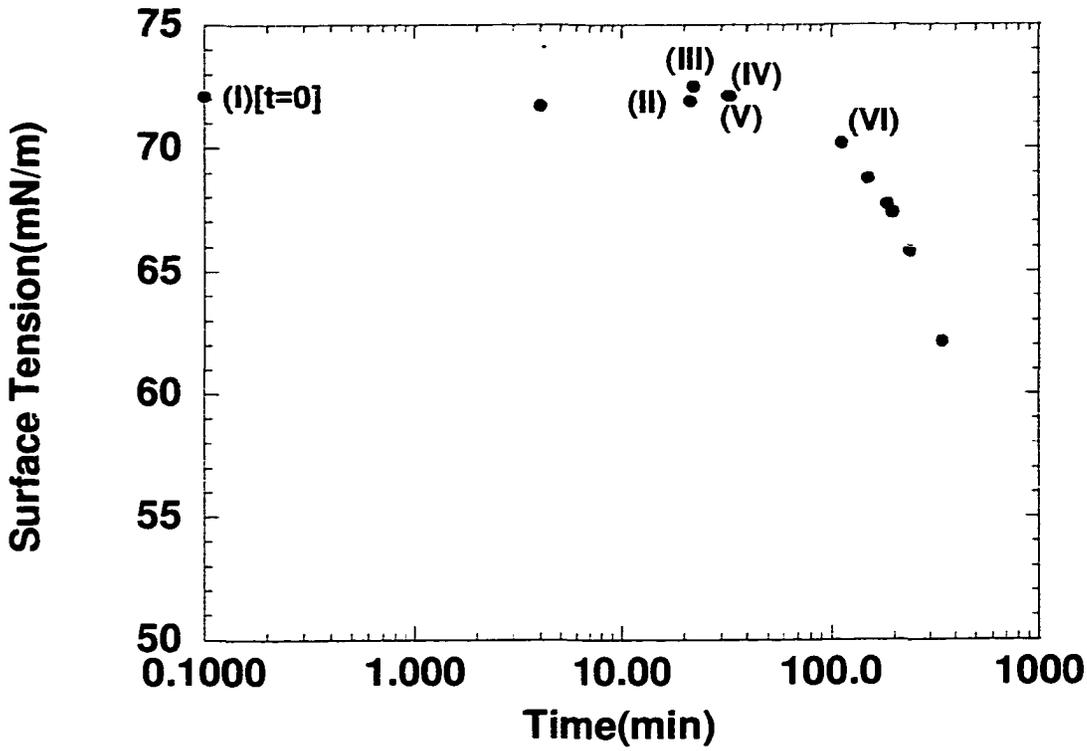

Fig. 3.3 (b): Trace of the Surface Tension During the Adsorption Process.

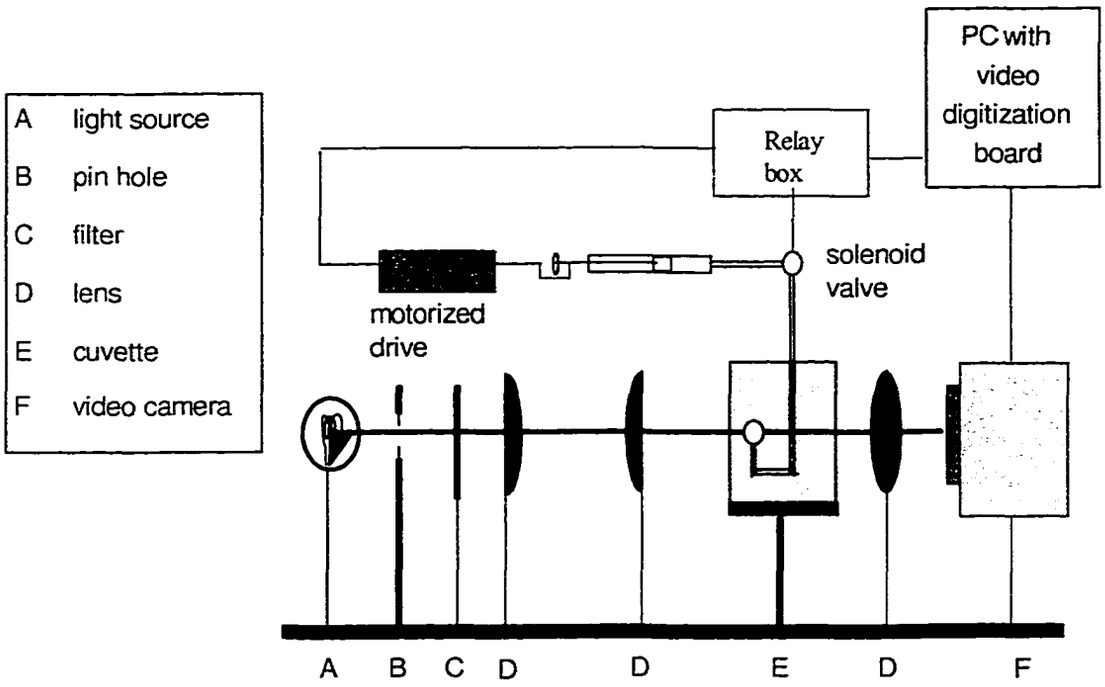

Fig. 3.4: Schematic of the Pendant Bubble Apparatus.

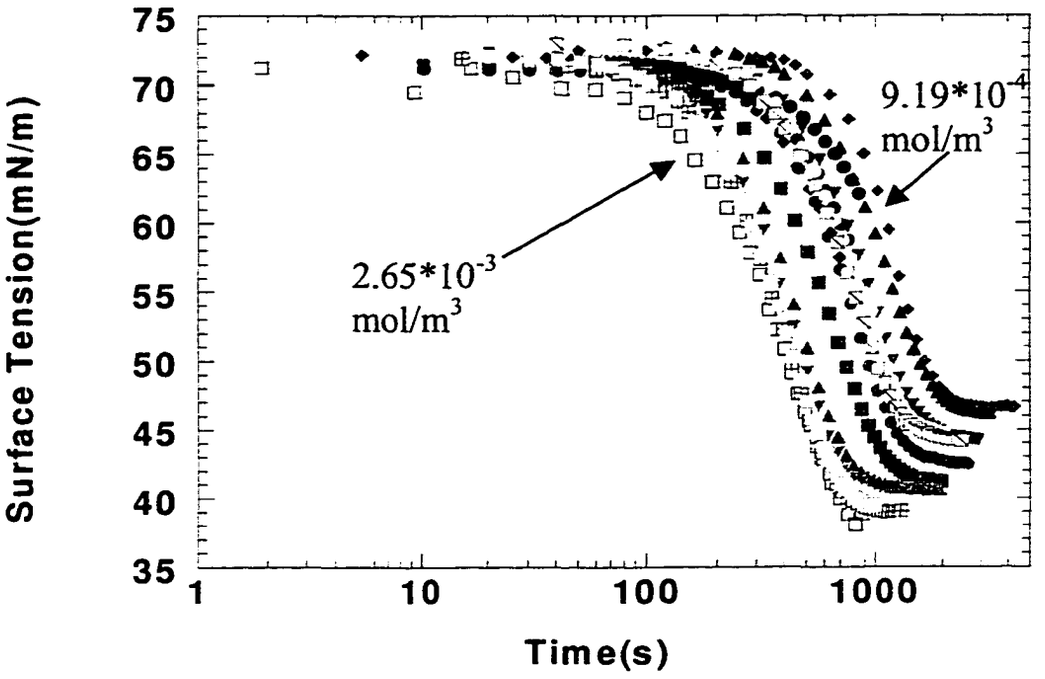

Fig. 3.5: Representative Dynamic Surface Tension Relaxations for $C_{14}E_6$ at Relatively Low Concentration Displaying an Induction Period in Tension Reduction.

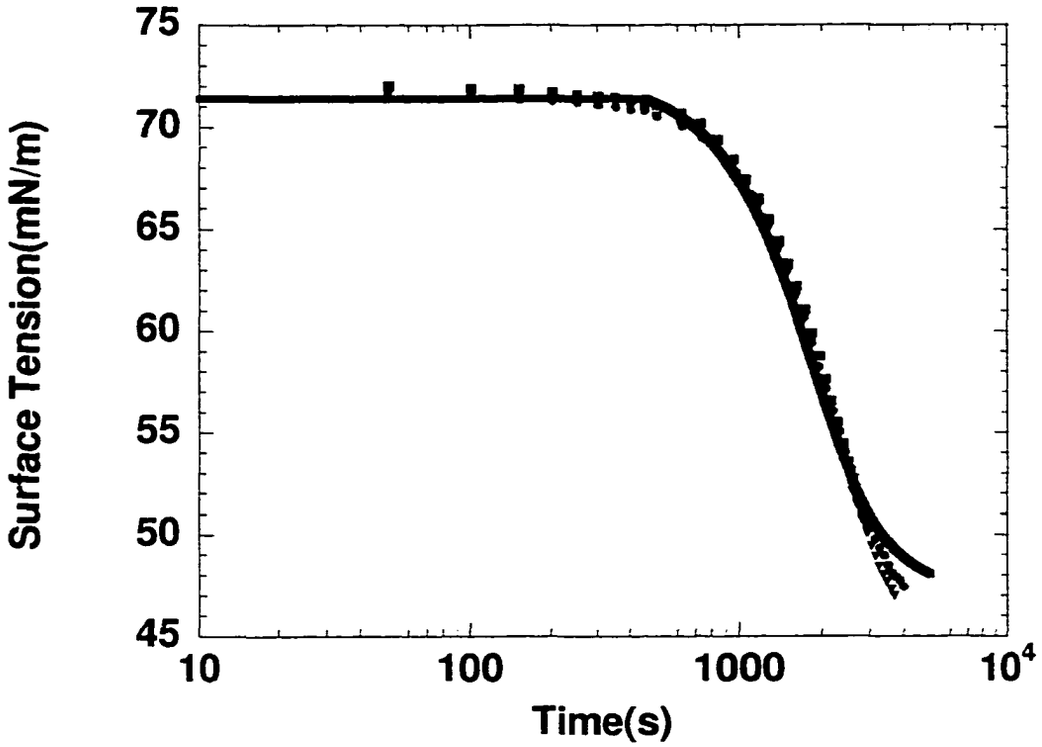

Fig. 3.6: Dynamic Surface Tension Relaxation For $C_{14}E_6$ at a Bulk Concentration of $8.77*10^{-4}$ mol/m^3 and the Fit Using the Kinetic-Diffusive Phase Transition Model.

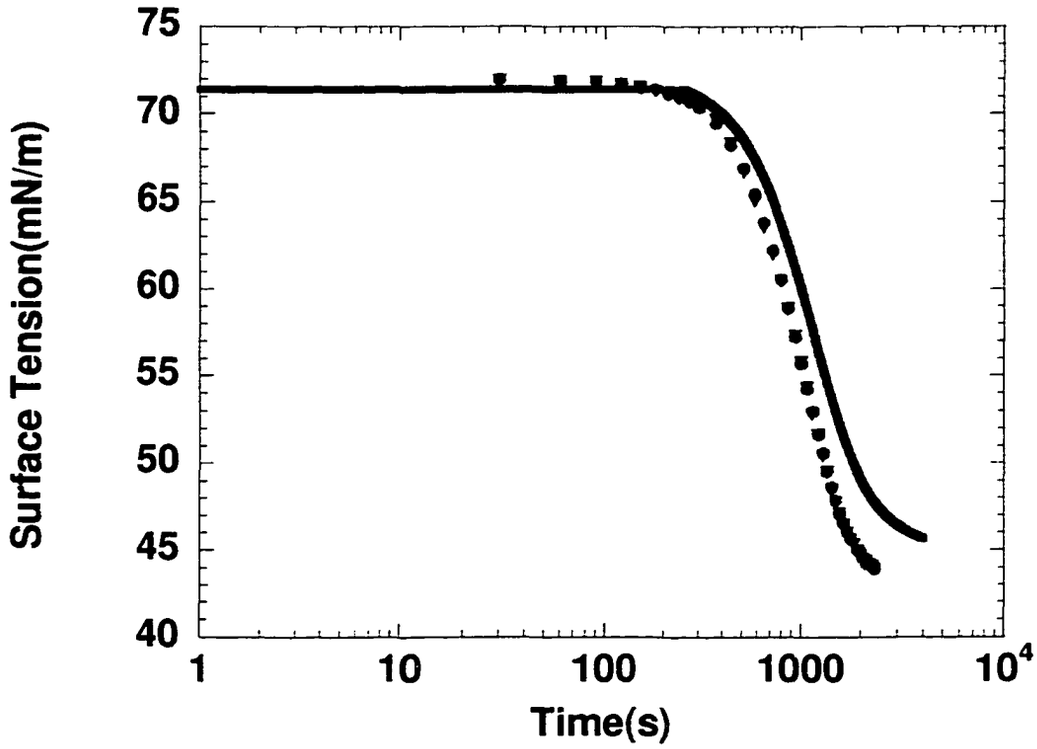

Fig. 3.7: Dynamic Surface Tension Relaxation For $C_{14}E_6$ at a Bulk Concentration of $1.25*10^{-3}$ mol/m^3 and the Fit Using the Kinetic-Diffusive Phase Transition Model.

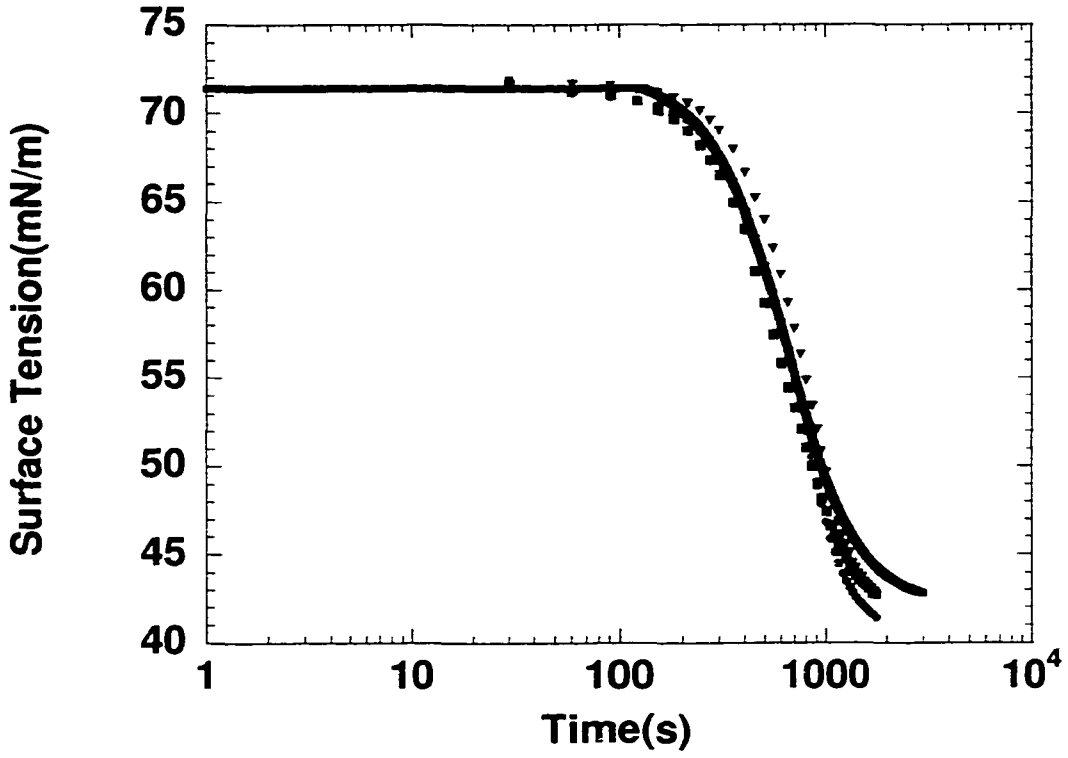

Fig. 3.8: Dynamic Surface Tension Relaxation For $C_{14}E_6$ at a Bulk Concentration of $1.88*10^{-3}$ mol/m^3 and the Fit Using the Kinetic-Diffusive Phase Transition Model.

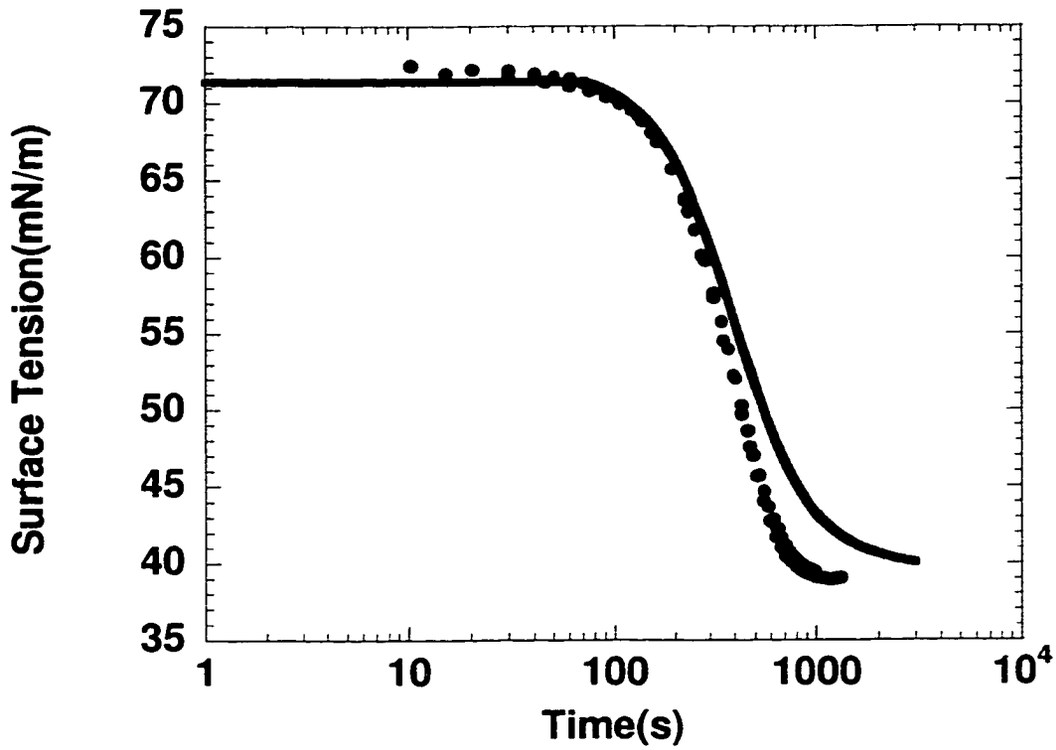

Fig. 3.9: Dynamic Surface Tension Relaxation For $C_{14}E_6$ at a Bulk Concentration of $2.65*10^{-3}$ mol/m^3 and the Fit Using the Kinetic-Diffusive Phase Transition Model.

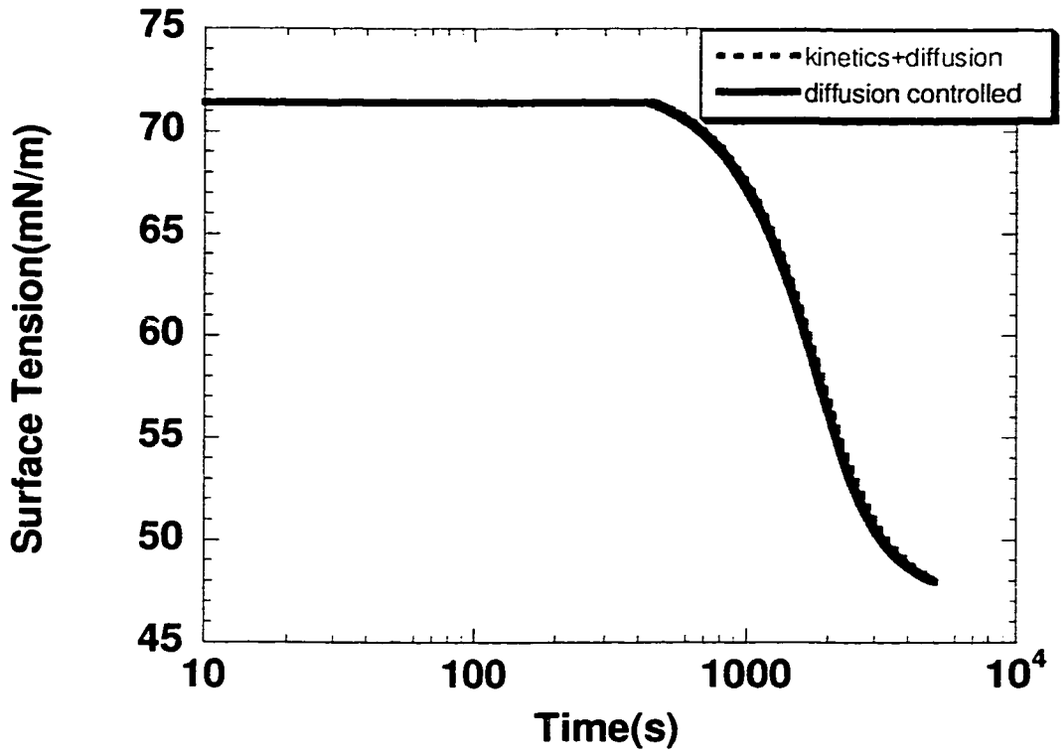

Fig. 3.10: Plot of Dynamic Tension Reduction Using the Phase Transition Model For the Diffusion Controlled and Mixed Diffusive-Kinetic Cases at a Bulk Concentration of $8.77*10^{-4}$ mol/m^3.

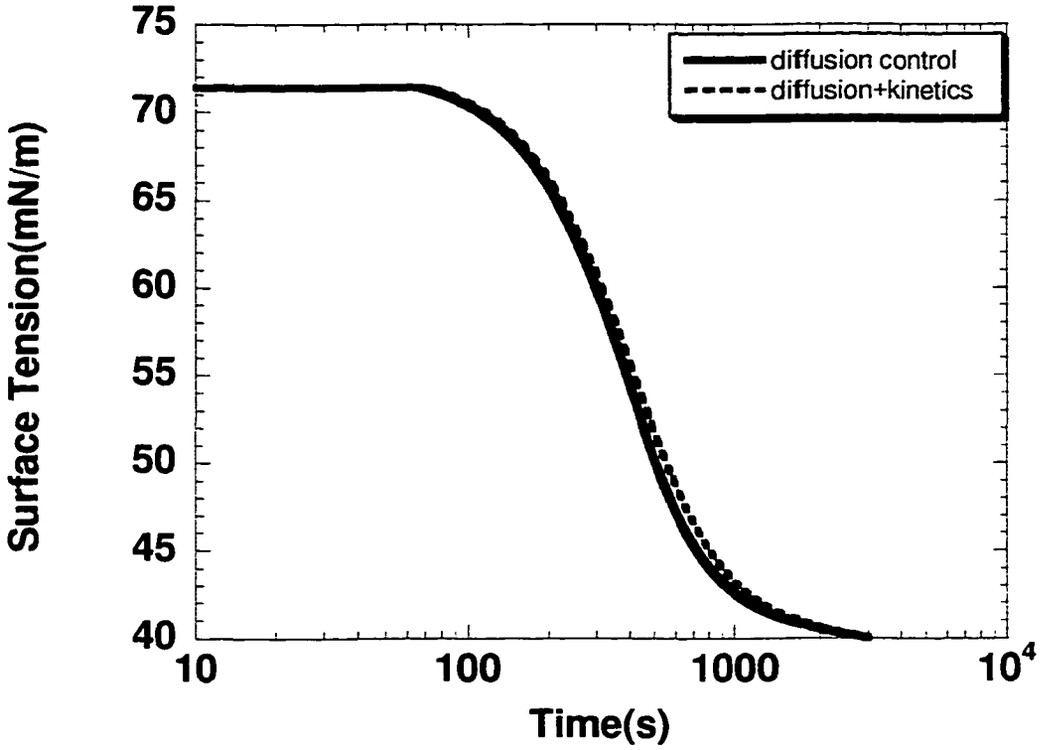

Fig. 3.11: Plot of Dynamic Tension Reduction Using the Phase Transition Model For the Diffusion Controlled and Mixed Diffusive-Kinetic Cases at a Bulk Concentration of $2.65*10^{-3}$ mol/m^3.

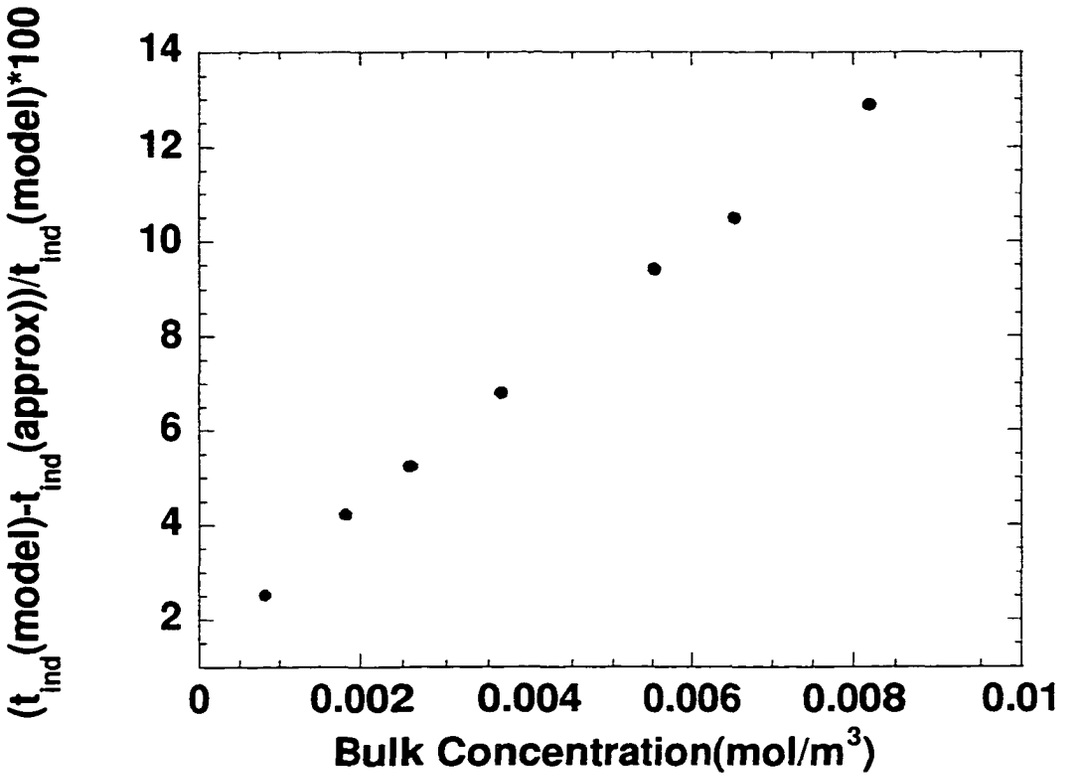

Fig. 3.12: Plot of the Normalized Difference in Induction Times Predicted by the Complete Phase Transition Model and That By Solution of Equation 3.9, Against the Bulk Concentration.

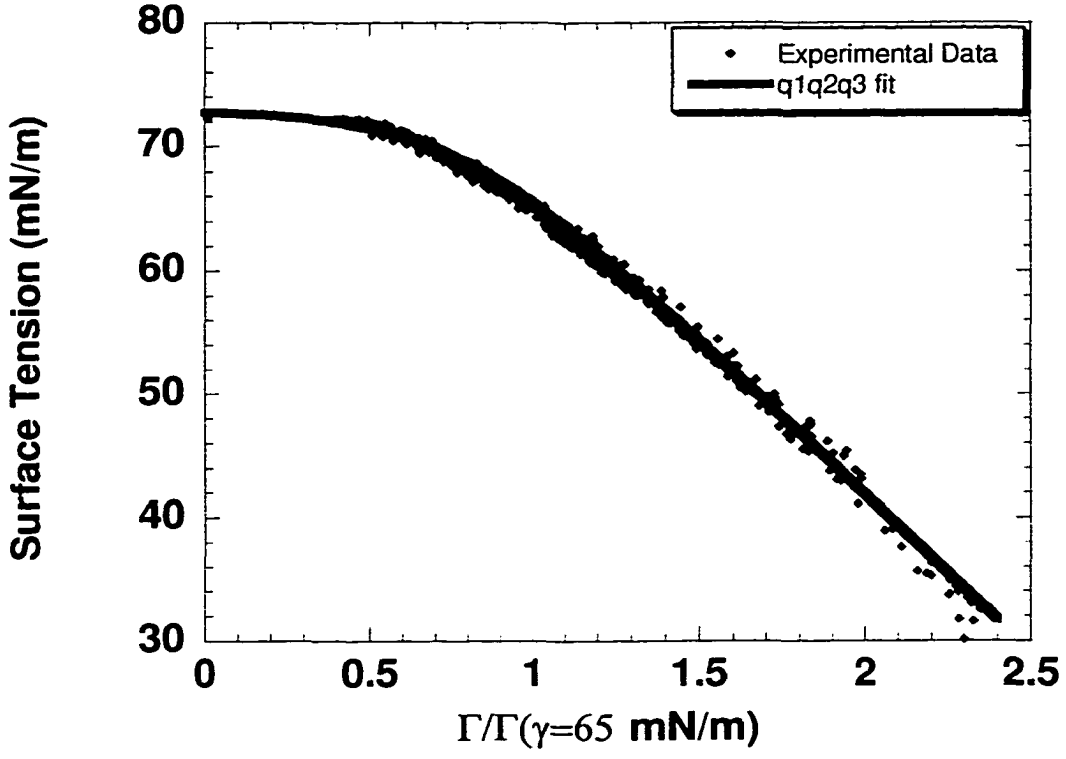

Fig. 3.A1: Surface Tension vs Relative Surface Concentration Data for $C_{14}E_6$ Using the Pendant Bubble as a Langmuir Trough and the Empirical Fit to the Data.

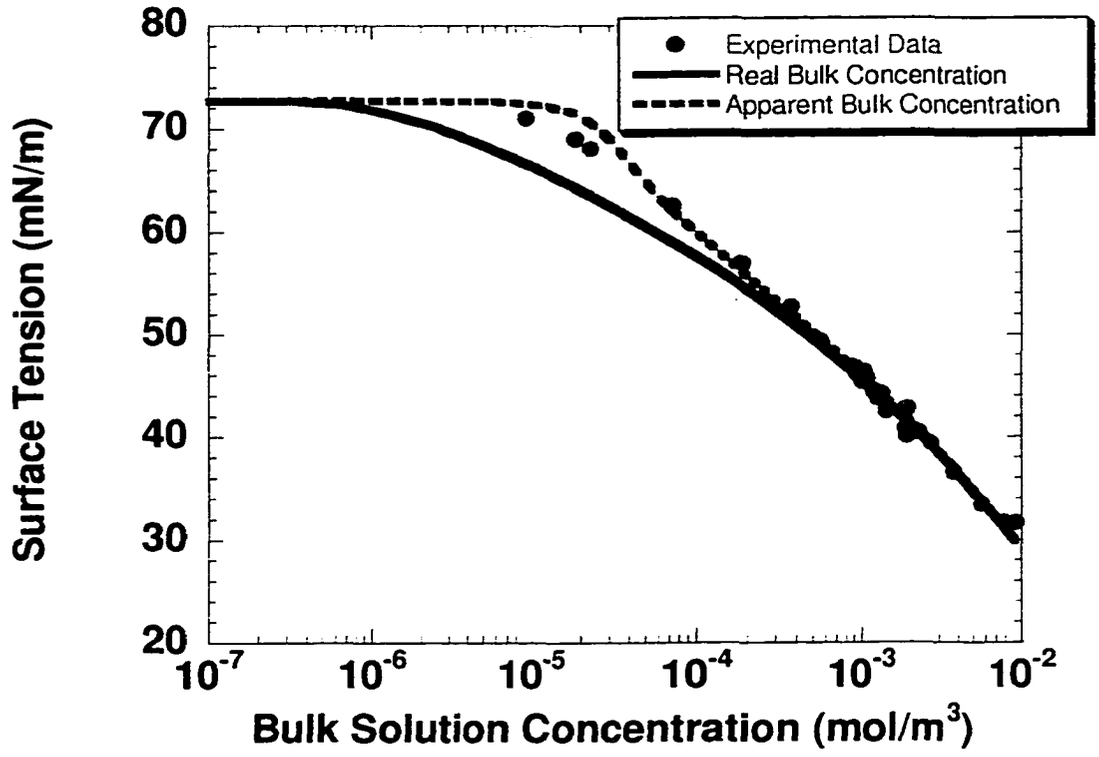

Fig. 3.A2: Surface tension - Bulk Concentration Equilibrium Data for $C_{14}E_6$ with the Fit Using the Runge-Kutta Integration for the Corrected and Uncorrected Concentrations.

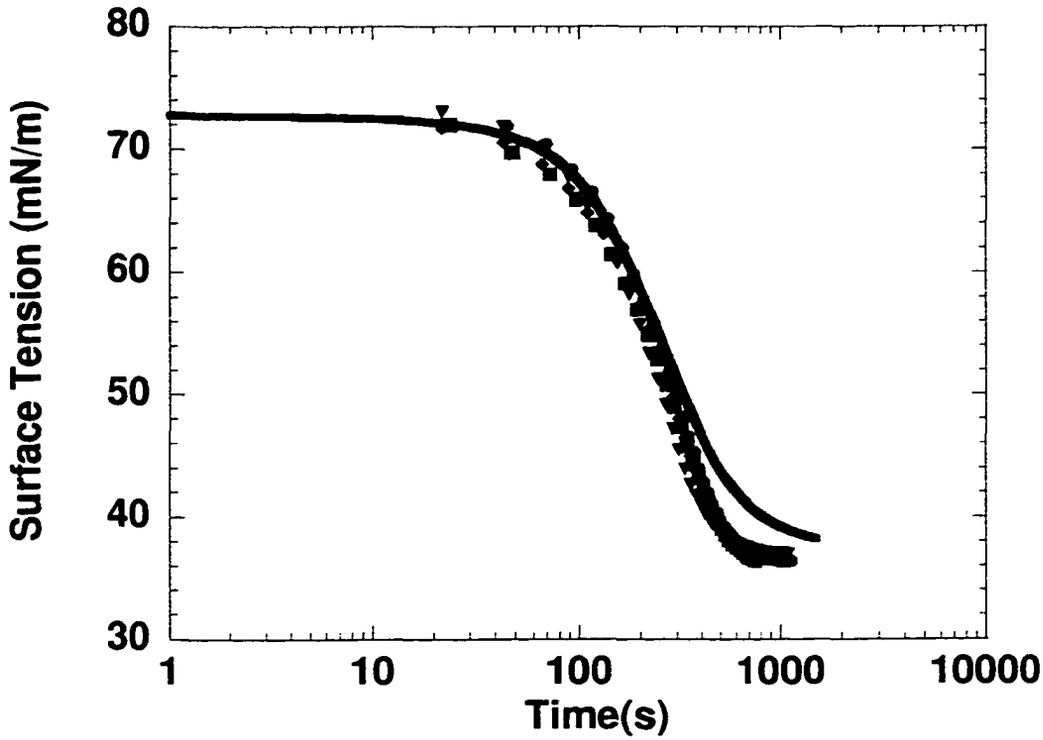

Fig. 3.B1: Fit of the Kinetic-Diffusive Model For the LE state to Relatively High Concentration ($3.74*10^{-3}$ mol/m^3) Dynamic Tension Data to Determine the Kinetic Adsorption Rate Constant and Diffusion Coefficient.

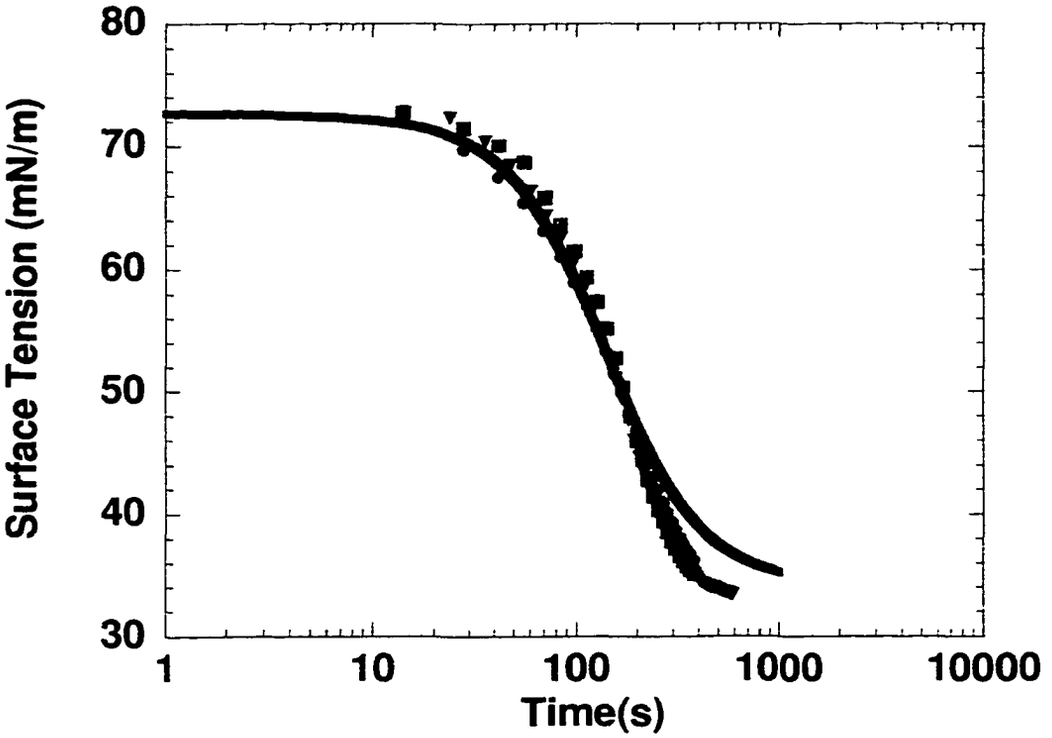

Fig. 3.B2: Fit of the Kinetic-Diffusive Model For the LE state to Relatively High Concentration ($5.60*10^{-3}$ mol/m^3) Dynamic Tension Data to Determine the Kinetic Adsorption Rate Constant and Diffusion Coefficient.

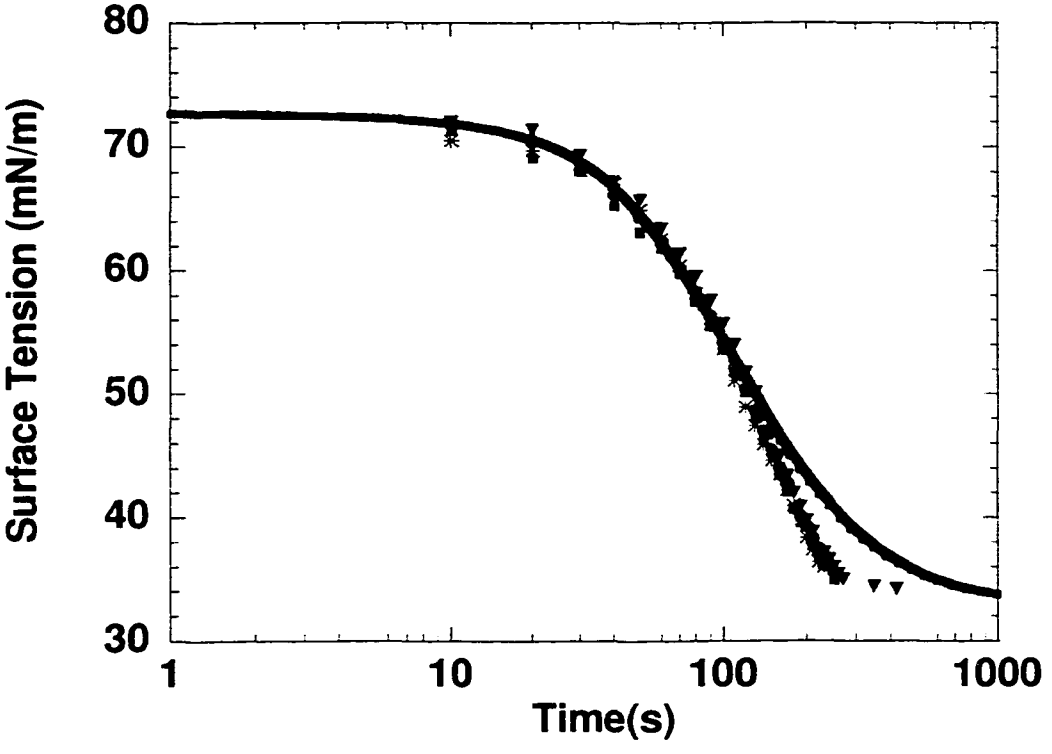

Fig. 3.B3: Fit of the Kinetic-Diffusive Model For the LE state to Relatively High Concentration ($6.62*10^{-3}$ mol/m^3) Dynamic Tension Data to Determine the Kinetic Adsorption Rate Constant and Diffusion Coefficient.

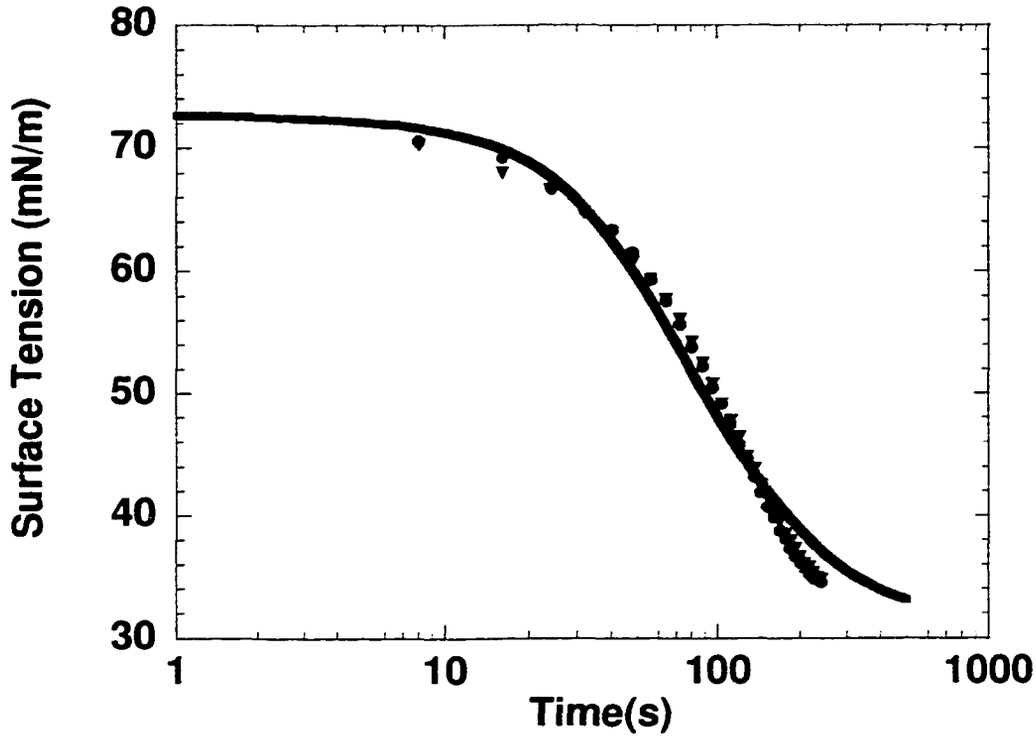

Fig. 3.B4: Fit of the Kinetic-Diffusive Model For the LE state to Relatively High Concentration ($8.27*10^{-3}$ mol/m^3) Dynamic Tension Data to Determine the Kinetic Adsorption Rate Constant and Diffusion Coefficient.

References

1)Rosen, M. *Surfactants and Interfacial Phenomena*; Second ed.; Wiley: New York, 1989.

2)Lin, S.-Y.; McKeigue, K.; Maldarelli, C. *Langmuir* **1991**, *7*, 1055-1066.

3)Lucassen-Reynders, E. H.; Lucassen, J.; Garett, P. R.; Giles, D.; way, F. *Advanced Chemical Ser* **1975**, *144*, 272.

4)Tempel, M. v. d.; Lucassen-Reynders, E. H. *Advances in Colloid and Interface Science* **1983**, *18*, 281.

5)Hua, X. Y.; Rosen, M. J. *Journal of Colloid and Interface Science* **1988**, *124*, 652-.

6)Joos, P.; Bleys, G. *Coll. Polym. Sci.* **1983**, *261*, 1038-1042.

7)Svitova, T. F.; Smirnova, Y. P.; Churaev, N. V.; Rusanov, A. I. *Coll. J. (Russia)* **1994**, *56*, 375-379.

8)Zhang, L. H.; Zhao, G. X. *Journal of Colloid and Interface Science* **1989**, *127*, 353.

9)Gao, T.; Rosen, M. J. *Jounal of Colloid and Interface Science* **1995**, *172*, 242-248.

10)Hénon, S.; Meunier, J. *J. Chem. Phys.* **1993**, *98*, 9148-9154.

11)Melzer, V.; Vollhardt, D. *Physical Review Letters* **1996**, *76*, 3770-3773.

12)Volhardt, D.; Melzer, V. *Jounal of Physical Chemistry* **1997**, *101*, 3370-3375.

13)Fainerman, V. B.; Volhardt, D.; Melzer, V. *Journal of Chemical Physics* **1997**, *107*, 243-251.

14)Melzer, V.; Vollhardt, D.; Brezesinski, G.; Mohwald, H. *Journal of Physical Chemistry B* **1998**, *102*, 591-597.

15)Pollard, M.; Pan, R.; Steiner, C.; Maldarelli, C. *Langmuir* **1998**, *14*, 7222-7234.

16)Lin, S.-Y.; McKeigue, K.; Maldarelli, C. *AIChE J.* **1990**, *36*, 1785-1795.

17)MacRitchie, F.; Alexander, A. E. *Journal of Colloid Science* **1963**, *18*, 458-463.

18)Joos, P.; Serrien, G. *Journal of Colloid and Interface Science* **1989**, *127*, 97-103.

19)Lin, S. Y.; McKeigue, K.; Maldarelli, C. *Langmuir* **1994**, *10*, 3442-3448.

20)Lin, S. Y.; Tsay, R.-Y.; Lin, L.-W.; Chen, S.-I. *Langmuir* **1996**, *12*, 6530-6536.

21)Pan, R.; Green, J.; Maldarelli, C. *Journal of Colloid and Interface Science* **1998**, *205*, 213-230.

22)Pan, R.; Green, J. H.; Maldarelli, C. M. *Langmuir,in press* **1999**.

23)Pan, R. *PhD Thesis,City University of New York* **1996**.

24)Subramanyam, R.; Pan, R.; Maldarelli, C. *Colloids and Surfaces A* **1998**, *Submitted for Publication*.

Chapter 4

Observations of LE/LC Phase Transitions in Slightly Soluble Surfactants

4.1 Introduction

In chapters 2 and 3, it was demonstrated that similar to insoluble surfactants spread and compressed at an air/water interface, aqueous soluble surfactants undergo gas to liquid expanded phase transitions as they adsorb onto interfaces from solution. Whether soluble surfactants can further undergo transitions from liquid expanded to liquid condensed states observed in insolubles has not been studied in detail. The ability of a surfactant molecule to assemble to a LC state is strictly a balance of the attractive van der Waals interactions between the hydrophobic chains and the repulsive forces among the hydrophilic polar head groups. It is necessary for the attractive forces to predominate the repulsion so that these molecules are able to stack tightly next to each other. In this context it is useful to note that surfactants with larger head groups/smaller chains (hydrophilic) are more soluble compared to amphiphiles with smaller head groups/longer chains (hydrophobic). So for simple amphiphilic molecules, the more insoluble a surfactant is, the greater is its ability to pack into a LC state. Thus many insoluble surfactants do undergo an LE/LC transition (e.g. PDA[1,2]), and soluble ones which undergo this transition are most likely sparingly soluble.

There is some evidence in the literature that conclusively establishes that sparingly soluble surfactants can assemble from solution into condensed phases.

The earliest evidence on the LE/LC phase transition in soluble surfactants was provided by Hutchinson[3,4] for films of a series of fatty acids assembled from benzene at the benzene-water interface. The force-area plots for the long chain fatty acids indicated transitions of films from expanded to condensed states. Similarly Lange's surface pressure isotherms for the sparingly soluble surfactants $C_{12}E_0$ and $C_{18}E_3$ displayed features characteristic of surface phase transitions. The isotherms for these surfactants displayed plateaus in the pressure at 20 mN/m at fairly high surface coverages indicative of a first order phase transition from an expanded to a condensed state. The corresponding isotherm for $C_{12}E_1$, as presented by Aveyard[5] also displayed unusual features at higher surface pressures suggesting phase transitions. In addition liquid/solid phase transitions of medium chain length normal alcohols (9-16) have been recently demonstrated using temperature tension measurements, ellipsometry, x-ray reflectivity and diffraction by Berge[6-8] and coworkers and ellipsometry and sum frequency spectroscopy by Bain[9,10] *et al.* These studies confirm earlier evidence of condensed states in sparingly soluble alcohols based on the increase in surface viscosity (see for example Trapeznikov [11] and Ross[12,13]).

More recently, direct visual evidence has been obtained for formation of condensed states by adsorption from solution. Melzer *et al.*[14,15] presented a study on formation and growth kinetics of condensed phases in adsorbed films of the slightly soluble N-dodecyl-hydroxybutric acidamide (DHBAA) in a static cell. Their BAM observations demonstrated a transition from a LE to a LC state during adsorption, and simultaneous tension measurements indicated that during the

transition the surface pressure was constant (although the plateau in tension lagged the appearance of the condensed phase). They also carried out dynamic adsorption studies for similar amphiphiles: N-Dodecyl-γ-hydroxy-butyric acidamide (DHBA), N-tetradecyl--γ-hydroxy-butyric acidamide (THBA) and N-(γ-hydroxypropyl) tridecanoic (and tetradecanoic) acid amide (HTRAA and HTEAA[16,17] and found plateaus in surface tension at intermediate times demonstrating transitions from liquid to condensed states. The work of Pollard *et al.*[18] also provided visual evidence of the assembly of surfactants into condensed states. Using fluorescence microscopy accompanied by surface tension measurements on the interface of an open channel, they studied a sparingly soluble surfactant $C_{14}E_1$. Once the surfactant adsorption had proceeded such that the interface was in a (bright) LE state, subsequent flow and adsorption induced the formation of round dark liquid condensed domains in a bright background. These domains grew in size and number, but at constant tension upon continued adsorption. Once the interface was mostly occupied by completely dark domains with just the dye trapped in-between the domains, the surface tension started to drop and finally the interface appeared to be like a spider web pattern. This clearly established that this surfactant undergoes a first order phase transition from an expanded to a condensed state (LE to LC). Similar results were obtained from spread monolayers of $C_{14}E_1$ along with the dye when visualized under fluorescence. Plateaus in surface pressure isotherms of spread monolayers of $C_{14}E_1$ and in independently measured dynamic tension relaxations due to surfactant adsorption onto freshly created interfaces, also

verified a phase transition at a surface pressure similar to that in the fluorescence adsorption experiments. Pollard *et al.* also suggested that the sparingly soluble surfactants $C_{12}E_o$ and $C_{16}E_2$ would also undergo a LE/LC transition and this was demonstrated by surface pressure isotherms (although not shown). Johal[19] also reported a structural phase transition in adsorbed dodecanol monolayers at the hydrophobic solid/liquid interface.

Based on the literature review, it is clear that a few sparingly soluble surfactants can assemble into liquid condensed phases. Of these, the observation that the alcohols condense is the more important from a technological point of view. In many interfacial technologies, alcohols are often added to surfactant systems to condense the monolayer. For instance, the presence of trace quantities of dodecanol in the bulk phase has been found to induce remarkable ordering and transitions to condensed phases in mixed monolayers of dodecanol with sodium dodecyl sulfate (SDS)[20], dodecanol with C_nTAB's[21] at the air/water interface and dodecanol with SDS at the hydrophobic solid/liquid interface[22]. It has been noted that surface films of sodium lauryl sulfate can be condensed by the addition of lauryl alcohol to form monolayers which restrict interphase transport of a gas[23]. The mechanism of action of alcohols as foam breakers is also related to their ability to condense monolayers. To make a liquid foam, surfactant is added to reduce the energy of the air/liquid surface so that a large interfacial area can be created. In a foam, when air bubbles approach one another, coalescence is caused by the thinning and rupture of the intervening liquid film. Surfactants dissolved in the liquid phase

adsorb onto the bubble surface where they are convected away from the centerline along which the particles approach. This increases the tension at the centerline, creating a Marangoni force that reduces the surface velocity, decreases the rate of thinning and increases the lifetime of the dispersion. To break the foam, an alcohol is added. Adsorbed alcohol causes liquid and condensed phases to co-exist on the surface, which can be compressed with minimal change in tension due to the phase co-existence. The resulting reduction in the Marangoni force increases the rate of thinning and destabilizes the foam. Previous studies on the condensation of alcohols by Berge, Bain and coworkers as cited above have not studied in detail the LE/LC phase co-existence, the concentrations of co-existing phases or the bulk concentrations necessary for co-existence. Our aim in this chapter is to study more completely the phase transition for an archetype of an alcohol undergoing the LE/LC transition. We choose dodecanol because the transition occurs at room temperature (at room temperature, in the C_{10} series, even the alcohol does not reach the LC state[24] (too small a chain)), and at bulk concentrations which are not too low to be accurately measured. The C_{16} and C_{18} homologues are too low in solubility. In addition, this alcohol has been found to play a crucial role as a contaminant in many surfactant systems: Nilsson first recognized[25] that trace amounts of dodecanol in the bulk could lead to a large proportion of the interface being contaminated with the same. This is reflected in the equilibrium γ-ln c_b measurements for the surfactant sodium dodecyl sulfate (SDS), where a prominent and unusual minima is observed. As was suggested by Mysels[26], the

partial hydrolyses of SDS to dodecanol with the dodecanol preferentially occupying the interface causes the occurrence of this minimum. He also established that SDS solutions, which could be purified enough and prevented from hydrolyses, did not show this unusual phenomenon[26]. Further, the presence of trace quantities of dodecanol has been found to have a marked effect on dynamic tension[27-29] and rheological properties[11].

In this chapter we provide four pieces of evidence for the LE/LC phase transition for dodecanol. The simplest approach to verify this phase coexistence is to treat this surfactant analogously to insoluble surfactants and measure surface pressure isotherms on a Langmuir trough. Although this technique does qualitatively provide direct evidence of two-phase coexistence (a plateau in the isotherm), the soluble surfactant will desorb into the sub-phase, at least at the higher surface concentrations, and consequently the measurements of the surface concentrations will be inaccurate. A second piece of evidence comes from the measurements of the γ–ln c_b curve. As mentioned earlier discontinuities in the slopes of these curves are suggestive of phase transitions, although clearly distinguishing a cusp is difficult and questionable. Dynamic tension measurements during adsorption of surfactant onto freshly created pendant bubbles provide the third piece of evidence demonstrating that these surfactants can self assemble from solution into condensed states. As was the case with $C_{14}E_1$, a phase transition will manifest itself as a plateau in dynamic tension reduction for a first order transition. The last piece of evidence will be obtained from fluorescence microscopy. This technique has previously been successfully

used to distinguish two-phase coexistence for insoluble and sparingly soluble surfactants. Here the interface shall be monitored as surfactant physically adsorbs from solution to see if it undergoes any phase transitions. Simultaneous measurements of the tension during the adsorption process as was done in Chapter 3 will also be carried out.

We extend our measurements of dodecanol to identify the range of insoluble surfactants that form the LC phase, and demonstrate that $C_{11}E_0$ (undecanol) and $C_{12}E_1$ also form this condensed phase at room temperature.

4.2 Experimental

Materials: The n-alkyl poly (ethylene glycol) ether surfactant ($C_{12}E_1$=$CH_3(CH_2)_{11}(OCH_2CH_2)_1OH$), >98% purity, was obtained from Nikko Chemicals, Japan. The alcohol surfactants $C_{12}E_0$ (Dodecanol) and $C_{11}E_0$ (Undecanol) of greater than 99.5% purity were obtained from Fluka. For fluorescence studies a fluorophore NBD-HDA (4-(hexadecylamino)-7-nitrobenz-2-oxa-1,3-diazole) supplied by Molecular Probes, OR was used. All chemicals were used as received without any further purification. The subphase in all experiments was deionized water purified by a Milli-Q filter system fitted with an Organex-Q column to remove trace contaminants (Millipore, MA). The resistivity of the deionized water was at least 15 MΩ- cm.

Methods: The techniques utilized were fluorescence microscopy, dynamic and equilibrium tension measurements and surface pressure measurements. These have been described in detail in the preceding chapters.

Preparation of Solutions: Two different approaches were used to prepare solutions. As we are dealing with sparingly soluble surfactants, most solutions were such that there was surfactant in excess of its solubility limit in water. For solutions that were above the solubility limit in water, they were gently stirred for at least 24 hours. The excess insoluble material was visible as macroscopic flakes in the aqueous solution.

Solutions of low concentration below the solubility limit cannot be prepared accurately from high concentration solutions because of the limited solubility and a new procedure had to be adopted. It must be understood that the concentrations we are dealing with are too small to be accurately directly weighed out, so dodecanol was first dissolved in ethanol at very high concentrations ($0.134*10^3$ mol dodecanol/m^3 ethanol). Then trace amounts of ethanol were dispersed in water. This is a commonly used method for preparing dilute solutions. The criterion for choosing ethanol as the dispersing solvent is that it is completely miscible with water, shows negligible surface activity of its own at these concentrations, and that dodecanol is infinitely soluble in ethanol. When dodecanol (in ethanol) was added beyond a certain amount to water, the dodecanol precipitated out. By adding different amounts of dodecanol (in the form of its solution in ethanol) to water, aqueous solutions of dodecanol at different low concentrations were prepared.

4.3 Results

4.3.1 The LE/LC Phase Transition for Dodecanol

As mentioned above, four different sets of results were used to verify the existence of an expanded to condensed phase transition for dodecanol. The pendant bubble technique was used for three important results: the equation of state measurements by using the pendant bubble as a Langmuir trough as in Chapter 3, the equilibrium γ–ln c_b measurements and the dynamic tension reduction accompanying clean interface adsorption. Fluorescence microscopy accompanied by dynamic surface tension measurements using a Wilhelmy plate provided the last piece of evidence.

(a) Langmuir Trough Measurements of the Surface Pressure Isotherm:

The simplest piece of evidence for the LE/LC phase transition comes as mentioned above from measurements of surface pressure isotherms on a Langmuir trough. Monolayers of dodecanol were spread onto the air/water interface of the trough from a chloroform solution. As we are dealing with soluble surfactants, most of the compression rates used were very high and little or no time was allowed for the chloroform to evaporate. This could certainly induce some complications such as nucleating phases not equilibrating rapidly enough during compression and the presence of the solvent in addition to the surfactant. Shown in Fig. 4.1 are surface pressure isotherms for dodecanol at 20^0 C at different compression speeds. At all compression speeds, it is immediately evident that dodecanol undergoes a phase transition from an expanded to a condensed state in the form of a plateau in surface pressure. This provides the

first piece of evidence. However it is also clear that at the lower compression speeds, the final packing concentration of the surfactant is too high and is not realistic. For alcohols the typical cross sectional area of the molecule permits a final crystalline packing concentration of 19-19.5 $Å^2$/molecule[30] and the final value obtained in these compressions is too high (Γ^{-1} too low). It must be noted here that for slender alcohols the hydrocarbon cross section area and not the polar alcohol group determines the limiting packing. At the higher compression speeds the isotherm does indeed shift to the right demonstrating more realistic coverages due to reduced desorption. However at higher speeds the plateau is not as flat as for the lower speeds perhaps because of non-equilibrium effects and presence of chloroform. Even at the highest speed used, the limiting surface concentration is a bit on the higher side (Γ^{-1}=17 $Å^2$/molecule). This implies that even at these compression rates, there is some desorption.

In Chapter 3, it was demonstrated that the pendant bubble could be used as Langmuir trough to directly measure the equation of state for soluble surfactants, as there was less exchange of surfactant between the interface and the bulk. As this can be carried out only in solutions of low concentration, solutions of different concentrations of dodecanol below the solubility limit were prepared by the procedure using ethanol as a dispersing solvent (as described earlier). Once these solutions were prepared, pendant bubbles were quickly formed and the tension monitored with time until equilibrium was reached. Once in equilibrium, the bubbles were compressed/expanded rapidly to measure the equation of state. Some experiments were also done without the bubble having

reached equilibrium, to verify that the equilibrium equation of state corresponds to the dynamic equation of state[31].

Shown in Fig. 4.2 are the complied results of compression of bubbles at different dilation rates and in different but somewhat low bulk concentrations. The plot is that of the surface tension against the relative surface concentration. These have been normalized by forcing the relative surface concentration at a tension of 60 mN/m to be unity. It is immediately clear that since all these sets of data overlap, there is indeed minimal exchange of surfactant with the bulk and we are measuring the true equation of state albeit with reference to a given surface concentration. It was also found that it was difficult to compress and expand the same bubble and get no hysteresis as was done by Pan *et. al.* This could be because this surfactant has faster kinetic exchange coefficients or because we are compressing to much higher surface concentrations as compared to conventional surfactants, thereby inducing higher desorption rates due to overcrowding. At higher dilation rates, the plateau corresponding to the phase transition was not as flat as before perhaps because of dynamic effects of non-equilibrium phases nucleating. However the fact that different sets of data of bubble compressions in different concentrations and dilation rates coincided with each other when normalized, is sufficient evidence to confirm that there is no surfactant exchange with the bulk and that we are truly measuring accurately the (relative) equation of state. Further the fact that we obtained a very flat plateau in the isotherm and that the surface pressure corresponding to the phase transition agreed well with similar measurements on the Langmuir trough, provides

concrete evidence that these solutions are indeed that of pure dodecanol in water and the ethanol used for solution preparation does not induce any complications.

Instead of employing a procedure to get the absolute equation of state as was done in Chapter 3, here the relative equation was converted to the absolute measurement by using a single point in the LE phase of the high compression rate Langmuir trough data as the reference. Choosing a point in the LE phase as a reference is somewhat justified because we expect minimal desorption in the Langmuir trough when the surface concentrations are not too high and so the area/molecule corresponding to a surface tension of 60 mN/m was chosen as the reference. This procedure is adopted because modeling a (apparent) cusp or cusps is significantly more difficult, although in principle it can be done. In Fig. 4.3 therefore is the absolute measurement of the equation of state with the Langmuir trough data shown alongside. In is apparent that the two sets of measurements match well in the LE phase but begin to depart at higher surface concentrations implying desorption in the Langmuir trough measurements at higher surface concentrations. The pendant bubble as a Langmuir trough data predicts a final packing density that seems to be more realistic (18 $Å^2$/molecule) and is in somewhat better agreement with independent measurements of this value reported in the literature. This also gives further support to the fact that we have measured the true equation of state. Further the bounds of the surface coverage at the two ends of the transition are approximately 24 $Å^2$/molecule for the LE end and 20 $Å^2$/molecule for the LC end of the transition by using the

pendant bubble as a Langmuir trough data. The most important conclusion however, is that from the surface pressure isotherm measurements, there is evidence from both spread and adsorbed monolayers that this surfactant undergoes the LE/LC phase transition.

(b) Equilibrium Surface Tension Measurements: Cusps in γ–ln c_b data:

The second piece of evidence comes from compilation of the long time equilibrium surface tension/bulk concentration data obtained from the pendant bubble measurements as shown in Fig. 4.4. Usually phase transitions are evident in the form of apparent cusps in the γ–ln c_b curve as cusps give two surface concentrations at a given bulk concentration implying a phase transition. These observations have traditionally been made for the G/LE transition [32-34], where there is a large difference in densities of the two phases. Here the density difference between the LE and LC phases is extremely small (ΔA~5 Å^2/molecule) and so it is extremely difficult to clearly distinguish a cusp. For dodecanol while the cusp signaling the G/LE transition is somewhat apparent, the cusp for the LE/LC transition is not so clearly evident (Fig. 4.5). However if one takes the slope of this curve for data just above (till 60 mN/m) and just below (till 40 mN/m) the surface tension corresponding to the phase transition (52 mN/m, from the pendant bubble as a Langmuir trough measurements), then it yields surface concentrations of 21 and 28 Å^2/molecule for the two ends of the transition. While the scatter and accuracy of the data does give rise to inaccuracy in these estimates and a large error bar should be provided, but the fact that two different slopes were obtained, suggests a discontinuity and a cusp. Also since they

somewhat agree with the equation of state measurements (20 and 24 $Å^2$/molecule for the two ends), they are at-least self-consistent. However large error bars have to be applied to the concentration axis as well because the true bulk concentration can be acutely depleted due to (a) adsorption of surfactant at the cuvette air/water and glass/water interfaces and (b) evaporation due to the volatility of the surfactant. Dodecanol by itself is volatile and therefore solutions that are left standing for longer periods of time are rapidly depleted of surfactant due to evaporation. So these slope measurements can be quite inaccurate. While this evidence is in no way conclusive or unambiguous, a cusp may be present in the data, thus further supporting the phase transition hypothesis and provides the second piece of evidence for the LE/LC phase transition.

(c) Plateaus in the Relaxation in Dynamic Tension for Adsorption at a Clean Interface:

The third piece of evidence comes from the dynamic tension experiments using the pendant bubble technique. Dynamic tension runs were carried out for these dodecanol solutions at a range of bulk concentrations (Fig. 4.6). For the low concentration solutions it was found that only very freshly prepared (within a couple of hours) solutions gave reliable and reproducible results. It must be mentioned that solutions that are left standing in the cuvette for extended periods of time are depleted of surfactant due to both the volatility of the surfactant and adsorption onto the water/air and glass/water interfaces. So runs for the lower concentrations were repeated by refilling the cuvette with fresh solution for every run. The first observation from these results is that, beyond a certain concentration, dynamic tension curves at increasing concentrations converged to

a single curve. This means that this single converged curve represents the relaxation of a solution in which the monomer concentration is exactly at its solubility limit. Filtered (<20 μm) and unfiltered solutions gave similar results implying that the excess macroscopic surfactant phase had no role to play in the rates. For these solutions with excess surfactant reproducible dynamic tension runs over extended period of days even after the stirring had been stopped were used to verify that the monomer had indeed reached its true solubility in water. Based on this, the solubility of dodecanol in water thus determined was close to 0.01502 mol/m^3 (between 0.0134 and 0.0161 mol/m^3) and is in good agreement with that from literature[19,35].

Secondly, from the dynamic tension curves we note two plateaus for the higher concentration solutions: one at early times at the clean interface tension, which corresponds to the G/LE transition discussed in Chapter 3, and a second at later times when the tension is reduced sufficiently from the clean interface value. This second plateau occurs at intermediate tensions and at the same tension as the pendant bubble film balance data and indicates a transition to a more condensed state. For lower bulk concentrations the final equilibrium surface concentrations are not high enough to form this state, and the equilibrium remains in the LE state. Also the time of formation of the LC state for dodecanol (about 200 s for the saturated solution) is much faster than $C_{14}E_1$[18] (3000 s), owing apparently to the higher solubility. This is the third piece of evidence for the LE/LC phase transition for dodecanol and perhaps the most important

because it clearly demonstrates that sparingly soluble surfactants can self assemble from solution into liquid condensed states.

(d) Fluorescence Microscopy Observations of Adsorption onto an Initially Clean Interface:

The final and most conclusive piece of evidence comes from direct visual observation of the interface as surfactant adsorbs from solution onto the interface. As was done in Chapter 3, aqueous surfactant (dodecanol) solution (excess dodecanol) was allowed to flow into an open channel flow cell whose interface was monitored by fluorescence and the tension measured using a Wilhelmy plate (Fig. 3.2). The temperature was 28^0 C. Fig. 4.7 (a)[I-IX] shows the progressive evolution of the interface as surfactant adsorbs onto the interface. Fig. 4.7 (b) shows the trace of the surface tension measured during this adsorption process. It is immediately evident that the surfactant in the monolayer first undergoes a G/LE phase transition at the clean interface tension and these progressive images are shown in Fig. 4.7 (a) (I)-(V). The interface is initially dark when just the dye is present and as surfactant adsorbs, the nucleation and growth of the bright LE phase follows. The tension starts dropping when the entire interface is in a bright LE state. Normally soluble surfactants stay even at maximum packing in a bright LE state. This was demonstrated in Chapter 3 for $C_{14}E_6$ (although we did not go all the way till maximum packing was attained). However for dodecanol, with the passage of time, one observed the nucleation of dark domains (LC) in a mainly bright background (LE) at a reduced tension value of 45 mN/m. These domains grew in number and size but at constant tension as further adsorption was permitted. Eventually as the monolayer was almost

completely covered with dark domains with the exception of a few bright spots where the dye is presumably trapped between the domains, the tension started dropping. Such a progressive evolution of the monolayer through a LE/LC phase transition is shown in Fig. 4.7 (a) (VI)-(IX) and is very similar to that observed by Pollard for $C_{14}E_1$. Here the surface tension at the plateau is different from that in the equation of state and dynamic tension measurements because the temperature was substantially higher. Pollard estimated a drop in the phase transition tension of 0.9 mN/m/ ^{0}C. for $C_{14}E_1$. As the dynamic tension experiments were conducted at 20-22^0 C, the plateau in the fluorescence experiments should be expected at a tension of 45-46 mN/m and this is what is observed. This provides the last and most cogent piece of evidence that a sparingly soluble surfactant can self assemble from solution into condensed phases.

4.3.2 The LE/LC Phase Transition for $C_{12}E_1$ and $C_{11}E_0$

The second surfactant studied was $C_{12}E_1$. Its dynamic tension relaxation is presented in Fig. 4.8 for the saturated solution at 21° C (excess added to maintain saturation). According to Aveyard[5] this surfactant undergoes a transition whose plateau pressure varies strongly with temperature. From our dynamic tension data we observe a sharp discontinuity in the tension relaxation and see a flat plateau in tension at a value of 30 mN/m. This plateau extends in time until the tension finally drops to its equilibrium value of 27-28 mN/m. Since the plateau tension is so close to the equilibrium value, it is very difficult to ascertain for sure if this is a phase transition or not. However the repeated

reproducibility of this plateau and the fact that the recorded movie sequence of the evolution of the shape of the bubble, when played back, clearly shows the pendant bubble having stopped its shape relaxation for a long time (at the times in which the tension remained constant) before it again relaxes, provides convincing evidence that we indeed observe a phase transition. The reason the plateau extends in time is because the surface density of the nucleating LC phase is almost equal to the equilibrium surface density of the LC phase for the saturated surfactant. Consequently the adsorption rates at densities so close to the equilibrium surface density are very slow and it takes a long time for the coverage to attain its equilibrium value. Further according to Aveyard[5] the tension (plateau) at this temperature should be at 28 mN/m which is in close agreement with our value of 30 mN/m for the phase transition. At a lower temperature (19^0 C) the plateau is again observed at a higher tension (in the right direction[18]) once again verifying that we are indeed observing a LE/LC phase transition for $C_{12}E_1$. Finally due to higher solubility, the dynamics are faster as compared to dodecanol despite the density of the nucleating LC phase being higher and the LE/LC transition begins in about 100 s.

The last homologue studied was $C_{11}E_0$. The dynamic tension relaxation for saturated solutions are shown in Fig. 4.9. There is clearly a plateau in tension once again demonstrating that even for this homologue, the cohesion is still strong enough to induce a phase transition and form a condensed phase. The dynamics of formation of the condensed state are much faster when compared with dodecanol (40 s compared to 200 s) owing to the higher solubility. It is also

faster when compared to $C_{12}E_1$ because the surface concentration required to form the condensed phase is not as high and hence shorter is the time to reach this surface concentration. This is verified by the fact that the plateau is not as extended as before and the equilibrium tension is at least a few dynes lower than the plateau tension, implying that the surface densities of the co-existing LE and LC phases are not as large as that for $C_{12}E_1$.

4.4 Conclusions and Discussion

In this chapter we demonstrate that at room temperature, sparingly soluble surfactants with small polar groups (j) relative to chain (i) length ($2j/(i-10)\leq 1$) can assemble from solution into liquid condensed phases. One surfactant dodecanol has been analyzed extensively to characterize its phase behavior. Evidence has also been provided for the existence of condensed phases among similar homologues such as $C_{12}E_1$ and $C_{11}E_0$. This suggests that in these molecules, the chain length is long enough compared to the polar group such that the cohesive (van der Waal) forces can overcome the repulsive interactions and permit tight packing in condensed states. Therefore similar to the insoluble surfactants, soluble surfactants under the limit of low solubility can form condensed states in addition to gaseous and liquid states.

For dodecanol, four different pieces of evidence have been provided to verify the formation of condensed states. Plateaus in surface pressure measurements as a function of surface concentration of surfactant by using a Langmuir film balance as well as pendant bubbles provide the simplest evidence for a transition from expanded to condensed states. Large desorption of

surfactant during compression on a Langmuir trough precludes the accurate measurement of surface pressure isotherms by this technique. More accurate surfactant equations of state (relative to a given coverage) are obtained by using the pendant bubble as a film balance as faster dilation rates minimize exchange of surfactant between the surface and the bulk. A reference surface concentration from the corresponding isotherm measured on the Langmuir trough is used to construct an absolute equation of state. Realistic values for the surface density at the maximum packing verifies that the absolute equation of state obtained this way is accurate. Estimates of the inverse surface densities of the LE and LC phases are found to be 24 and 20 $Å^2$/molecule respectively at 20-22^0 C.

Compilation of the long-time equilibrium surface tension-bulk concentration data provides the second piece of evidence for a phase transition. Phase transitions manifest themselves as cusps in the data. Here although a cusp is not immediately apparent from the measurements, two different values are obtained from calculations of surface coverages using the Gibbs adsorption equation for data just above and just below the phase transition tension. Further these values are in reasonable agreement with the corresponding values from the equation of state measurements. Therefore a cusp may be present and it is proof of a phase transition.

Plateaus in dynamic tension reduction upon surfactant adsorption onto freshly created interfaces provide the third piece of evidence for transitions to condensed states. These transitions occur if the bulk concentration of surfactant

is high enough and the surface tension corresponding to the onset of these is exactly same as that in the surface pressure measurements. However, owing to the low solubility of these surfactants, the rate at which these condensed states form by adsorption is very slow: from tens to hundreds of seconds at the solubility limit in water. For gently stirred solutions (not dispersions), the presence of excess surfactant present as insoluble flakes in the solution was found to have no contribution in enhancing the transport rates of these surfactants to the interface. This is presumably because the time for breakup of these aggregates is slow when compared to the adsorption rates and hence they do not act as effective reservoirs of surfactant.

Fluorescence monitoring of the interface during adsorption provides the most direct evidence for the formation of condensed states for dodecanol. Here once the adsorption proceeds such that the interface attains a bright (LE) state, dark (condensed) domains nucleate and grow in size and number in co-existence with the diminishing LE phase at constant tension. Once the interface is covered with the dark domains (with the exception of the bright dye trapped between these phases), the tension drops with the interface attaining a spider-web like pattern. This most conclusively establishes the formation of condensed states by adsorption for dodecanol.

Similar amphiphiles such as $C_{12}E_1$ and $C_{11}E_0$ that are more soluble than dodecanol also undergo a phase transition to a condensed state. This is observed as a plateau in dynamic tension reduction. Again the rates at which the

condensed states are formed are slow due to the limited solubility, although they are faster than dodecanol because of their higher solubility.

There is evidence in the literature that $C_{10}E_0$[24], $C_{12}E_2$[31] etc. do not form condensed phases at room temperature. Based on this, a simple table can be constructed of chain length vs ethoxy no. for poly-ethylene oxide surfactants to show the limits at which the formation of condensed phases is still permissible at room temperature. This is shown in Table 4.1 and it demarcates the phase envelope for the LE/LC transition with regard to the polar group size and chain length.

One question which remains to be answered is whether the condensed states observed are equilibrium states. The condensed states that occur in insoluble surfactants spread at an interface may or may not be equilibrium states. For instance in stearic acid monolayers, the equilibrium spreading pressure (esp), which is the pressure at which the monolayer is in equilibrium (hence the lowest free energy) with the stable bulk phase is about 5 mN/m at 25^0 C[36], but condensed states (LS) exist at elevated pressures upto 40 mN/m before "apparent" collapse. So any condensed state at pressures above the esp is a non-equilibrium metastable state. Here these states exclusively form because of the action of an external force, for instance the compression of a monolayer by the motion of the barriers of a Langmuir trough. Any non-equilibrium state will eventually go back to a stable equilibrium state. On the other hand for pentadecanoic acid (PDA), condensed states occur at surface pressures[2] (10 mN/m at 25^0 C) lower than the equilibrium spreading pressure of 20-25 mN/m at

this temperature[37]. Hence these states are perhaps stable equilibrium states. In general as the chain length is lowered for these fatty acids, the equilibrium spreading pressure increases. Hence by the time the somewhat soluble homologues (of lower chain length) of this series are reached, the esp is fairly high and most states are therefore equilibrium states.

For soluble surfactants that adsorb from solution, every state is an equilibrium state. This is because the assembly at interfaces occurs spontaneously without the action of any external force and so the system reaches a state of minimum free energy by itself. Indeed it has also been found that for fairly and sparingly soluble alcohols, the esp is high, of the order of 45 mN/m[10], so most states are equilibrium states. So any condensed states that form spontaneously by adsorption for these surfactants are equilibrium states[10]. In addition, for dodecanol it has been rigorously demonstrated by using the pendant bubble as a Langmuir trough that the equilibrium equation of state matches the dynamic equation of state. This further verifies that the condensed states studied in this chapter are truly equilibrium states.

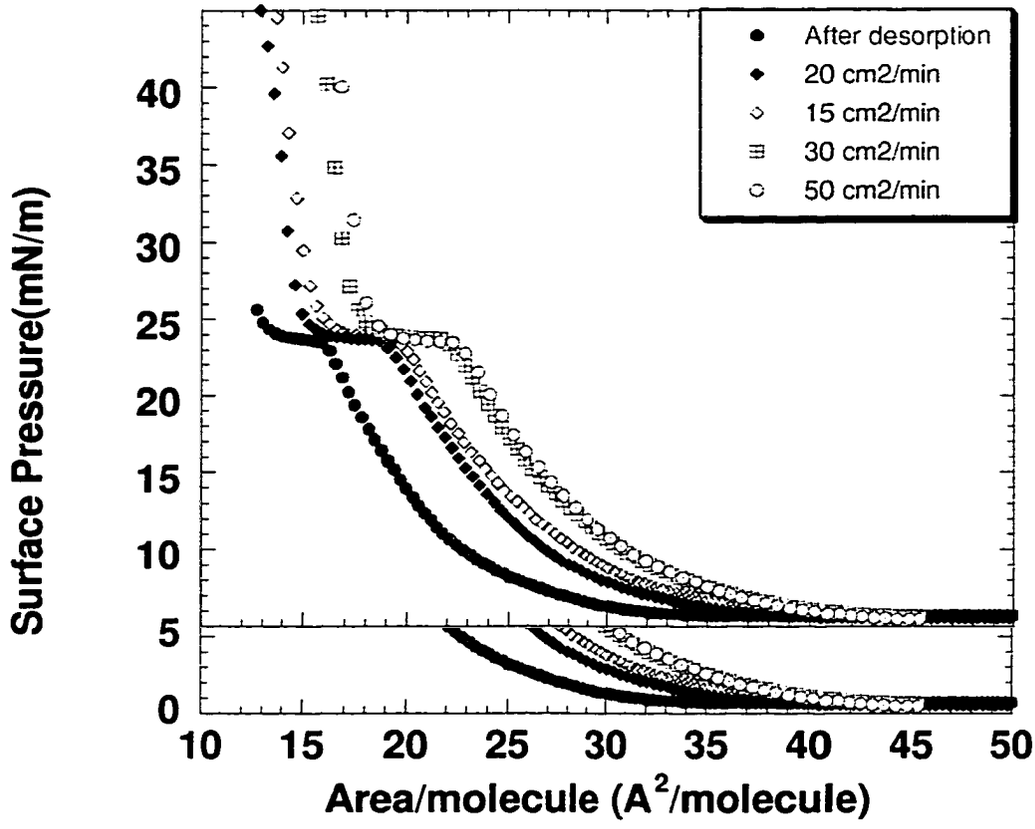

Fig. 4.1: Surface Pressure Isotherms For Dodecanol on a Langmuir Trough at Variable Compression Speeds Verifying Two-Phase Co-existence (LE/LC).

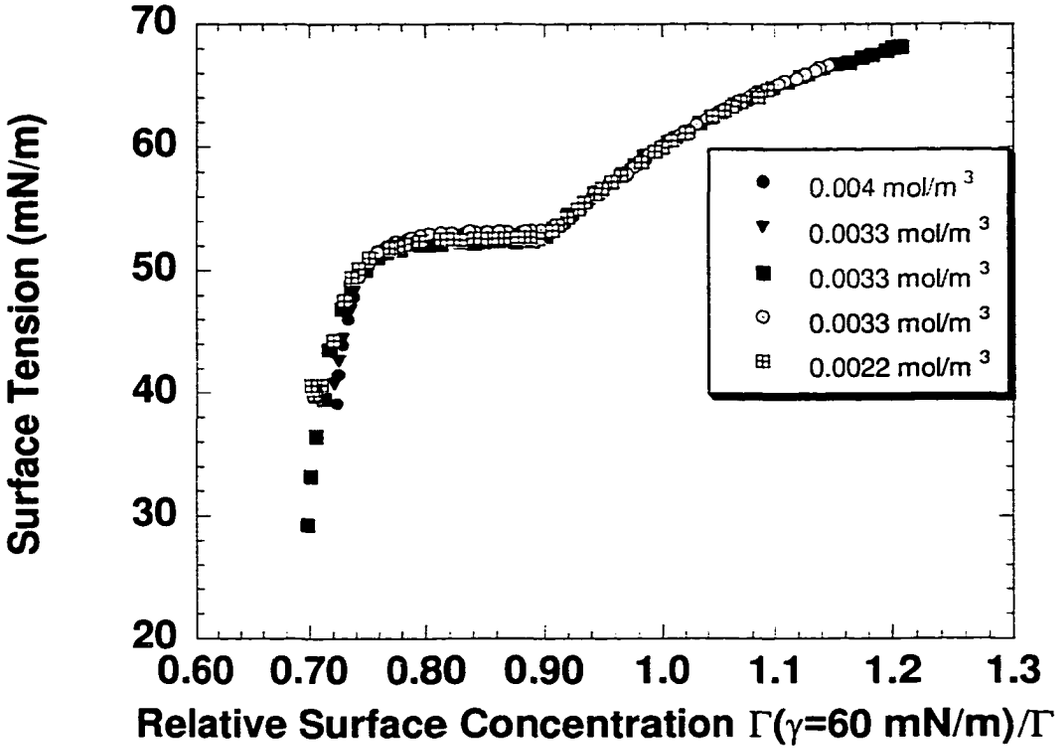

Fig. 4.2: Plot of the Surface Tension Against Relative Surface Concentration by Using the Pendant Bubble as a Langmuir Trough at Different Dilation Rates and in Different Bulk Concentrations.

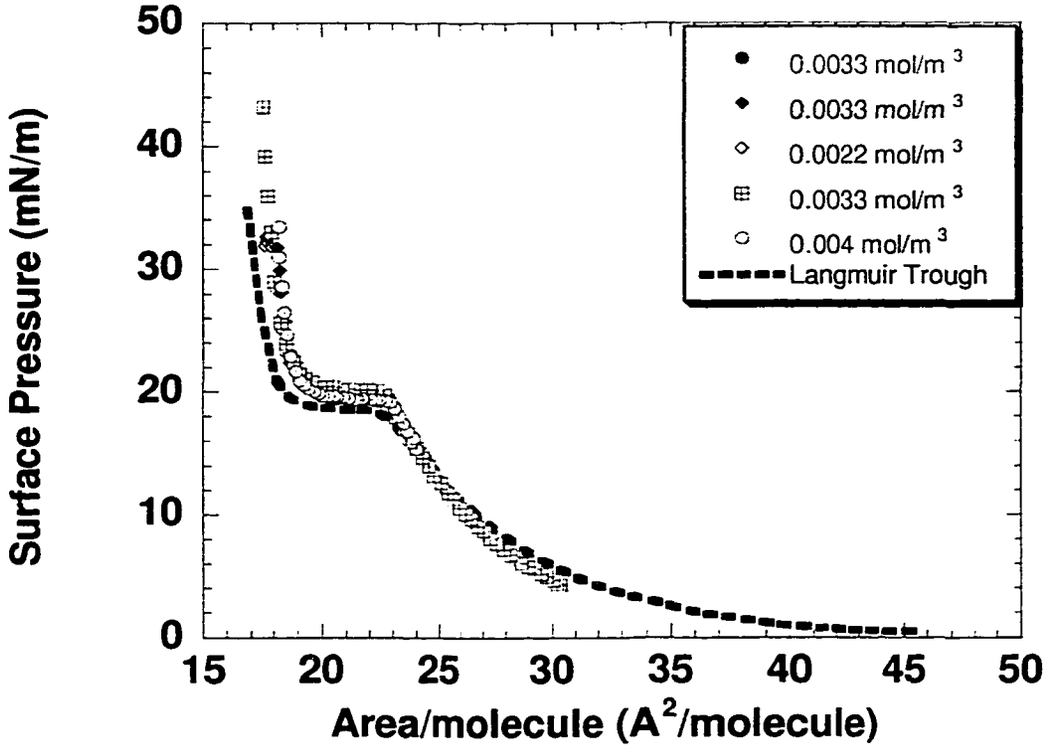

Fig. 4.3: Comparison of the Langmuir Trough Isotherm and the Pendant Bubble as a Langmuir Trough Measurements by Using a Point in the LE Phase as Reference (Area/Molecule at γ=60 mN/m).

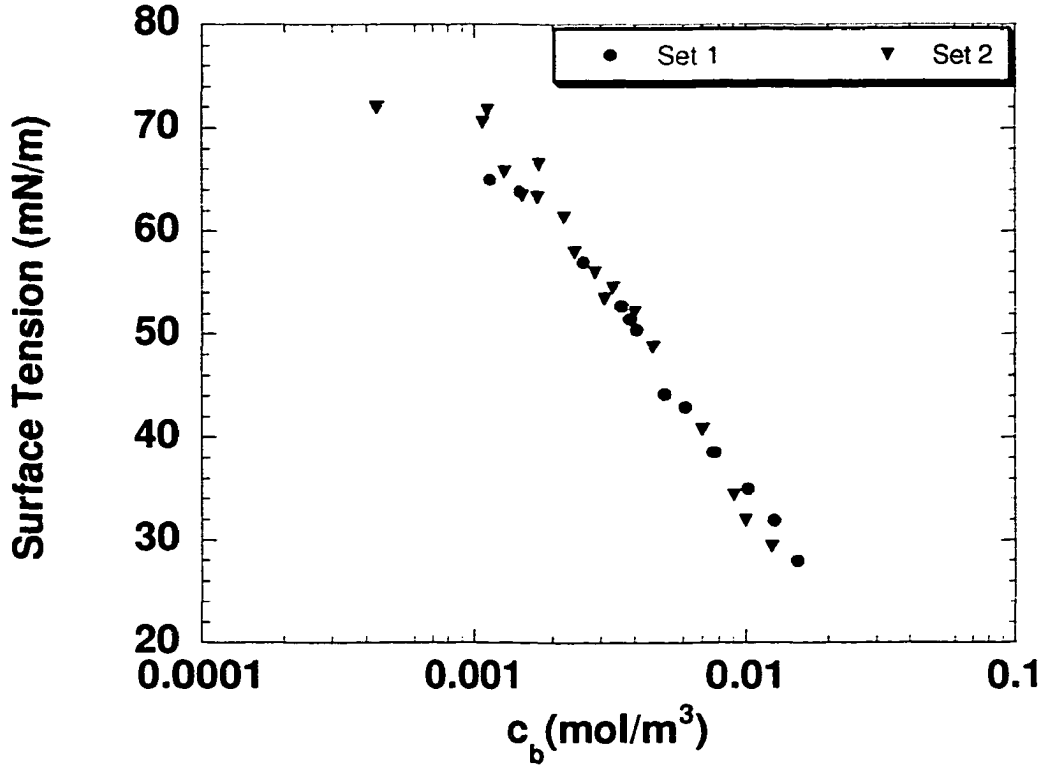

Fig. 4.4: Surface Tension-Bulk Concentration Equilibrium Data for Dodecanol.

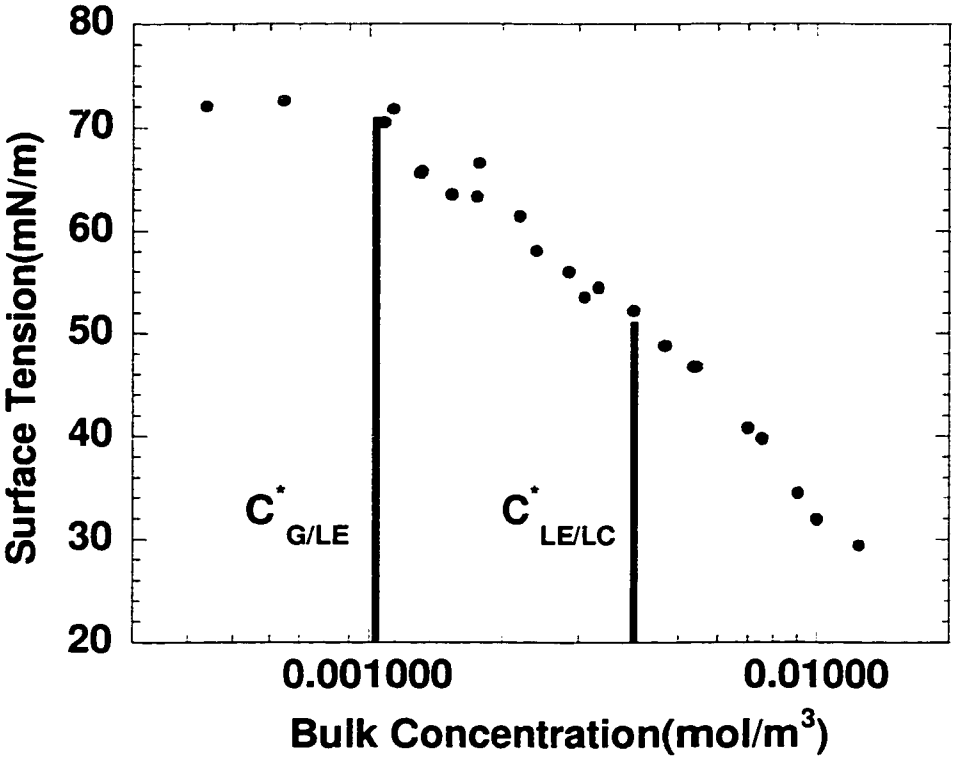

Fig. 4.5: Surface Tension-Bulk Concentration Equilibrium Data Demonstrating the Existence of Cusps For G/LE and LE/LC Phase Transitions.

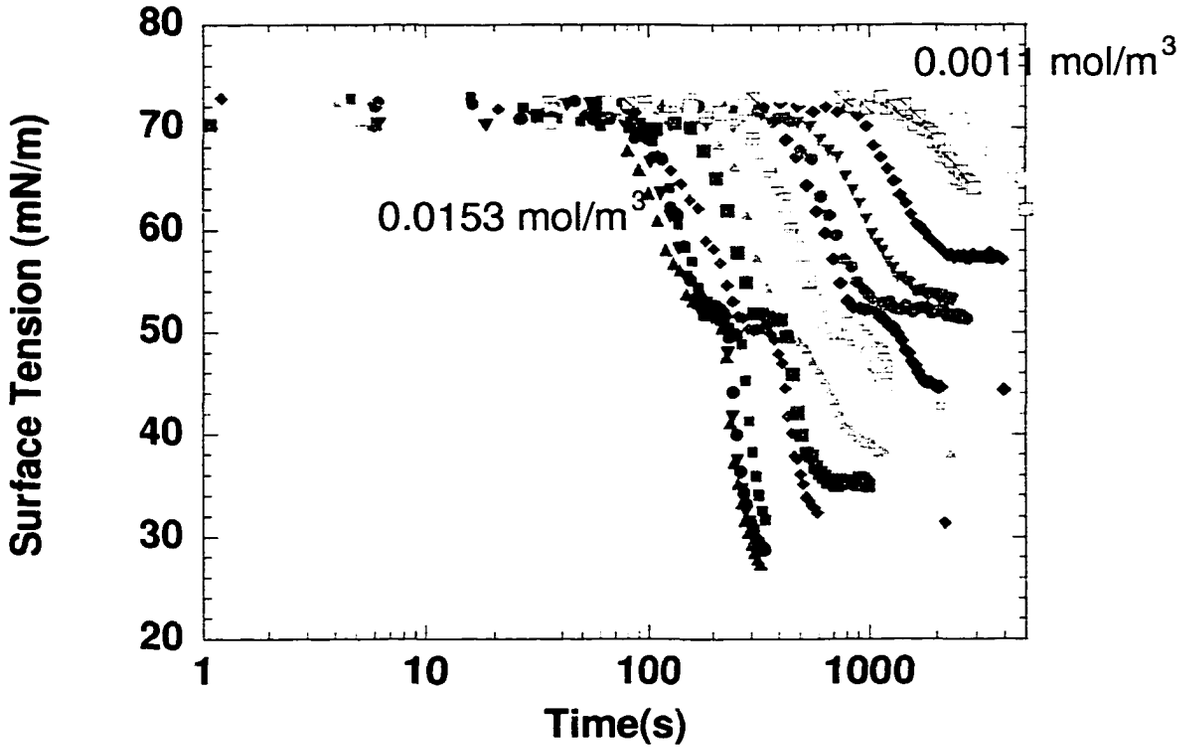

Fig. 4.6: Representative Dynamic Tension Relaxations for Dodecanol at Different Bulk Concentrations Providing Evidence of Self-Assembly to a LC State if the Concentration is High Enough.

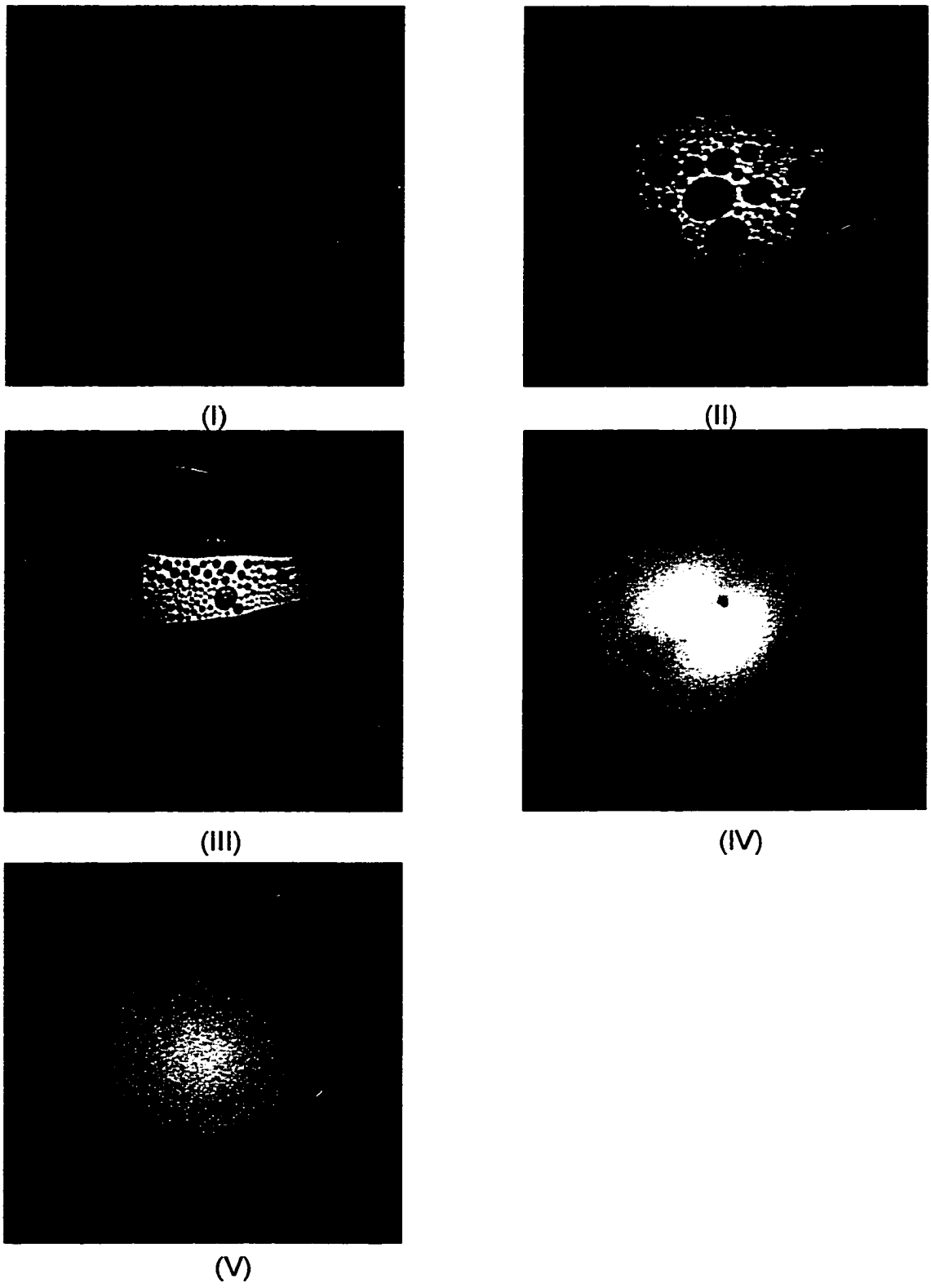

Fig. 4.7 (a): In-Situ Adsorption Monitored by Fluorescence Through a G/LE Phase Transition For Dodecanol.

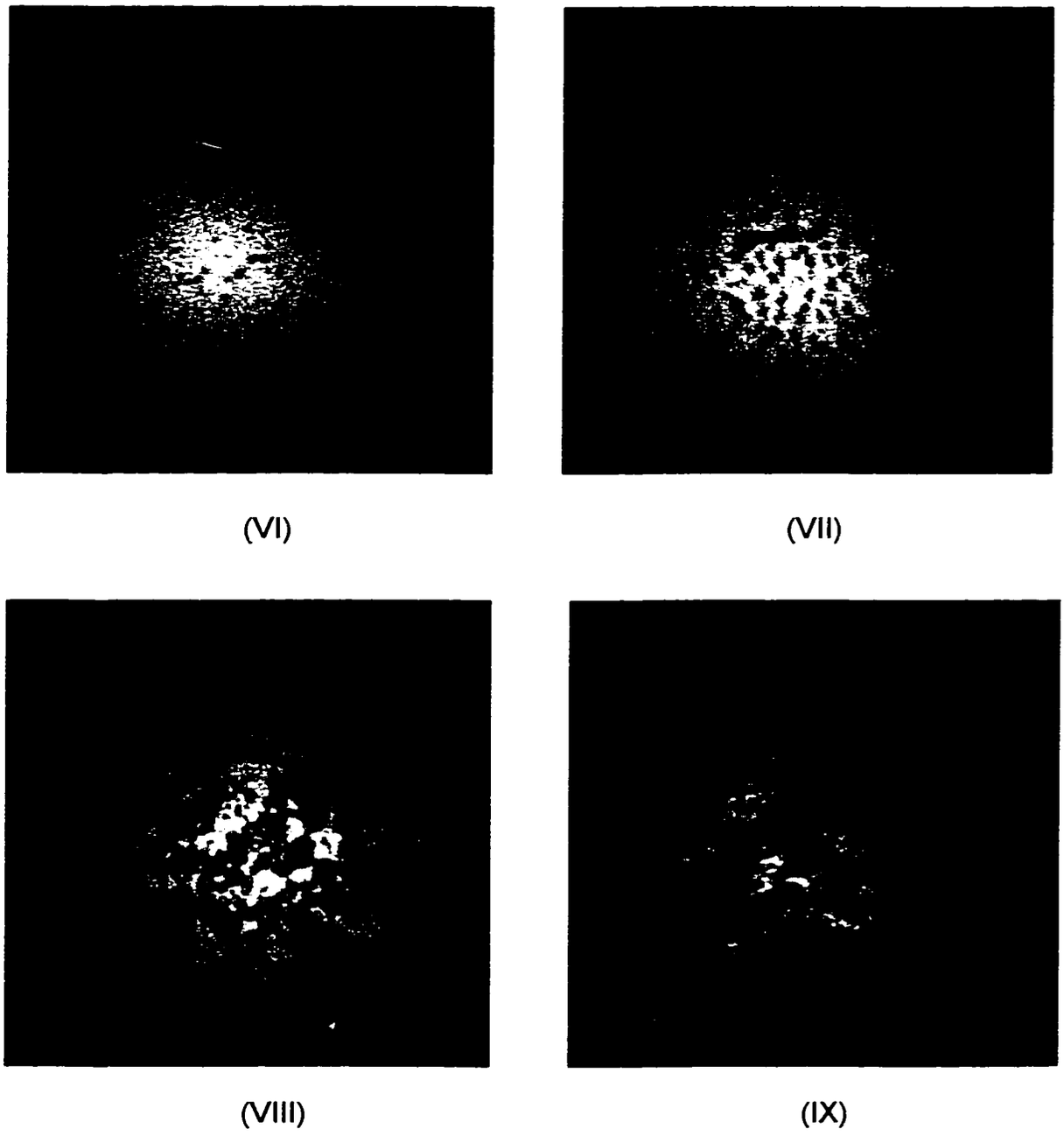

Fig. 4.7 (a) (contd.): In-Situ Adsorption Monitored by Fluorescence Through a LE/LC Phase Transition For Dodecanol.

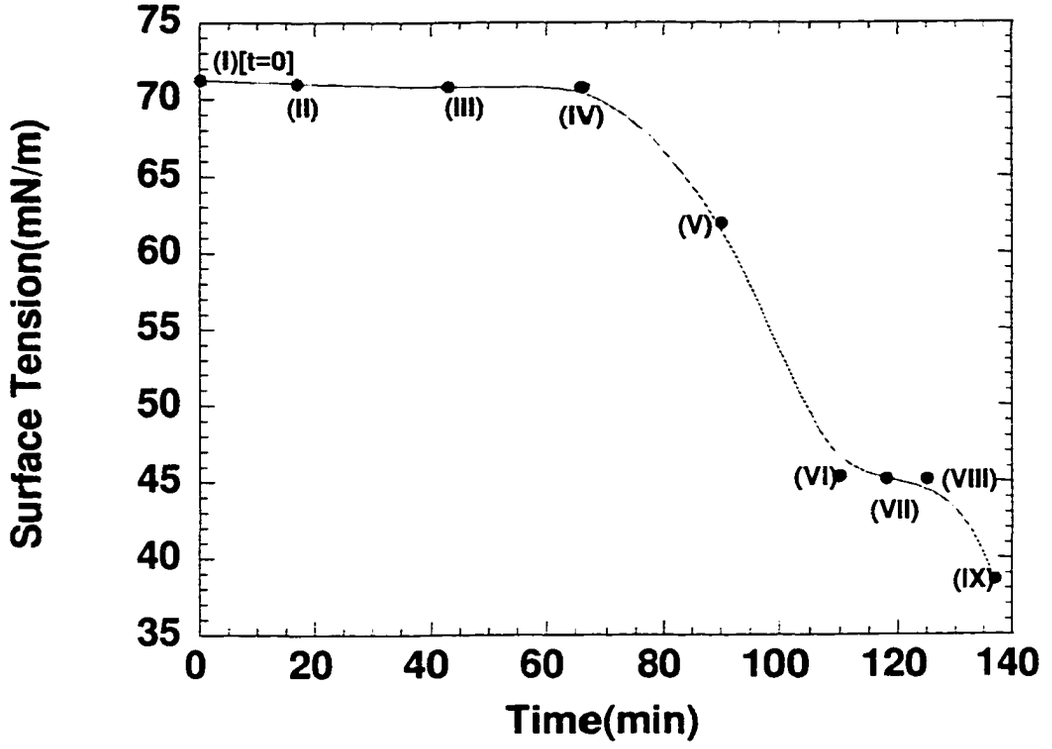

Fig. 4.7 (b): Dynamic Tension Relaxation Measured Simultaneously During the Clean Interface Fluorescence Adsorption Experiment.

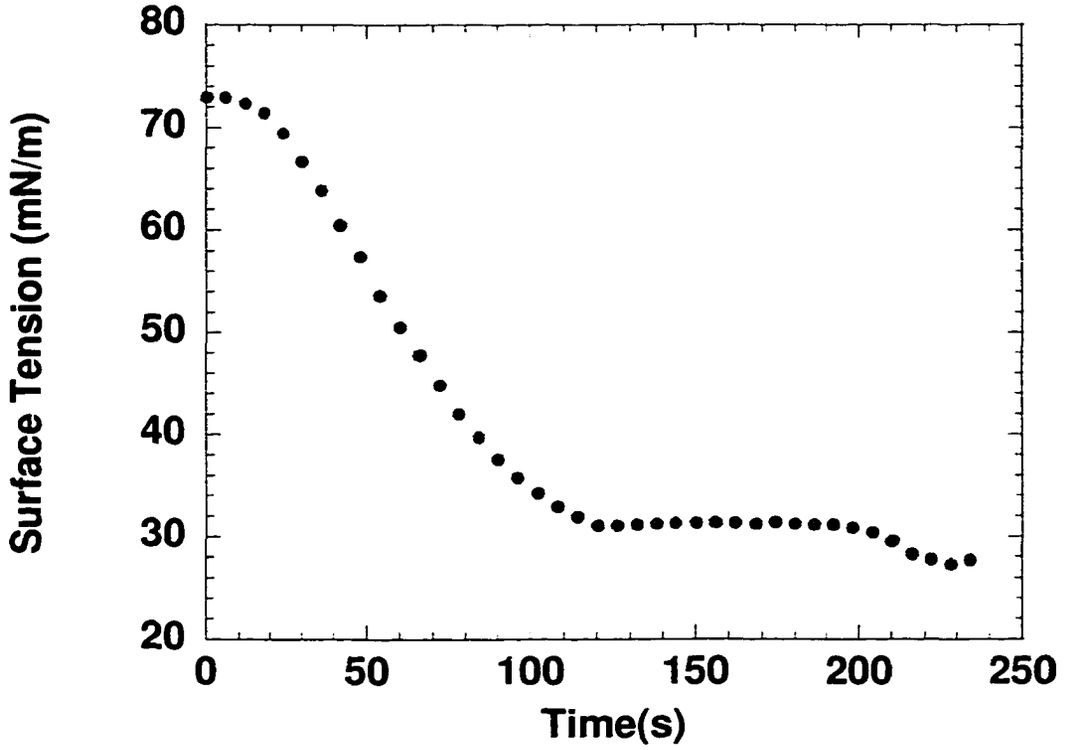

Fig. 4.8: Dynamic Surface Tension Relaxation For a Saturated Aqueous Solution of $C_{12}E_1$.

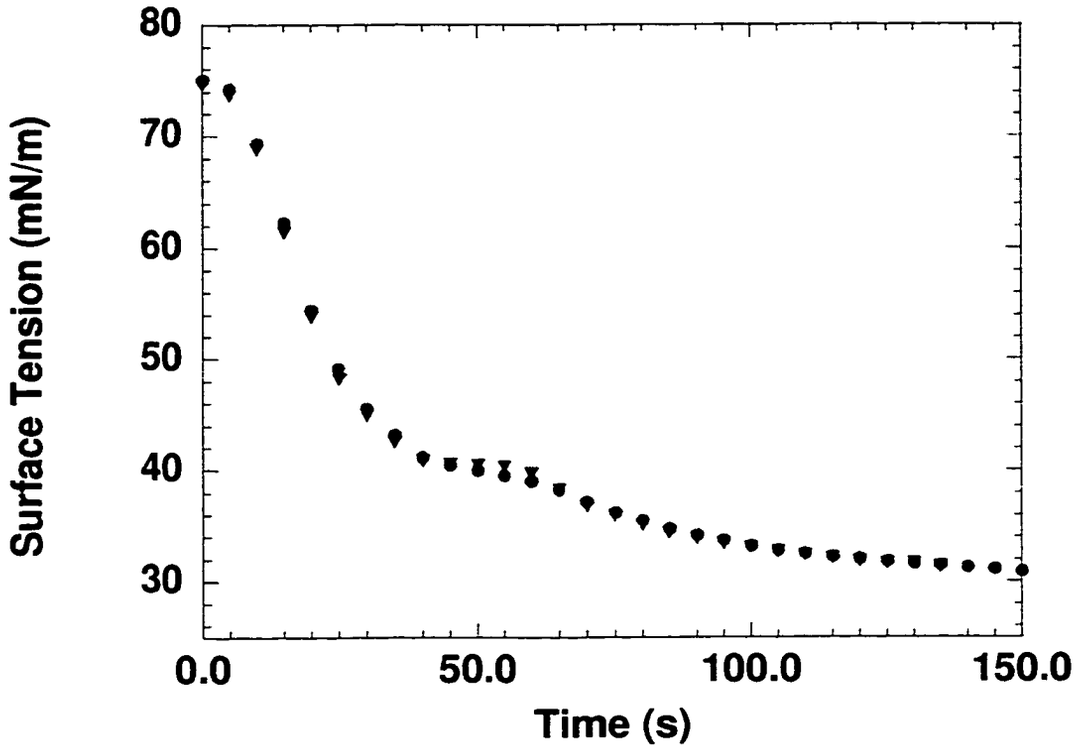

Fig. 4.9: Dynamic Surface Tension Relaxation For a Saturated Aqueous Solution of $C_{11}E_0$.

m n→ ↓	0	1	2	3
10	NO	NO	NO	NO
12	**YES**	**YES**	NO	NO
14	**YES**	**YES**	NO	NO
16	**YES**	**YES**	**YES**	NO

Table 4.1: Phase Envelope For the Poly-(ethyleneoxide) Surfactants (C_mE_n: $CH_3(CH_2)_{m-1}(OCH_2CH_2)_nOH$) Forming Condensed (LC) States at an Air/Water Interface at 20^0 C With Respect to Polar Group Size (n) and Chain Length (m).

References

1)Pallas, N. R.; Pethica, B. A. *Lang.* **1993**, *9*, 361-362.

2)Winch, P. J.; Earnshaw, J. C. *J. Phys.: Condens. Matter* **1989**, *1*, 7187-7205.

3)Hutchinson, E. *Journal of Colloid Science* **1948**, *3*, 219-234.

4)Hutchinson, E. *Journal of Colloid Science* **1948**, *3*, 235-250.

5)Aveyard, R.; Carr, N.; Slezok, H. *Can. J. Chem.* **1985**, *63*, 2742-2746.

6)Berge, B.; Renault, A. *Europhysics Letters* **1993**, *21*, 773-777.

7)Berge, B.; Konovalov, O.; Lajzerowicz, J.; Renault, A.; Rieu, J. P.; Vallade, M. *Physical Review Letters* **1994**, *73*, 1652-1655.

8)Rieu, J. P.; Legrand, J. F.; Renault, A.; Berge, B.; Ocko, B. M.; Wu, X. Z.; Deutsch, M. *Journal of Physics II France* **1995**, *5*, 607-619.

9)Braun, R.; Casson, B. D.; Bain, C. D. *Chemical Physics Letters* **1995**, *245*, 326-334.

10)Casson, B. D.; Braun, R.; Bain, C. D. *Faraday Discussions* **1996**, *104*, 209-229.

11)Trapeznikov, A. *Acta Physicochim URSS* **1945**, *20*, 597.

12)Ross, J.; Epstein, M. B. *Journal of Physical Chemistry* **1958**, *62*, 533-535.

13)Ross, J. *Journal of Physical Chemistry* **1958**, *62*, 531-533.

14)Melzer, V.; Vollhardt, D. *Physical Review Letters* **1996**, *76*, 3770-3773.

15)Volhardt, D.; Melzer, V. *Jounal of Physical Chemistry* **1997**, *101*, 3370-3375.

16)Fainerman, V. b.; Vollhardt, D.; Melzer, V. *Journal of Chemical Physics* **1997**, *107*,
243-251.

17)Melzer, V.; Vollhardt, D.; Brezesinski, G.; Mohwald, H. *Journal of Physical Chemistry B* **1998**, *102*, 591-597.

18)Pollard, M.; Pan, R.; Steiner, C.; Maldarelli, C. *Langmuir* **1998**, *14*, 7222-7234.

19)Johal, M. S.; Usadi, E. W.; Davies, P. B. *Journal of Chemical Society:Faraday Transactions* **1996**, *92*, 573-578.

20)Casson, B. D.; Bain, C. D. *Journal of Physical Chemistry B* **1998**, *102*, 7434-7441.
21)Casson, B. D.; Bain, C. D. *Journal of Physical Chemistry B* **1999**, *103*, 4678-4686.

22)Bain, C. D.; Davies, P. B.; Ward, R. N. *Langmuir* **1994**, *10*, 2060-2063.

23)Brown, A. G.; Thuman, W. C.; McBain, J. W. *Jounal of Colloid Science* **1953**, *8*, 508-514.

24)Lin, S.-Y.; McKeigue, K.; Maldarelli, C. *Langmuir* **1991**, *7*, 1055-1066.

25)Nilsson, G. *Jounal of Physical Chemistry* **1957**, *52*, 1135-1142.

26)Mysels, K. J. *Langmuir* **1986**, *2*, 423-428.

27)Mysels, K. J.; Florence, A. T. *Journal of Colloid and Interface Science* **1973**, *43*, 1973.

28)MacLeod, C. A.; Radke, C. J. *Journal of Colloid and Interface Science* **1993**, *160*, 435-.
29)Czichocki, G.; Volhardt, D.; Seibt, H. *Tenside Detergents* **1981**, *18*, 320.

30)Harkins, W. D.; Copeland, L. E. *Journal of Chemical Physics* **1942**, *10*, 272-277.

31)Pan, R. *PhD Thesis,City University of New York* **1996**.

32)Motomura, K.; Matuura, R. *J. Coll. Int. Sci.* **1969**, *29*, 617-622.

33)Motomura, K.; Matuura, R. *J. Coll. Int. Sci.* **1969**, *29*, 623-628.

34)Motomura, K.; Iwanaga, S.; Hayami, Y.; Uryu, S.; Matuura, R. *J. Coll. Int. Sci.* **1981**, *80*, 32-38.

35)Lu, J. R.; Purcell, I. P.; Simister, E. A.; Thomas, R. K.; Rennie, A. R.; Penfold, J. *Journal of Colloid and Interface Science* **1995**, *174*, 441-455.

36)Gaines, G. L. *Insoluble monolayers at liquid-gas interfaces*; Wiley-Interscience: New York, 1966.

37)Boyd, G. E. *J Phys Chem* **1958**, *62*, 536-541.

Chapter 5

Accelerating the Rate of Formation of Condensed States at the Air/Water Interface

5.1 Introduction

In Chapter 4, it was demonstrated than sparingly soluble surfactants such as dodecanol can assemble from solution onto the air/liquid interface into condensed states. Any potential applications such as those mentioned in Chapter 1 deem that these phases should assemble at an interface fairly rapidly e.g. in the agrochemical spray application, it should take no more than a few seconds. In Chapter 4, we had also seen that at the air/liquid interface, the rate at which the LC phase forms for dodecanol and other similar surfactants is fairly slow owing to their low solubility. It takes for example, more than 300 s for the equilibrium LC state to be reached for a monolayer of dodecanol by assembly from a solution where the surfactant is at its solubility limit. This is by far too slow to be useful in any application.

To accelerate the rate of formation of condensed states there are two approaches. The first is to just accelerate the adsorption rates of the sparingly soluble surfactant. To do that a technique has been suggested by Franses and co-workers[1]. They showed that if the sparingly soluble surfactant could be finely dispersed in aqueous solutions by either sonnication or vigorous stirring or a combination of both, then the finely dispersed (~5 μm) surfactant micro-phases act as reservoirs of surfactant that could rapidly break up due to their small size and easily maintain a high concentration of surfactant monomer (till the solubility

limit). Therefore when the surfactant concentration is depleted in the sublayer due to adsorption, the rapid breakup of these reservoirs prevents reduction in monomer concentration and enables rapid adsorption due to sustenance of high concentration of surfactant near the interface. This is especially true if the monomeric adsorption process is diffusion controlled (no kinetic barriers), because the fast breakup of these reservoirs eliminates diffusional resistance and thereby makes the adsorption process infinitely fast. Indeed, it has been shown by Franses *et al.*[1] that rapid adsorption rates are attainable by dispersed solutions of similar surfactants despite the solubility being extremely low. However it is quite obvious that only freshly prepared dispersed solutions of these surfactants will exhibit fast adsorption dynamics. If the solution is left standing then the particles (surfactant aggregates) will agglomerate to a large size (if solid) or coalesce and phase separate completely to a bigger sized droplet (if liquid) because surface energetics will try to minimize the contact area between the surfactant phase and the aqueous phase. Furthermore the monomer concentration in the bulk would still be at the solubility limit while the breakup times now would be much larger than the adsorption time-scales due to the larger size of these phases. This could create large diffusional resistance and the adsorption process would slow down. Ultimately if the solution is left standing for extended periods of time then the adsorption dynamics will be same as that for a solution in which exactly the amount corresponding to the solubility limit was added. Gentle stirring does not cause the formation of such a dispersed state and therefore does not induce such a supersaturated state as was seen in

Chapter 4 for dodecanol where the adsorption dynamics were slow despite the presence of excess surfactant. There it was also seen that independent of the amount of excess surfactant present as large macro-phases, the dynamic tension reduction was slow and always the same.

The second approach to accelerate the rate of formation of a condensed state is to use a co-surfactant. There is an enormous amount of experimental data in the literature dealing with adsorption and dynamic tension relaxations in binary mixtures of surfactants and a number of attempts have been made to model the same[2,3]. There has been relevant research conducted which quantified individual component amounts in adsorbed films of binary surfactant solution mixtures[4-8] using neutron reflectivity. Their results indicate that in mixtures of surfactants with different surface activity, even a small amount of the more surface active component in the bulk can lead to an increased (much larger) presence on the interface. For example in the SDS/dodecanol mixture a concentration of 2% dodecanol (relative to SDS) in the bulk can cause upto 80% of the interface being populated by dodecanol molecules[6], dodecanol's surface activity being two orders of magnitude larger than SDS. The dodecanol/SDS results provide an explanation for the high surface shear viscosity of mixed monolayers of SDS/dodecanol[9] i.e. it also shows that most of the interface is populated by dodecanol and the that trace amounts of dodecanol in the bulk can induce a surface condensation in the mixed monolayer. Further there is a maxima in dodecanol adsorption at close to but less than the CMC of SDS. Similarly in mixture of polyethoxylates, the more surface-active component,

preferentially adsorbs onto the interface in a large proportion [4]. Bain and co-workers have also shown that mixed surfactant systems of SDS and dodecanol[10] and C_nTAB's and dodecanol[11] also undergo condensation to solid states despite dodecanol being present in very minute quantities in the bulk. The interface in these condensed states has both surfactants present in almost equimolar ratios. These are equilibrium measurements, but non-uniformities during dynamic adsorption of mixed surfactant systems in which one component is much more surface active when compared to the other have also been noticed even at very short times [12-14]. This suggests that even in very short times, the more surface active component can significantly alter the relaxation dynamics, despite being present only in a small quantity in the bulk. Whether the actual transport of the relatively insoluble component has been enhanced or if trace quantities of it can induce "island formation"[6] (understood as a phase change) in the mixed monolayer is not clear.

Based on this available evidence, the idea behind using a second non LC phase forming component is simply that at any given time, two components would have adsorbed instead of one and this gives a higher total surface concentration. The second non-LC forming component can be dissolved in greater amounts in water due to its higher solubility and hence it has higher transport rates to the interface. Further even trace amounts of the condensed phase forming component could significantly effect a mixed monolayer structure and perhaps even lead to the formation of a condensed state. Hence the rate of formation of a condensed state could be accelerated just because there is a

greater adsorbed quantity at a given time and the cohesion between the two components may be enough for the mixed monolayer to form a condensed state. An added advantage of using a second component is that, binary systems are often synergistic and hence the mixed system could prove more effective than the single component. We expect this to be the case for mixtures with small molecules such as dodecanol because they can readily fill voids in the monolayer of the second non-LC forming component and thereby create a close-knit packed structure and this could significantly lower interfacial tensions. Furthermore the second component could even stabilize a dispersion of the LC phase forming component, thereby accelerating the adsorption of this component and the formation of a mixed monolayer in the LC state.

The goals of this chapter are twofold. The first is to see if the rates of formation of condensed states for the LC phase forming surfactants studied in Chapter 4 can be accelerated by dispersing these surfactants finely in water solutions as has been suggested by Franses *et al.*[1]. In this approach a much faster dynamic adsorption process is enabled because the small dispersed aggregates act as reservoirs of surfactant and rapidly breakup to replenish any depleted regions. No mention of the stability of these solutions was discussed as only very freshly prepared solutions were used. If the adsorption dynamics are indeed accelerated then, the solution will be analyzed for its stability to study if the adsorption rates of surfactant from solutions left standing are also fast or does the surfactant precipitate out and reduce the adsorption rates.

The second approach to hasten the formation of condensed states is by addition of a second component. Mixtures of a LC phase forming sparingly soluble surfactant and a second more soluble non-LC phase forming surfactant will be studied to see if the cohesion among the two components is enough to preserve the condensed state and if the time of formation of a condensed state is reduced due to net increased adsorption of surfactant. Dynamic surface tension will be used to study how quickly the condensed states can be formed and fluorescence microscopy will be used to verify the formation of condensed states. The experimental techniques used are given in Sec. 5.2. Sec. 5.3 gives the results of both the dynamic tension and fluorescence experiments. These results are summarized and discussed in Sec. 5.4.

5.2 Experimental

Materials: The poly-(ethyleneglycol) n-alkyl ether surfactants (C_mE_n=CH_3 $(CH_2)_{m-1}(OCH_2CH_2)_nOH$, m=10,12,14;n=4,6),>98% purity, were obtained from Nikko Chemicals, Japan. All chemicals were used as received without any further purification. The medium chain alcohol surfactants (CH_3 $(CH_2)_{m-1}$ OH, m=11,12)>99.9% purity were supplied by Fluka and decanol (>99% purity) from Aldrich. All aqueous solutions were prepared using deionized water purified by a Milli-Q filter system fitted with an Organex-Q column to remove trace contaminants (Millipore, MA). For fluorescence studies, a fluorophore NBD-HDA (4-(hexadecylamino)-7-nitrobenz-2-oxa-1,3-diazole) supplied by Molecular Probes, OR was used. The resistivity of the deionized water was at least 15 MΩ cm.

Preparation of solutions: For surfactants, whose solutions were below the solubility limit, solutions were prepared in the usual way. But for solutions in which surfactants were above the solubility limit in water, two different approaches were adopted. In the first, only gentle stirring over a period of days was carried out. As seen in Chapter 4 for dodecanol, this leads to solutions in which the surfactant monomer reaches its true equilibrium solubility in water. Solutions prepared this way, display the same dynamic tension reduction as those solutions made by adding increasing amounts slightly above the solubility limit. These solutions are very stable over periods of weeks. Further every new solution prepared this way displayed the same dynamic tension reduction despite adding different excess amounts. Thus a solution of dodecanol in water would have a monomer concentration in the bulk of 0.0134-0.0161 mol/m^3 with the excess amount as insoluble flakes whose dissolution/breakup time is large compared to adsorption time scales.

The second protocol adopted for preparing solutions is the dispersion approach suggested by Franses[1]. Aqueous solutions of sparingly soluble surfactants will be prepared by vigorous stirring of these solutions in addition to sonnication. The stability of these dispersions will be studied by leaving them standing over a period of days and measuring the dynamic tension relaxation. If the surfactant precipitates out into large size macro-phases, then the dynamic tension will be slowed down.

Dynamic and Static Interfacial Tension Measurements: For all the solutions used both static and dynamic surface tension measurements were carried out

using the Pendant Bubble and/or the Wilhelmy plate method. These techniques have been described in detail in the preceding chapters.

Fluorescence Microscopy Experiments: Both in-situ and "single shot" fluorescence experiments were carried out. These have also been discussed in detail in the preceding chapters.

5.3 Results

5.3.1 Single component systems

The first results discussed are for the single component LC phase forming surfactants $C_{12}E_0$, and $C_{11}E_0$ and these are contrasted with that for a non-LC phase forming surfactant of comparable size, decanol as well as other non-LC phase forming surfactants of different structure $C_{12}E_6$ and $C_{14}E_6$. It was shown in Chapter 4 that the transport rates of the LC phase forming surfactants to the air/liquid interface with the monomer at its solubility limit is fairly slow and equilibrium is achieved in hundreds of seconds. Aqueous solutions of these surfactants in a dispersed form were prepared by the second protocol described in the experimental section to study if the dynamic adsorption rates can be accelerated. Only freshly prepared dispersed solutions were used. For these solutions attempts were made to measure the dynamic tension reduction due to clean interface adsorption but no realistic dynamic measurements could be made as the adsorption was too rapid (equilibrium reached in a few tenths of a second), thus verifying Franses' results for tetradecanol. It can be presumed that the rates of breakup of aggregates in these solutions are fairly rapid as the adsorption is very fast despite the low solubility (by the mechanism described

earlier). So only the equilibrium values were recorded reliably using both the pendant bubble technique and the Wilhelmy plate. However when these solutions were left standing (no stirring) for extended periods of time, then the excess surfactant precipitated out into large aggregates (for solid) or big drops (for liquid) forming a different phase. Dynamic tension measurements on these solutions could be carried out, as they were far slower (tens of seconds). Hence it is clearly established that dispersed solutions are metastable. The equilibrium surface tension measurements for the dispersed as well as gently stirred solutions are tabulated in Table 5.1[1].

From the results of Table 5.1 we can conclude the following. The first is that the equilibrium tensions for all three-alcohol surfactants (non-dispersed) is about the same although slightly lower for the LC phase forming surfactants (27-28 mN/m). Secondly the freshly dispersed solutions have a lower equilibrium tension than the true saturated solution indicating some degree of super-saturation in the dispersed solutions (when these are left standing, then the equilibrium tension rises to that of the non-dispersed solution and dynamics are slowed down). Dodecanol gives the lowest surface tension among the three surfactants presumably because it packs the tightest. For the other two surfactants $C_{12}E_6$ and $C_{14}E_6$, the equilibrium surface tensions are higher with $C_{12}E_6$ being the highest. This is because of their final state being a loosely packed amorphous state [16].

---

[1] For decanol the equilibrium (non-dispersed) surface tension value was taken from the literature[15]

5.3.2 Results of Mixed Surfactant Systems

From the results of dynamic relaxations of single components $C_{12}E_0$ and $C_{12}E_1$ it is evident that these surfactants do undergo the LE/LC phase transition. However due to the low solubility of these surfactants, the time for assembly into the LC state is too large. To accelerate the rate of formation of condensed states, the first approach adopted was to hasten the adsorption of the single component by itself and one suggested by Franses to produce dispersions of these solutions was adopted. It was seen that the transport rates were indeed accelerated, but the solutions were metastable i.e. the surfactant precipitated out when left standing. Therefore a second approach needs to be devised and this involves using a second component. The motivation behind using a second component as mentioned earlier is that two components may synergistically interact and be more effective in lowering interfacial tensions due to an accelerated formation of the condensed state.

The first dynamic tension experiments were carried out for mixtures of saturated dodecanol solutions in water (gently stirred and not dispersed) and $C_{14}E_6$. If one uses dispersed solutions, then the adsorption rates are too fast and the only measurable quantity is the final equilibrium surface tension. For such an experiment there would be no evidence to prove whether the final packing state of the monolayer was condensed or expanded. However if one uses saturated solutions, then the dynamics are measurable and evidence of phase changes (if any) would be immediately noticeable and it would become clear if the final packing state of the monolayer was condensed or expanded.

The preliminary results on dynamic relaxations in mixed surfactant systems are presented in Fig. 5.1. All the solutions were made by mixing up a small amount of a concentrated solution (>0.063 mol/m^3) of $C_{14}E_6$ in a saturated solution of dodecanol in water (with excess dodecanol) to bring the $C_{14}E_6$ concentration to a pre-calculated level assuming the dodecanol solution to be water. The dynamic tension relaxations for mixtures of saturated dodecanol with $C_{14}E_6$ at four different concentrations (0.0078, 0.0125, 0.0156 and 0.025 mol/m^3) are presented on a single plot (Fig. 5.1). We can clearly see that in each of the first three curves there is a plateau in tension relaxation, almost at the same tension as pure dodecanol, indicating apparently a transition for the mixed monolayer from a LE to a LC state. More importantly there is acceleration by almost an order of magnitude in time for the assembly to a LC state (beginning of the transition). The time for assembly to this state is approximately 200 s for dodecanol and is 50,35 and 25s respectively for the three different solutions (fastest for 0.0156 mol/m^3). Further the equilibrium tension of the mixture (<26 mN/m) is lower than that for any of the individual components (~28mN/m for dodecanol and 31.5 mN/m for $C_{14}E_6$) indicating miscibility of the two components and a synergistic effect in tension reduction. On the other hand in the fourth relaxation (0.0251 mol/m^3l $C_{14}E_6$), the plateau is no longer present, suggesting that eventually due to the increased concentration of the non-LC forming $C_{14}E_6$, its adsorption dominates the mixed monolayer and does not allow the formation of the condensed state. The synergism in dynamic as well as equilibrium tension

reduction is also lost, although eventually dodecanol may replace $C_{14}E_6$ from the interface.

This clearly establishes that by using a co-surfactant one can accelerate the assembly to a LC state upto a certain limit of the concentration of the second component. It is not yet clear if this apparent phase change for the mixed system is brought about by an increased dodecanol transport rate to the interface (the plateau pressure of the phase transition of the mixed monolayer is close to the signature pressure of dodecanol ~50mN/m) or whether a small amount of dodecanol at the interface can precipitate a phase change in the mixed monolayer as has been suggested[6]. In Fig. 5.2, the tension relaxations for pure dodecanol, pure $C_{14}E_6$ at one of the above concentrations and for the mixture with $C_{14}E_6$ at the same concentration are plotted. There is clearly a synergistic interaction among the two surfactants as the relaxation of the mixture is faster than the single component relaxations, and it is much faster than a simple additive effect. For example at 50s, the maximum amounts of dodecanol and $C_{14}E_6$ on the interface (assuming individual adsorption and a diffusion limited case and short times) are 50 and 95 $Å^2$/molecule respectively, while the mixture tension of 50 (beginning of plateau) would indicate a packing in the monolayer of less than 25 $Å^2$/molecule (based on the surface coverage at the beginning of the LE/LC transition for pure $C_{12}E_0$ as measured in chapter 4).

For a two component system, the phase rule does not require a plateau in tension for a phase transition to occur. Therefore to verify if the mixture is indeed undergoing a transition to a condensed state, fluorescence experiments were

undertaken. There are two possibilities. Either the mixed monolayer is a miscible one with both phases containing both components or they are acting as a host-guest system. The fact that there is a plateau in surface tension and because the surface tension at which the dynamic tension plateaus off for the mixture is close to that for dodecanol by itself, seems to suggest that the system is behaving like a host-guest system. In this picture, the isolation of the dodecanol molecules and subsequent squeezing of it by $C_{14}E_6$ causes the phase transition with the condensed state consisting primarily of dodecanol molecules. This state would then be in equilibrium with an expanded state consisting of both components. However the synergism among the two components suggests that the monolayer is a miscible one and both components co-exist in both phases.

In either case, to understand why the rate of formation of the condensed state has been accelerated, we need to verify if trace amounts of the LC phase forming component can induce a phase transition in the mixed monolayer. For this we carried out single-shot spreading fluorescence experiments on a constant area teflon cell. Similar experiments have been carried out in Chapter 2 but are briefly described here. Chloroform solutions of two-component surfactant systems (mixtures of $C_{14}E_6$ and $C_{12}E_0$) in different proportions with a fluorescent dye were quickly spread onto the air/water interface of a teflon cell at initially known coverages. The images were then recorded rapidly.

Two such experimental results are shown in Figs. 5.3 (a) and 5.3 (b). It is clear that based on the amount initially spread, the mixed monolayer is in two-phase coexistence with dark condensed domains in a bright background.

Surfactant immediately begins to desorb off the surface and the monolayer goes into a bright LE state. The important result however is that the mixed monolayer forms a condensed state at surface concentrations lower than that is required for dodecanol to form the condensed state by itself. As seen in Fig. 5.3 (b) even when the dodecanol concentration is 41 $Å^2$/molecule which is much lower than that is required for it to form the condensed state by itself (25 $Å^2$/molecule), the mixed monolayer is in two phase coexistence or a condensed state. This implies that small quantities of the non-LC phase forming component are enough to induce a phase transition in the mixed monolayer. This could explain why the dynamic surface tension for the mixed monolayer shows an apparent transition to a condensed state at times much shorter than that is required for the individual components.

While these results are promising in itself and demonstrate that mixtures of polyethoxylates and alcohols are synergistic in tension reduction while maintaining a condensed state of the monolayer, the dynamics are still too slow for any application. Hence it was decide to test solutions made by dispersing the LC phase forming surfactant in aqueous solutions of high concentrations of the second component instead of water. Hence dispersed solutions of dodecanol in aqueous solutions of both $C_{14}E_6$ (0.48 mol/m^3) and $C_{12}E_6$ (0.69 mol/m^3 and 0.72 mol/m^3) at concentrations much greater than the CMC were prepared. As no dynamic tension measurements could be carried out for these solutions, only equilibrium surface tension measurements were carried out. Table 5.2 gives these results. It is clear that mixtures of $C_{12}E_6$ and $C_{12}E_0$ are more synergistic in

reducing the surface tension than mixtures of $C_{14}E_6$ and $C_{12}E_0$. This can be attributed to the better isolation of the hydrophobic chain from water in the surfactant combination whose chain lengths are identical. Also the mixture of $C_{12}E_6$ and $C_{12}E_0$ is highly synergistic in lowering the air/liquid surface tension (21 mN/m). This value is attained almost spontaneously indicating extremely fast dynamics. Further these solutions appear to be more stable and demonstrate similar tension lowering ability even when left standing even over a period of days when compared to the single component system which is highly metastable. This suggests that the non-LC phase forming component somehow contributes to the stability of the dispersion of the LC phase forming component and adsorption rates of both surfactants are fast.

To verify that the mixed surfactant system of $C_{12}E_6$ and $C_{12}E_0$ is so synergistic in tension reduction because they too form a condensed state, it was decided to undertake in-situ fluorescence adsorption experiments. The experiment was very similar to that carried out in Chapter 3 for $C_{14}E_6$ and that in Chapter 4 for $C_{12}E_0$. The only difference here was that only small quantities of the aqueous solution of the mixed surfactant system were injected beneath the interface. Since all solutions are either above the CMC ($C_{12}E_6$) or above the solubility limit ($C_{12}E_0$), we expect the final equilibrium state to be the same as in the pendant bubble surface tension experiments. At these concentrations, the initial water in the cell is not sufficient to dilute the surfactant concentration enough, so as to cause a change in the final surface equilibrium composition.

Again the surface tension was monitored during the adsorption process by using a Wilhelmy Plate electrobalance.

Shown in Fig. 5.4 is the sequence of images for the evolution of phases with adsorption for the mixed surfactant system at 25^0 C. Fig. 5.4 (a) is the image of the clean interface with just the dye present, and the measured surface tension was 72.4 mN/m. Immediately after the flow was started the monolayer turned into a completely bright LE state (Fig. 5.4 (b)) this was accompanied by a drop in surface tension to 60 mN/m (Here the G/LE transition is not evident because the bulk concentration was very high and thereby the critical density of the nucleating LE phase was presumably achieved instantaneously). Upon continuation of flow, the dark domains nucleated in a bright background at a tension of 38-39 mN/m. These grew in number and size (Figs. 5.4 (c)- (e)) with further adsorption but with the tension staying nearly constant at this value. Eventually when most of the surface was dark (LC) (Fig. 5.4 (f)), other than the dye trapped between the dark domains, the tension dropped rapidly to 30 mN/m. Eventually with the interface staying in the LC state the tension dropped to 21 mN/m which was exactly the same value as in the pendant bubble measurements. This experiment therefore verifies that the synergistic surfactant mixture of $C_{12}E_6$ and $C_{12}E_0$ also undergoes a phase transition to a LC state. The formation of the condensed state in the mixed monolayer is the cause for the synergism in tension reduction.

5.4 Summary and Discussion

From results of Chapter 4, we had been able to identify bulk soluble surfactants $C_{12}E_0$ and $C_{12}E_1$ that have the ability to assemble from solution to a LC state. However owing to the limited solubility of these in water the dynamics of assembly to a LC state is not rapid enough to be applicable directly in industrial processes. Two approaches have been used to accelerate the formation of condensed states at interfaces using these surfactants. In the first, the procedure adopted by Franses is utilized. Here the surfactant is finely dispersed in water by vigorous stirring or sonnication or a combination of both. Enhanced transport rates of the sparingly soluble surfactants to interfaces where achieved using this approach. However solutions prepared this way are metastable and surfactant precipitation upon standing reduces the adsorption rates to that of a solution with the monomer at the solubility limit in water.

In the second approach, a co-surfactant is used to accelerate the assembly to a LC state. Combinations of dodecanol and $C_{14}E_6$ have been shown to be able to assemble to a LC state in an order of magnitude less time as compared to dodecanol by itself. In addition the mixed surfactant system is synergistic in reducing the equilibrium surface tension. Spread monolayers of the two component systems demonstrated that condensed states could form in mixtures at surface concentrations much lower than that required for the single LC phase forming component by itself and this explains the accelerated formation of the condensed state. Investigation of other pairs demonstrated that the combination of $C_{12}E_6$ and $C_{12}E_0$ was the most synergistic in surface tension

reduction. Also dispersions of $C_{12}E_0$ in high concentration aqueous solutions of $C_{12}E_6$ were able to reduce the surface tension to very low values very rapidly. These dispersed solutions were found to be more stable than the single component systems when left standing. In-situ fluorescence microscopy conformed that this system too forms condensed states at the air/liquid interface.

Solution	Equilibrium Surface Tension (mN/m) (Non-Dispersed)	Equilibrium Surface Tension (mN/m) (Dispersed)
Water	72.5	--------
$C_{12}E_0$	27-28	24-26
$C_{11}E_0$	28	26-27
$C_{10}E_0$	29	27-28
$C_{12}E_4$	29	28
$C_{12}E_6$	32.5	---------
$C_{14}E_6$	31	---------

Table 5.1: Equilibrium Surface Tension Measurements For the Dispersed as well as Non-Dispersed Solutions.

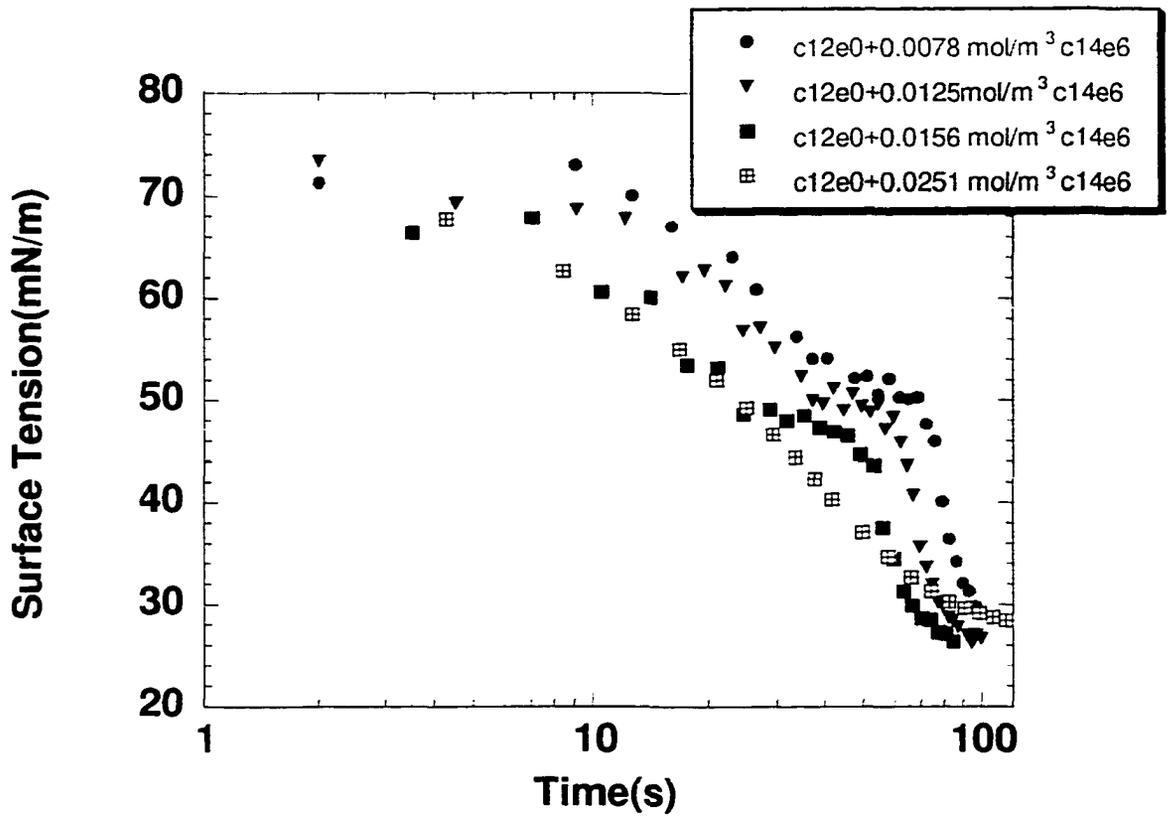

Fig. 5.1: Dynamic Surface Tension Relaxations For Mixtures of Saturated Solutions of Dodecanol With Increasing Concentrations of $C_{14}E_6$ Demonstrating the Formation of Condensed States in the Mixed Monolayer at Shorter Times and the Synergism among the Two Components.

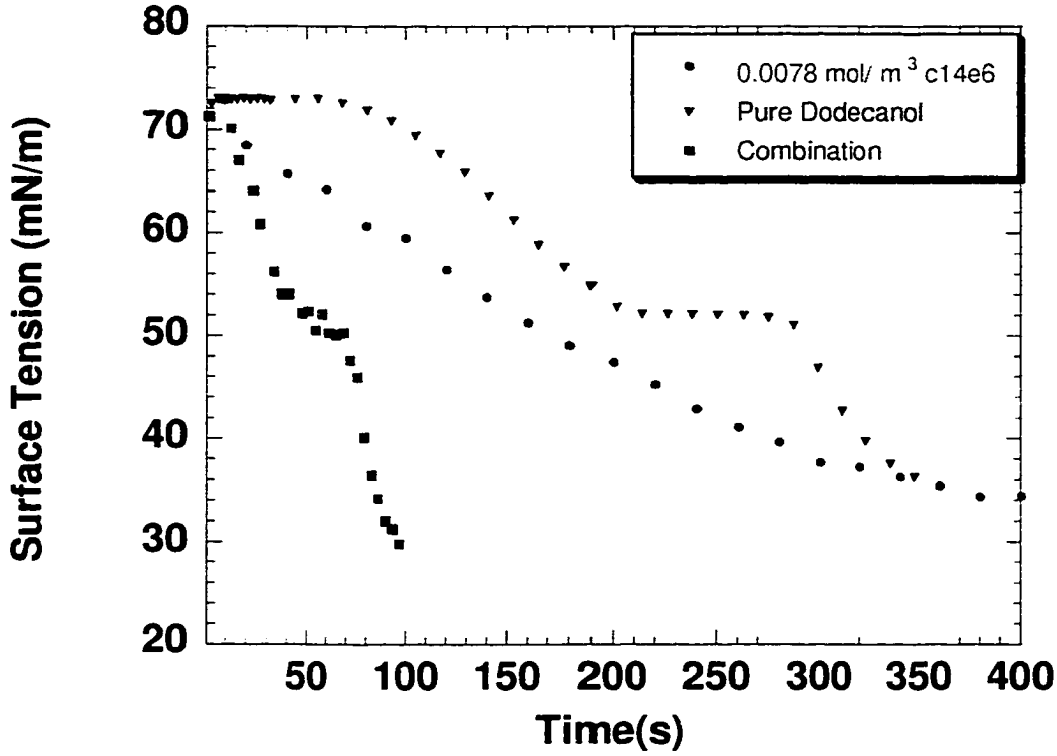

Fig. 5.2: Comparison of Dynamic Surface Tension Relaxations For Dodecanol at its Solubility Limit, A Solution of $C_{14}E_6$ at a Known Concentration and the Mixture of The Two Demonstrating the Acceleration in Formation of Condensed States in the Mixed Monolayer at Shorter Times due to the Synergism Among the Two Components.

(a)

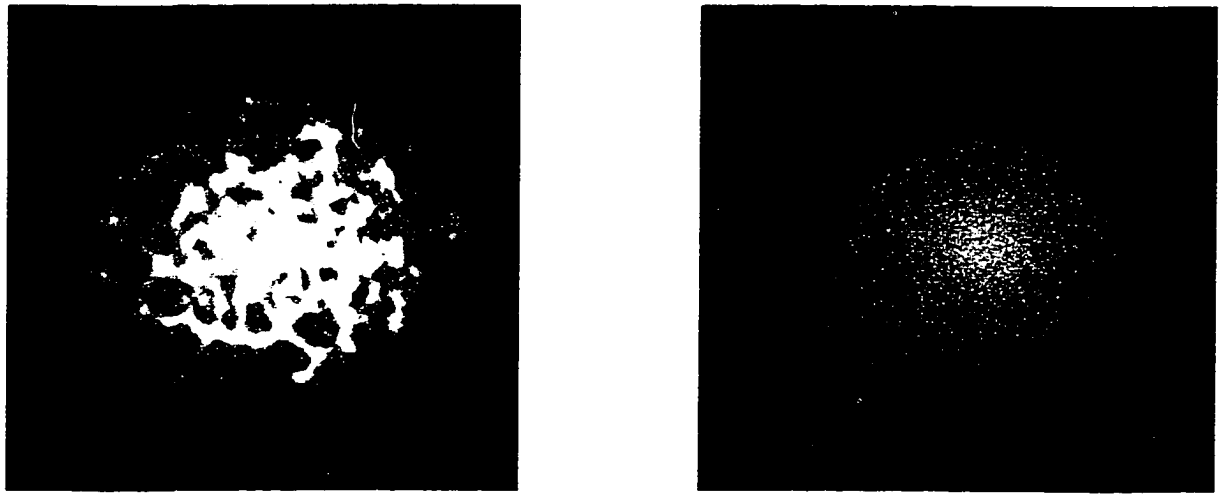

(b)

Fig. 5.3: Single Shot Fluorescence Images For Mixed Monolayers of $C_{12}E_0$ and $C_{14}E_6$ Verifying the Formation of Condensed States in the Mixed Monolayer ((a) $C_{12}E_0$ at 28 $Å^2$/molecule and $C_{14}E_6$ at 102 $Å^2$/molecule (b) $C_{12}E_0$ at 41 $Å^2$/molecule and $C_{14}E_6$ at 95 $Å^2$/molecule). The Image on the Right is the Monolayer after the Surfactant(s) Begin to Desorb.

Binary Mixture	Equilibrium Surface Tension (mN/m)
$C_{12}E_0$/ $C_{12}E_4$	22-23
$C_{12}E_0$/ $C_{12}E_6$	21-22
$C_{11}E_0$/ $C_{12}E_6$	24-25
$C_{10}E_0$/ $C_{12}E_6$	25.5
$C_{12}E_0$/ $C_{14}E_6$	22-23.5

Table 5.2: Equilibrium Surface Tension Measurements For Solutions of Binary Surfactant Mixtures.

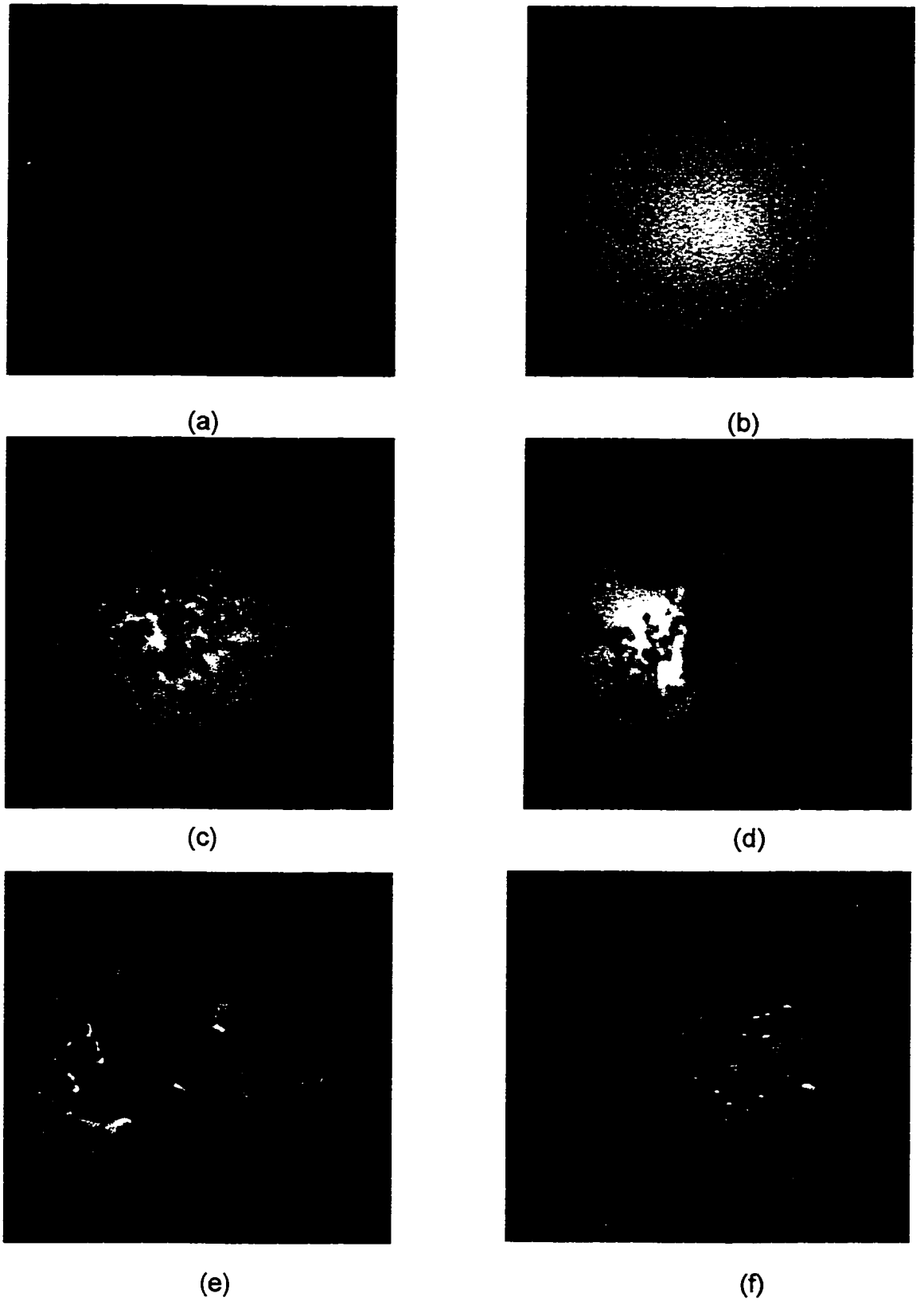

Fig. 5.4: In-Situ Adsorption Monitored by Fluorescence Through a LE/LC Phase Transition For the $C_{12}E_6/C_{12}E_0$ Mixture.

References

1)Myrick, S. H.; Franses, E. I. *Langmuir* **1999**, *19*, 1556-1561.

2)Siddiqui, F. A.; Franses, E. I. *AIChE* **1997**, *43*, 1569-1578.

3)Nikas, Y. J.; Puvvada, S.; Blankschtein, D. *Langmuir* **1992**, *8*, 2680-2689.

4)Penfold, J.; Staples, E.; Thompson, L.; Tucker, I. *Colloids and Surfaces A* **1995**, *102*, 127-132.

5)Penfold, J.; Staples, E.; Thompson, L.; Tucker, I.; Hines, J.; Thomas, R. K.; Lu, J. R. *Langmuir* **1995**.

6)Lu, J. R.; Purcell, I. P.; Simister, E. A.; Thomas, R. K.; Rennie, A. R.; Penfold, J. *Journal of Colloid and Interface Science* **1995**, *174*, 441-455.

7)Staples, E.; Thompson, L.; Tucker, I.; Penfold, J.; Thomas, R. K.; Lu, J. R. *Langmuir* **1993**, *9*, 1651-1656.

8)Staples, E. J.; Thompson, L.; Tucker, I.; Penfold, J. *Langmuir* **1994**, *10*, 4136-4141.

9)Poskanzer, A. M.; Goodrich, F. C. *The Journal of Physical Chemistry* **1975**, *79*, 2122-2126.

10)Casson, B. D.; Bain, C. D. *Journal of Physical Chemistry B* **1998**, *102*, 7434-7441.

11)Casson, B. D.; Braun, R.; Bain, C. D. *Faraday Discussions* **1996**, *104*, 209-229.

12)Czichocki, G.; Volhardt, D.; Seibt, H. *Tenside Detergents* **1981**, *18*, 320.

13)Fainerman, V. B.; Miller, R. *Colloids and Surfaces A* **1995**, *97*, 65-82.

14)MacLeod, C. A.; Radke, C. J. *Journal of Colloid and Interface Science* **1993**, *160*, 435-.

15)Lin, S.-Y.; McKeigue, K.; Maldarelli, C. *Langmuir* **1991**, *7*, 1055-1066.

16)Pan, R.; Green, J.; Maldarelli, C. *Journal of Colloid and Interface Science* **1998**, *205*, 213-230.

Chapter 6

Using Surfactant Mixtures to Promote Spreading and Minimize Droplet Rebound upon Impact on Hydrophobic Surfaces

6.1 Introduction

Spreading of aqueous solutions on solid surfaces is an important phenomenon not only in nature but also in a broad spectrum of industrial applications. Aqueous formulations do not wet hydrophobic surfaces. When an aqueous drop is placed on such a surface, the liquid subtends a large contact angle with the solid. Hydrophobic surfaces are low energy, non-polar surfaces and consequently the solid liquid tension is high (polar/non-polar) and the air-liquid tension is low (non-polar/non-polar) and this causes the drop to bead up and not spread. The ability of the drop to spread out or bead up on surfaces is dictated by the balance of the air/liquid ($\gamma_{L/A}$), the solid/liquid ($\gamma_{S/L}$) and the air/solid ($\gamma_{S/A}$) interfacial tensions at the three phase contact line. Fig. 6.1 is a schematic of a droplet sitting on a hydrophobic surface with the three interfacial tensions subtending an obtuse contact angle ($\theta > \pi/2$). Here the air/liquid tension acts in conjunction with the air/solid tension to balance the high solid/liquid tension. This balance (eq. 6.1) is expressed mathematically by the Young-Dupré equation which fixes the equilibrium static contact angle (θ_e):

$$\gamma_{S/A} - \gamma_{S/L} = \gamma_{L/A} \cos\theta_e \qquad [6.1]$$

Examples of low energy surfaces commonly encountered include teflon, parafilm and many foliate surfaces in nature. Besides the surface properties

(polarity etc.), the second factor which dictates spreading of drops on surfaces is the roughness of the substrate. Rough surfaces consist of macroscopic crests and troughs. On rough surfaces, the three-phase contact line can get pinned very easily in a trough for instance[1] and the drop will stop spreading. Fig. 6.2 is a schematic of a section of a drop on a rough surface and a simple free energy calculation for the change in energy for the water to spread yields Wenzel's equation[2] (eq. 6.3). The main assumption made in deriving this equation is that the surface is assumed to be of uniform roughness (r is the ratio of the length of a smooth to a rough surface and is always greater than unity). For water to spread by a length dx the free energy change[2] is:

$$dG_s = r * dx * (\gamma_{S/L} - \gamma_{S/V}) + dx * \gamma_{L/V} * \cos(\theta) \qquad [6.2]$$

To obtain the equilibrium configuration, we differentiate eq. 6.2 with respect to r to minimize the free energy change with respect to r. This yields:

$$\cos(\theta^{*}) = r * \cos(\theta_e) \qquad [6.3]$$

Since r>1, roughness amplifies the hydrophobicity if the initial contact angle is greater than 90^0 and causes the drop to achieve much higher contact angles on the rough surface as compared to the smooth surface. This equation obviously is not always applicable because the cos function is bounded whereas r is unbounded. A detailed thermodynamic analysis using the concepts of surface energies has been utilized to study the effect of surface roughness[2] on spreading by many groups. Such an analysis yields for instance the Cassie-Baxter equation.

The amplification of de-wetting due to roughness has also been demonstrated experimentally in recent publications[2-4]. Surfaces were modified by melting alkylketenedimer (AKD) on solid surfaces of glass. Scanning electron micrographs (SEM) of these surfaces showed an extremely rough fractal pattern and water contact angles of even 174^0 were observed. When these surfaces were flattened out by physical means the contact angle was reduced to 109^0. Thus super-water repellant surfaces can be obtained if the surface is extremely rough in addition to being hydrophobic. A more systematic experimental study of roughened surfaces was carried out by Bico *et al.*[2] where the effect of different controlled patterned roughness' on the contact angle was studied. Here substrates of silicon were made hydrophobic by grafting a self-assembled monolayer of a fluorosilane, after inducing microstructure using a sol-gel casting process using tetramethyorthosilicate. The different patterns studied were shallow cavities, stripes and spikes. All defects were in the micrometer range. The roughness increased water contact angles from 110 for the planar surface to about 170 for the spikes. They claimed that the main criterion for increased hydrophobicity was not just the roughness but the fraction of solid in contact with the liquid. Thus spiked interfaces (fraction=0.05) had the highest contact angle despite the roughness 'r' being only 1.15. Once again surface inhomogeneities amplify the non-wettability of surfaces.

One instance where such an amplification of surface hydrophobicity is problematic in day-to-day life is the spray delivery of agro-chemicals (pesticides, insecticides and fungicides) onto foliar surfaces. Leaf surfaces are often

unusually hydrophobic for two reasons. The first is that the leaf epidermis is covered with a layer of wax crystals. Plants secrete wax to make the leaf surface more hydrophobic. This is nature's self cleaning mechanism in which a lack of water retained on leaf surfaces leads to low germination and growth of spores, parasites and other fungi. The size and the density of these crystals determine the extent of hydrophobicity of the surface. The waxy layer causes an increase in the solid/liquid tension. The second factor contributing to the hydrophobicity is that leaf surfaces are extremely rough and have bumps and trichomes (hairs). This roughness amplifies the hydrophobicity due to reasons discussed above. Typically foliate surfaces subtend equilibrium water contact angles greater than 90^0 and therefore these formulations do not wet them readily. This prevents the active from readily penetrating the leaf surface as the contact area is reduced, and this reduces the efficacy of the formulation. In a static case of drops beaded up on a hydrophobic leaf surface, they can easily roll-off once the leaf is tilts due to the weight of the drop. From an environmental point of view, this effect of the formulation directly draining into the soil is not acceptable.

Hydrophobic surfaces are even more problematic in dynamic conditions, for instance when droplets of a spray formulation impact on a leaf surface. Reichard[5] studied retention of water droplets of typical spray drop sizes on different foliate surfaces and found that on some hydrophobic surfaces such as cabbage leaves, there was a 100% reflection of droplets of all sizes. Table 6.1 gives Reichard's data on reflected amounts on different leaf surfaces. This underscores the importance of this problem in day-to-day life.

Quiere[6] *et. al.* also carried out drop impact experiments on the unusually rough patterned surfaces they developed. They very nicely demonstrated that water drops could even undergo multiple rebounds literally like a bouncing ball before the viscous effects damped out the oscillations. This once again verified that roughness and surface properties could cause reflection of water drops impacting on the surface.

Why do droplets reflect off from hydrophobic surfaces? As a spray droplet first impacts on such a surface, the drop fluid is pushed sideways and it begins to spread. Spreading of liquids on solids has been studied extensively [7-10]. The regime of spreading we are interested in is the case of dry spreading in the absence of an initial water layer (hydrophobic surface) or a precursor film drawn out in advance of the spreading drop. Here, the drop begins to move over the surface when the instantaneous contact angle $\theta(t)$ increased by the lateral motion of the liquid, becomes larger than the static advancing angle (θ_A). If the surface is atomically smooth then θ_A is equal to θ_e. The more heterogeneous the surface is, the greater is the difference θ_A-θ_e as the liquid has to develop angles greater than θ_e to pass over non-uniformities on the surface. Similarly as liquid recedes on a surface the angle must be less than the static receding angle θ_R. The contact line stays pinned or near pinned for $\theta_A > \theta(t) > \theta_R$. Since $\theta_A > \pi/2$, the initial spreading rate along the contact line is slow. As the fluid is forced out laterally with the contact line not moving appreciably, the curvature of the drop near the equator increases and thereby raises the pressure in the liquid in the curved region. This increased capillary pressure at the bulging ends forces a reversal of flow towards

the drop center with a receding contact angle that can cause the drop to detach. This has been demonstrated experimentally by Mao *et al.*[11] for water droplets impacting on a hydrophobic paraffin wax surface and by Reichard[5] on hydrophobic leaf surfaces. It has also been shown experimentally [11] that if the surface is more hydrophilic and the static advancing angle is lower, then the drop spreads further as the contact line moves further and only a small radius of curvature develops. Consequently the droplet does not rebound from such surfaces as was demonstrated for stainless steel and glass.

As mentioned earlier and as is discussed in Reichard's paper, the rebound of spray droplets off of actual leaf surfaces is of major concern to the agrochemical industry. Surfactants dissolved in the aqueous drop phase have long been used to promote retention of drops on hydrophobic leaf surfaces. This adjuvacy has been attributed to the tension lowering ability of surfactants. When surfactant adsorbs onto the air/liquid or solid/liquid interfaces, the polar groups remain in contact with the aqueous phase while the non-polar chains are removed from the water interior and cohere together either in air (air/water interface) or against the hydrophobic solid surface. This adsorption lowers the surface energies and tensions in proportion to the amount adsorbed Γ. Below the CMC, for a given bulk concentration c_b there is an equilibrium-adsorbed amount $\Gamma(c_b)$ and an equilibrium tension $\gamma(c_b)$ at either interface. The adsorption of surfactant therefore lowers both the air/liquid and solid/liquid tensions and thereby the equilibrium as well as static advancing and receding contact angles. Now as the contact line advances, the curvature (and therefore the capillary

pressure) at the drop equator does not increase sufficiently to cause reflection. For a surfactant to be effective, it must rapidly adsorb onto the air/water interface in the time of flight of the drop (typical size 100-1000μm) which is of the order of a few seconds at most. In addition it must also adsorb onto the solid/water interface within the typical drop impact and spreading time scales (~50 ms). To rapidly and significantly lower the interfacial tensions, bulk concentrations much greater than the CMC are used in commercial formulations. Dynamic tension measurements have shown that micellar solutions can cause this rapid air/water tension reduction in time scales shorter than the time of flight [12].

While studies of adsorption and tension dynamics at the air/liquid interface are numerous, the adsorption dynamics and tension reducing ability of surfactants at the solid liquid interface, despite being extremely crucial have been largely ignored. For a drop to spread on a hydrophobic surface ($\theta>90^0$, $\cos\theta<0$), it is immediately evident from the Young-Dupré equation written in a modified form in eq. 6.4

$$\cos\theta_e = \frac{(\gamma_{S/A} - \gamma_{S/L})}{\gamma_{L/A}} \qquad [6.4]$$

that reducing only the air/liquid tension will cause the drop to bead up even further in the hypothetical case of zero reduction of the solid/liquid tension. This illustrates the importance of effectively reducing the solid/liquid tension.

Efforts to use surfactants to spread aqueous drops on hydrophobic surfaces have demonstrated that with the exception of the trisiloxane "super-wetters", the conventional ones are not effective (large equilibrium contact

angles) even at elevated concentrations. Naturally therefore they are not effective in eliminating or suppressing rebound from such surfaces. While the trisiloxane surfactants are effective in reducing the contact angle to near zero values, they are not always the most dependable wetting agents. They are photoliable, they do not function in a dry environment, are expensive and their super-spreading ability is readily compromised in the presence of other phases/components. On the other hand the conventional poly-(ethyleneoxide) non-ionic surfactants C_iE_j's are very stable, eco-friendly and cheap but do not spread readily on hydrophobic surfaces[13].

However as was demonstrated in Chapter 4, there exist certain sparingly soluble surfactants, which form tightly packed condensed phases at least at the air/liquid interface. If the very same surfactants could form condensed phases at the solid/liquid interface then they could perhaps be more effective in reducing the solid/liquid tension due to the tight packing. This tight packing would cause a significant reduction of the solid/liquid tension due the removal of a water layer from the surface. It would also be interesting to study the effect of such surfactants on drop spreading and rebound.

This hypothesis while being intuitive also has some factual backing to it. Indeed it has been shown that these surfactants pack tightly at the solid/liquid interface as was demonstrated by Kumar[14] for $C_{14}E_1$ using Fourier Transformed Infrared (FTIR) Spectroscopy. Johal[15] and Bain[16] using sum frequency spectroscopy further established that a similar surfactant dodecanol undergoes a structural phase transition to an ordered state at the hydrophobic solid/liquid

interface. Further the presence of trace amounts of dodecanol has been found to induce a remarkable crystalline ordering in the structure of a film of SDS adsorbed at the hydrophobic solid/liquid interface[16].

While this is evidence that the surfactants which form condensed phases at the air/liquid interface also aggregate in these phases at the hydrophobic solid/liquid interface, there is no study on the dynamics of the assembly of these phases i.e. how quickly can they be formed (although Kumar's study for $C_{14}E_1$ demonstrated extremely slow adsorption rates because of the low solubility of these surfactants[14]). There is also no evidence whether these surfactants are superior in spreading and related applications. For any potential applications it is essential that these phases assemble fairly rapidly e.g. in the agrochemical spray application, it should take no more than a few seconds. In Chapter 4, we had seen that at-least at the air/liquid interface, the rate at which the LC phase forms for dodecanol and other similar surfactants is fairly slow owing to their low solubility. It takes for example, more than 300 s for the equilibrium LC state to be reached for a monolayer of dodecanol by assembly from a solution where the surfactant is at its solubility limit. This is by far too slow to be useful in any application. In Chapter 5 we had demonstrated how dispersing the surfactant finely could accelerate the transport rates of these surfactants. This approach was only partially successful, as such solutions were metastable. With the addition of a second component, more stable solutions were formed. In addition the two components were synergistic with the very low equilibrium tensions

attained. Fluorescence was used to verify that these systems form condensed states at the air/water interface.

The goals of this chapter are twofold. The first is to study if the surfactants/surfactant mixtures forming condensed phases (at-least at the air/liquid interface) similar to those analyzed in chapters 4 and 5, are effective in promoting spreading on hydrophobic surfaces i.e. do they demonstrate enhanced spreading characteristics. Secondly, if they are more effective in causing spreading in an equilibrium situation, then how efficient are they in minimizing rebound from hydrophobic surfaces under dynamic conditions?

For the former, static contact angle measurements for sessile drops on hydrophobic surfaces will be carried out. For the latter impact experiments for both water and surfactant laden drops on the very same substrates using a high speed video setup will be carried out. The experimental techniques used are given in Sec. 6.2. Sec. 6.3 gives the results of both the spreading and impact experiments. These results are summarized and discussed in Sec. 6.4.

6.2 Experimental

Materials: The poly-(ethyleneglycol) n-alkyl ether surfactants (C_mE_n=CH_3 $(CH_2)_{m-1}(OCH_2CH_2)_nOH$, m=10,12,14;n=4,6,8),>98% purity, were obtained from Nikko Chemicals, Japan. The medium chain alcohol surfactants (CH_3 $(CH_2)_{m-1}$ OH, m=11,12)>99.9% purity were supplied by Fluka and decanol (>99% purity) from Aldrich. All chemicals were used as received without any further purification. All aqueous solutions were prepared using deionized water purified by a Milli-Q filter system fitted with an Organex-Q column to remove trace contaminants (Millipore,

MA). The resistivity of the deionized water was at least 15 MΩ cm. Polished single crystal silicon wafers (100) used for substrate preparation were supplied by Semiconductor Processing Company. Octadecyl-trichlorosilane (OTS) >95% purity used for hydrophobically modifying silica surfaces was obtained from Aldrich, MA.

Preparation of Substrates: Surfaces of polymer films such as polyethylene, teflon, or parafilm have been traditionally used for wetting experiments. However they do not have uniform surface properties, are extremely rough and consequently no realistic quantitative studies can be carried out on such surfaces. On the other hand model organic hydrophobic surfaces created by self-assembled monolayers with a $-CH_3$- termination offer a very attractive alternative because of their ease of preparation and long term stability[17]. Further polished silica surfaces are cleaved in such a way that they are smooth on an atomic level and hence are ideal for quantitative studies. The substrates therefore used for all studies were polished silica wafers hydrophobically modified by self-assembled monolayers (SAM's) of OTS although some experiments on parafilm were also conducted. To form these surfaces a strict protocol proposed by Sagiv [18,19] as well as methods developed in our laboratories were employed. In brief, the substrates were first cleaned by sonnicating them in solutions of Nochomix dissolved in sulfuric acid. Subsequently they were sonnicated in distilled water, then dried with compressed nitrogen and then plasma cleaned in a plasma chamber (Harrick Scientific). The substrates were then allowed to stand for half an hour to an hour in freshly prepared solutions (2mM concentration) of

Octadecyltrichlorosilane (OTS) in a mixture of hexadecane, chloroform and carbon tetrachloride in the volume ratio of 20:2:3. The substrates were then sonnicated in chloroform for an hour to get rid of any loosely adhered particulates/polymerized OTS. Such a rigorous protocol has been found to give atomically smooth substrates with water contact angles varying from 104^0-108^0 as has been analyzed in detail by Kumar[20] using atomic force microscopy (AFM) (this study presents a detailed analysis of ideal conditions for obtaining uniform monolayers). After contact angle or impact experiments, the substrates were re-used after sonnicating in acetone, rinsing with deionized water and drying. Measurement of water contact angles using sessile drops of deionized water placed on such cleaned substrates were used to verify that the monolayer was intact (same water contact angle as before). Further the air/liquid interfacial tension and contact angles of these drops were measured by edge analysis of sessile drops similar to pendant bubbles to make sure that all contaminants were removed (no drop in the interfacial tension). The substrates were found to be stable over extended periods of time.

Dynamic and Static Interfacial Tension Measurements: For all the solutions used both static and dynamic surface tension measurements were carried out using the Pendant Bubble and/or the Wilhelmy plate method. These techniques have been described in detail in the preceding chapters.

Contact Angle Measurements: Contact angles measurements for sessile drops on hydrophobic surfaces were obtained in two ways. In the first method the image was captured using a Scion digitizing card (LG-3) in a 200 MHz PC using

Scion Image software and subsequently the manual built-in protractor of this software was used to directly determine the angle. In this approach it must be noted that although the card corrects the optical distortions of the video signal, the video ratio is 0.98 and not unity, so a minor correction for this had to be incorporated. At least five measurements on each droplet were carried out to minimize manual errors. In the second method, the drops were subjected to an edge detection procedure, and then the edge points near the three phase contact line were fit to a straight line using a least squares fitting procedure. The number of points used in the fitting was varied till the slope of the fit remained more or less constant when compared to the fits with fewer points. The results obtained through both techniques were in excellent agreement with each other for drops with contact angles from 45^0-90^0 with minor differences when the angle was smaller or larger. For very small angles, only the manual technique was used.

As contact angle measurements were undertaken for solutions of low as well as high concentration of surfactant, it was imperative to ensure that there is no evaporation of the water phase as this leads to unnecessary complications in any quantitative measurements. Hence all contact angle measurements were carried out by placing the substrate in a humid environment. For this an environmental chamber (Ramé-Hart) was humidified by filling available pockets in the chamber with water and suspending wet filter paper strips from the top into the water troughs. Before placing the water drop on the substrate, care was taken to ensure that the surface was level by checking the height (pixel level) of the substrate on both the left and right ends of the screen. The chamber efficacy

in minimizing evaporation was tested using sessile water drops placed on the substrate and it was observed that there was negligible evaporation over even a couple of hours (drop volumes were monitored by image digitization followed by edge detection and an integral calculation for the volume). For surfactant systems, all measurements reported were equilibrium values in which the contact angle reached a somewhat constant value.

Drop Impact Experiments: High speed video experiments of droplets hitting a surface were carried out in a setup similar to the pendant bubble apparatus: the only difference was that the regular CCD camera was replaced by a Kodak Ektapro digital camera capable of acquiring 1000 full frames/sec and up to 12000 partial frames/sec. The drops were discharged from a 20-22 gauge stainless steel needle (teflon tips were added to the needle tips for the surfactant experiments) either manually or by suddenly opening and closing a solenoid valve through a D/A card (VB-EZ, Data Translation) installed in a 486 PC. The capturing procedure was triggered manually. For water variable drop sizes were obtained by simple changing the needle gauge; for surfactant solutions the drop sizes were not manipulated (the size of the drop for a given outlet radius is dependent on the surface tension and cannot be controlled easily (drop volume technique)). The velocity of drops was varied by either changing the free fall height or by varying the manual impulse force provided for the drop to detach. Only qualitative conclusions were drawn based on the impact experiments and hence it was not crucial to create drops of exactly same size and velocity. The

drops did not attain their terminal velocity in either case. The substrates on which the drops impacted were the same as in the contact angle experiments.

6.3 Results

6.3.1 Contact Angle Measurements

For sparingly soluble surfactant solutions which are at the solubility limit (non-dispersed), the breakup rates of excess aggregates are slow compared to adsorption rates of the monomer and so it is not very prudent to do contact angle/interfacial tension or impact experiments with these solutions. This is because drops have limited reservoirs of surfactant which will be rapidly depleted and the results will not be representative of adsorbed saturated monolayers in a condensed state. Hence the procedure suggested by Franses was utilized for these experiments. Aqueous solutions of these surfactants in a dispersed form were prepared by the second protocol described in the experimental section of chapter 5. Only freshly prepared dispersed solutions were used. All solutions were prepared at concentrations much higher that either the CMC or the solubility limit. By using this procedure for solution preparation it was ensured that both interfaces were saturated with their respective maximum packing surface concentration. Using these solutions, contact angle measurements using sessile drops placed on the substrates described earlier were carried out. These measurements are tabulated in Table 6.2[1]. The equilibrium surface tension

[1] For decanol the equilibrium (non-dispersed) surface tension value was taken from the literature[21]

measurements for these solutions are reproduced alongside from Chapter 5 for comparison.

From the contact angle measurements, it is clear that among the LC phase forming surfactants, dodecanol is the one that lowers the contact angle the most. The lower equilibrium air/liquid tension is reflected in the contact angle measurements. However *none of these surfactants reduce the contact angle to near zero in fact they are far from zero.* So a tight packing of the monolayer is not sufficient to enable complete wetting of hydrophobic surfaces as these surfactants are perhaps are not as effective in lowering the solid/liquid tension. One reason why this may occur is because the hydrophobic chains of these surfactants may not be effectively shielded from water due to the small polar groups and thereby not allowing an efficient solid/liquid tension reduction.

For the two polyethoxylated surfactants, the contact angles are higher than that for dodecanol but lower than for decanol. The difference between the two themselves is negligible ($C_{14}E_6$ is lower though) suggesting that the big polar group dictates the final packing and the small difference in chain length causes very small difference in air/liquid and solid/liquid tensions. For the air/liquid interface there is evidence that the final packing surface concentration is almost the same and so is the CMC surface tension[22,23]. Hence this result is not completely unexpected.

To compare this to dodecanol, at first sight one would conclude that dodecanol spreads a little better because the tight packing lowers the solid liquid tension more effectively. However this is not necessarily true as the air/liquid

tension for dodecanol is lower and hence the difference in the solid/air and solid liquid tensions ($\gamma_{S/A} - \gamma_{S/L} = \gamma_{L/V} \cos\theta_e$) is approximately same for both and this implies that the final solid liquid tension is also approximately the same. Thus dodecanol, the best candidate among the sparingly soluble surfactants studied does not seem to be significantly more effective in assisting spreading on hydrophobic surfaces when compared to conventional surfactants. Hence it is necessary to resort to mixed surfactant systems, which may be more effective because they are synergistic in the air/liquid tension reduction. The cohesion among the two components may also be strong enough to permit stacking in a condensed state at the hydrophobic surface and the effective isolation of water from the hydrophobic chains may prove to be very effective in promoting spreading on hydrophobic surfaces. Thus rapid achievement of low equilibrium contact angles may be possible by using a two-component system.

The contact angle measurements for the different mixed systems along with their equilibrium surface tension measurements are tabulated in Table 6.3. It is clear that mixtures of $C_{12}E_6$ and $C_{12}E_0$ which are more synergistic in reducing the surface tension, are also capable of promoting spreading on hydrophobic surfaces. Also, they are superior to mixtures of $C_{14}E_6$ and $C_{12}E_0$. This can be attributed to better isolation of the hydrophobic chain from water in the surfactant combination whose chain lengths are identical. This effectively reduces the interfacial tensions and promotes spreading. The mixture of $C_{12}E_6$ and $C_{12}E_0$ is highly synergistic in lowering the contact angle (13^0-19^0).

6.3.2 Drop Impact Experiments for Water as Well as Surfactant Laden Drops

In the previous section it was demonstrated that there exist binary surfactant mixtures which significantly lower the interfacial tension synergistically and exhibit superiority in promoting spreading on hydrophobic surfaces. It was also seen (though not shown explicitly) that these mixtures attain their equilibrium contact angles fairly rapidly, so the dynamic rates of adsorption are fairly rapid. Based on these results, the efficiency of these mixtures in eliminating rebound from hydrophobic surfaces can also be tested. We expect surfactants that rapidly lower the static equilibrium contact angles to smaller values, to be more effective in suppressing rebound from hydrophobic surfaces as compared to conventional surfactants which do not assist spreading on these surfaces. This is based on drawing the analogy between a rapid attainment of low contact angle on a hydrophobic surface to that of the surface being hydrophilic. Mao *et al.*[11] demonstrated that if the surface was sufficiently hydrophilic, then the droplets do not rebound from such surfaces as was shown for stainless steel and glass surfaces. From their images of water drops impacting on paraffin, stainless steel and glass surfaces, it is clear that more hydrophilic the substrate was, the less was the retraction and rebound. This is because of the reason discussed in the introduction. If the surface is hydrophilic then the static advancing contact angle is small and therefore it does not allow the build up of a high radius of curvature at the advancing end of the drop equator that causes the subsequent reversal of flow and reflection. Surfactants that adsorb and lower the contact angle rapidly and efficiently act so as to make the hydrophobic surface hydrophilic and thereby should be able to suppress rebound. In fact the binary mixtures studied in the

previous section cause water to spread to a much lower contact angle than that of water on the glass case in Mao's experiments. Hence it is not unreasonable to expect that these mixtures will prove effective in reducing retraction and hence reflection of impacting droplets. We expect surfactants that lower the contact angle to minimal values rapidly, to be the most effective in eliminating rebound.

The first set of experiments carried out was for impact of pure water drops on the same hydrophobic surfaces as were used earlier. This is to verify the results obtained by Mao *et al.* and Quere *et al.* i.e. to show clearly that water drops indeed rebound from our hydrophobic surfaces. Water drops of different sizes and velocities (though not controlled) were allowed to impact on the OTS modified hydrophobic surfaces (Fig. 6.3). Although many experiments were conducted, only two of them are shown here. Fig. 6.4 shows one such set of the sequence of a drop impacting, spreading then retracting and finally reflecting off the surface. The sequence does not consist of images at equal intervals of time, but just illustrates all modes of the spreading/retracting cycle The entire cycle takes about 50 ms. It is clear that as the drop first hits the surface, the initial momentum causes it to spread out and attain a pancake like configuration in which it completely flattens out. Subsequently it begins to retract and it is clear that the contact angle when the drop fully retracts is fairly high. Eventually almost the entire drop breaks off and gets free of the surface. While it may be argued that the drop barely bounces off the surface and will land back on the same spot, the same may not be true for a case where the drop hits a leaf surface. The leaf will be displaced due to the momentum of the impacting drops and this may allow

the reflected drop to miss the leaf and fall directly into the soil. Furthermore as is seen in the next sequence, if the drop velocities are higher, then the reflected drop or part of the drop that breaks off could completely get displaced from near the leaf.

The second sequence of water drops impacting on the surface (Fig. 6.5) is for a smaller drop of higher velocity. Here again the water drop follows the same progressive sequence as above, but during retraction the top portion of the drop pinches off and breaks free far from the surface. The lower part of the drop also breaks free but stays close to the surface. Also it is clear that the velocity of the broken part is higher and it departs far away from the surface. Based on this and the previous experiment it is clear that drops can completely reflect from hydrophobic surfaces. While a more systematic study of the effect of size and velocity of impacting drops on the percentage reflected needs to be carried out, it can be concluded from the experiments shown and other experiments conducted that small (but not too small) drops with highest velocities are the likely candidates for rebound. If drops are too small or the velocity too low then they do not have enough kinetic energy to allow for reflection. If drops are too large then the inertia is too difficult to overcome for the drop to recoil. Also large drops with high velocity breakup on impact and do not reflect.

The second set of impact experiments were for droplets laden with different surfactants. The first surfactant tested was $C_{14}E_6$, a commonly used surfactant to study if it was effective in reducing rebound. Under static conditions, the contact angle on the hydrophobic surface is 45^0. Aqueous solutions of $C_{14}E_6$

at three different bulk concentrations were prepared: CMC, 6*CMC and 52*CMC. The drops were formed at the tip of a capillary and allowed to age so that the tension was reduced, the aging time varying from a few minutes to a few seconds as the concentration was increased. Once they were aged the drops were allowed to impact on the substrate either by an impulsive force or by engaging the syringe pump. The other experimental details of the impact experiments have been discussed earlier.

Fig. 6.6 gives the sequence of images of the impact of the solution of $C_{14}E_6$ at the CMC. The images are indistinguishable from a water drop impacting on the surface. The droplet (at least a part) breaks free and rebounds off of the surface. The contact angle of the droplet during the retraction mode is still high and this is why the droplet rebounds. The reason there is no lowering of contact angle is because, despite the drop being aged there is not enough surfactant in the bulk to populate both the air/liquid and solid/liquid interfaces and lower the contact angle. Further at these concentrations the adsorption rates are fairly slow and equilibrium in reached only in a few hundred seconds, so practically no adsorption would have occurred onto the freshly created solid/liquid interface during the impact cycle. This is why the droplet behaves exactly as if it were a droplet of pure water and the surfactant has no effect.

The second sequence of images in Fig. 6.7 is for that of a drop containing $C_{14}E_6$ at a higher bulk concentration of 6*CMC. Here as the drop hits the surface, it too completely flattens out before retracting. During retraction the contact angle is marginally reduced when compared to that or water or $C_{14}E_6$ at the lower

concentration. As a result the top portion of the drop barely survives pinch off and breakup. Had the drop velocity been higher, then it would definitely have detached. The adsorption rates of surfactant at these concentrations are of the order of a few seconds and this is again not fast enough to cause the surfactant to completely populate the solid/liquid interface. This is the reason why there is only a minute lowering of contact angle and the drop still almost rebounds.

The last sequence of images for $C_{14}E_6$ are for a bulk concentration of approximately 52*CMC. At these high concentrations we expect rapid adsorption of surfactant and both interfaces should be populated with the equilibrium surface concentration as the drop first impacts and then spreads. The drop should therefore reach its equilibrium contact angle in time scales comparable to the spreading/retraction. Therefore the true efficacy of this surfactant in eliminating rebound can be tested. Shown in Fig. 6.8 are these images. Again the drop flattens out at first and then retracts. However here the contact angle the drop makes with the substrate is much lower than that of water and therefore the drop does not detach. However the drop does retract and had the velocity been higher, a part of it could very easily have detached.

Based on these experiments it is clear as to why conventional surfactants are only partially effective in reducing rebound and may not work in all cases. It is clear that only if the contact angle is reduced to very low values, is there a chance of reducing retraction and rebound. This is because, if the contact angle is low then there are no pressure gradients built up in the bulk to cause a flow reversal and hence there will not be any retraction. Also there may exist a critical

contact angle, such that the drop will not retract if the actual contact angle is lowered than this critical value during retraction.

To check this contact angle hypothesis and to see if the so-called "super-wetters" are effective in eliminating rebound upon impact, similar experiments were carried out for one such tri-siloxane surfactant E8 at a concentration of 1wt%. Under static conditions this surfactant causes aqueous formulations to completely wet the surface i.e. reduce the contact angle to near zero. The results of this impact experiment are shown in Fig. 6.9. Here as the drop impacts and spreads out, it immediately attains a very low contact angle. Subsequently the drop does not retract, but forms a very thin film that covers a large area of the surface. Here the concentration is high enough, so there is enough surfactant to rapidly populate both interfaces. More importantly though, this causes the contact angle to be reduced to a very low value and this completely eliminates retraction.

The fact that using a super-spreader eliminates rebound and causes complete wetting is proof that a low contact angle can prevent rebound. However in many applications, one cannot use these surfactants. For instance in the agrochemical industry, they are not compatible with other components of the formulation and their spreading ability is readily compromised in the presence of other components. In addition the formation of a very thin layer as was seen in the impact experiments is often not desirable as the film can easily drain into the soil. In addition the thinning of the film depletes the concentration of the active as it is spread over a larger area, and this reduces the cuticular penetration

efficiency of the active. So too efficient spreading is also not very good for this and other applications.

It was demonstrated earlier than mixed surfactant systems could reduce the static contact angle significantly without lowering it to zero. It would therefore be interesting to see what happens when a surfactant drop saturated with such a mixture impacts a hydrophobic surface. Such a test was carried out for the synergistic mixture of $C_{12}E_0/C_{12}E_6$. Fig. 6.10 is the sequence of images for such an experiment. Here again the drop begins to spread when it first impacts. Once it flattens out, there is hardly any retraction because it has attained its low equilibrium contact angle and this prevents flow reversal. In addition this does not cause the film to thin out as was for the super-spreader. So these mixtures are equally effective in eliminating rebound.

6.4 Summary and Discussion

Contact angle measurements on the single component as well as mixed surfactant systems revealed that conventional soluble surfactants do not promote complete spreading on hydrophobic surfaces. This is attributed to the fact that the loose packing of the monolayer does not prove to be effective in lowering the solid/liquid tension. However, even dispersed solutions of the condensed phase forming surfactants do not assist in complete spreading on hydrophobic surfaces. Here despite the close packed monolayer, the solid liquid tension is not reduced significantly, perhaps because the hydrophobe is not effectively isolated from water. Synergistic surfactant mixtures on the other hand, lower the contact angles significantly and promote spreading. Here in addition to the lower air/liquid

tension (due to the formation of a condensed state), the superior isolation of water from the hydrophobic chains due to the monolayer packing structure is the likely reason for the enhanced spreading characteristics.

High-speed visualization of water droplets hitting a hydrophobic surface clearly show that as a drop impacts on a surface, it can easily reflect off of the surface depending on the size and the velocity. This agrees with the results obtained by Mao *et al.* and Quere *et al.* As the drop first hits the surface, it flattens out to a pancake like configuration. The fluid in the droplet then undergoes a flow reversal due to the build up of pressure at the leading end due to the high radius of curvature. As the drop retracts it maintains a very high contact angle with the surface and because of this the drop gets extended into a long cylinder type configuration. This causes either a portion of the drop or the entire drop to come off the surface.

When droplets laden with surfactant impact the very same surface, the droplet spreading and retraction cyclic characteristics are markedly different. If the bulk concentration of surfactant is not high enough, then the droplet essentially behaves like a water droplet and reflects easily. This is because surfactant adsorption rates are fairly slow at these concentrations and there is no contact angle reduction during the impact cycle. On the other hand if the bulk concentration is high enough such than the adsorption rates at interfaces are comparable to the time scales of the droplet oscillations, then there is a large reduction in contact angle during the droplet retraction cycle. Reasonable reductions in contact angles may prevent the drop from detaching but does not

prevent the retraction. This is why conventional surfactants which lower the contact angle significantly but to far from zero values, are not very effective is suppressing rebound from hydrophobic surfaces. This is illustrated for one such surfactant $C_{14}E_6$. On the other hand surfactants which lower the contact angle to zero or near zero values are very effective in eliminating rebound as is seen for one trisiloxane super-wetter. Here as the droplet hits the surface, it completely spreads and forms a very thin film on the surface. There is consequently no retraction of the droplet and hence no rebound. Synergistic blends of poly-(ethylene-oxide) surfactants and alcohols which form condensed states are equally effective in suppressing rebound. Here although the equilibrium contact is not zero, it is still low enough and this prevents the build up of any pressure gradients in the bulk fluid which can cause rebound. A very low contact angle is attained instantaneously and this prevents the drop from retracting. Here the droplet does not form a very thin film and hence in some ways this surfactant blend is superior to the super-wetters in the applications considered here. The stability, biodegradability, cost-effectiveness and commercial availability of these blends make them a very viable alternative in many applications involving spreading on hydrophobic surfaces.

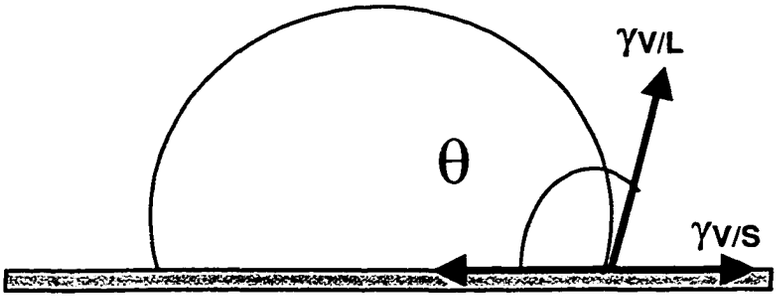

$$\cos(\theta) = (\gamma_{V/S} - \gamma_{L/S}) / \gamma_{V/L}$$

Fig. 6.1: Schematic of a Water Droplet Sitting on a Hydrophobic Surface with the Three Interfacial Tensions Determining the Equilibrium Contact Angle as Give by the Young- Dupré Equation.

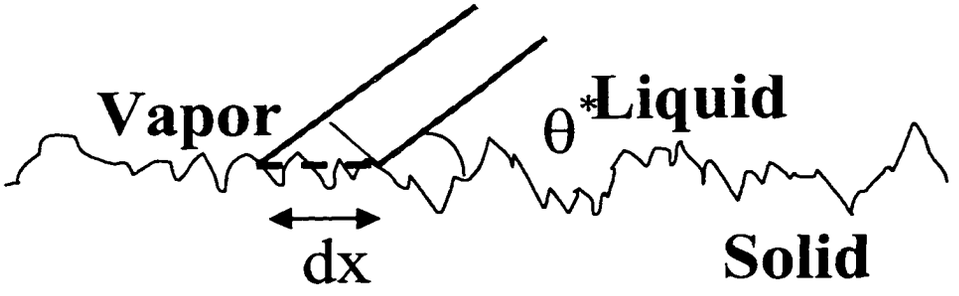

$$dG_s = r^*dx^*(\gamma_{SL} - \gamma_{SV}) + \gamma_{LV}^*\cos(\theta^*)^*dx$$

$$\cos(\theta^*) = r^*(\gamma_{SL} - \gamma_{SV})/\gamma_{LV} = r^*\cos(\theta)$$

Fig. 6.2: Amplification of Wetting/De-wetting of a Surface Due to Roughness.

Plant	Percent Reflected 160 μm	230μm	340 μm
Cabbage	100	100	100
Wheat	80	70	100
Soybean	70	60	50
Pear	0	0	0
Foxtail	50	80	70

Table 6.1:Reflection of Water Droplets from Different Foliate Surfaces (From Reichard *et al.*).

Solution	Equilibrium Surface Tension (mN/m) (Non-Dispersed)	Equilibrium Surface Tension (mN/m) (Dispersed)	Contact Angle on Hydrophobic Surface[2]
Water	72.5	--------	104^0-108^0
$C_{12}E_0$	27-28	24-26	34-36
$C_{11}E_0$	28	26-27	60-65
$C_{10}E_0$	29	27-28	55-60
$C_{12}E_4$	29	28	30-35
$C_{12}E_6$	32.5	---------	46.5
$C_{14}E_6$	31	---------	45
$C_{12}E_{23}$	----	---------	54

Table 6.2: Equilibrium Surface Tension For the Dispersed as well as Non-Dispersed Solutions and Contact Angle Measurements on the OTS Modified Hydrophobic Surfaces.

[2] For Sparingly Soluble Surfactants, Contact Angle Measurements were made for the dispersed solutions alone.

Binary Mixture	Equilibrium Surface Tension (mN/m)	Contact Angle
$C_{12}E_0$/ $C_{12}E_4$	22-23	18-20
$C_{12}E_0$/ $C_{12}E_6$	21-22	13-18
$C_{11}E_0$/ $C_{12}E_6$	24-25	19-20
$C_{10}E_0$/ $C_{12}E_6$	25.5	25.5-30
$C_{12}E_0$/ $C_{14}E_6$	22-23.5	20-24

Table 6.3: Equilibrium Surface Tension and Contact Angle Measurements For Solutions of Binary Surfactant Mixtures on the OTS Modified Hydrophobic Surfaces.

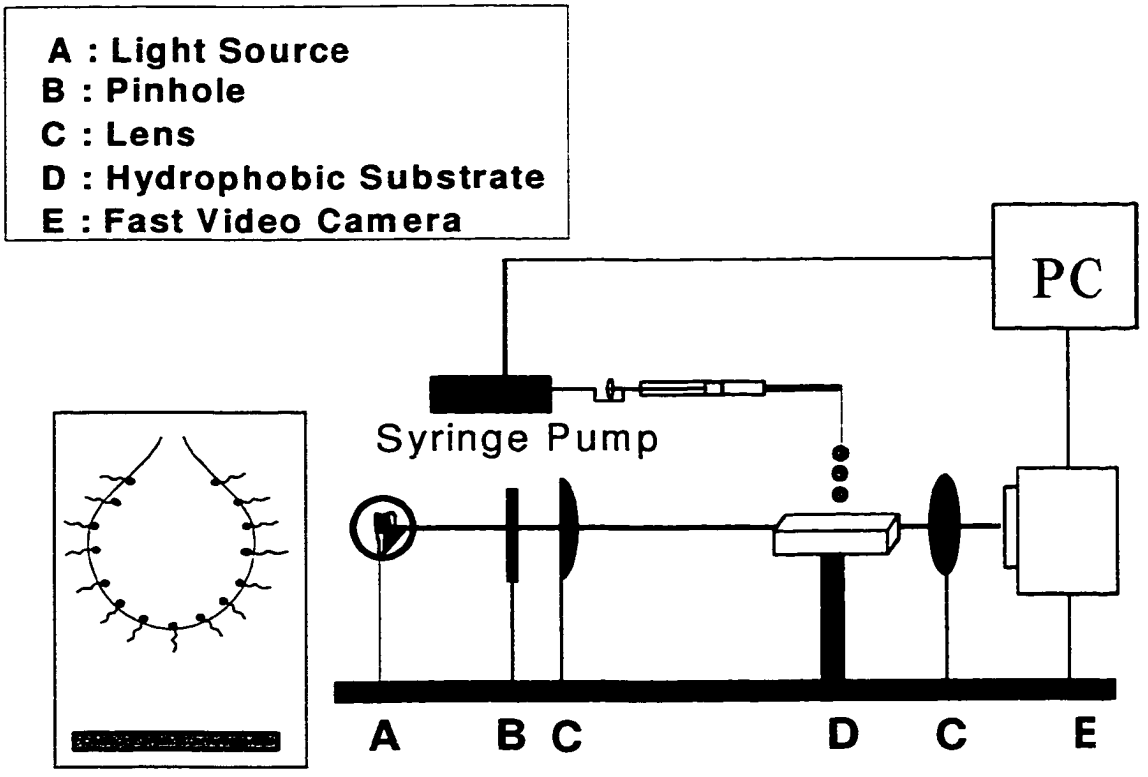

Fig. 6.3: Schematic of the High Speed Video Setup for the Drop Impact Experiments.

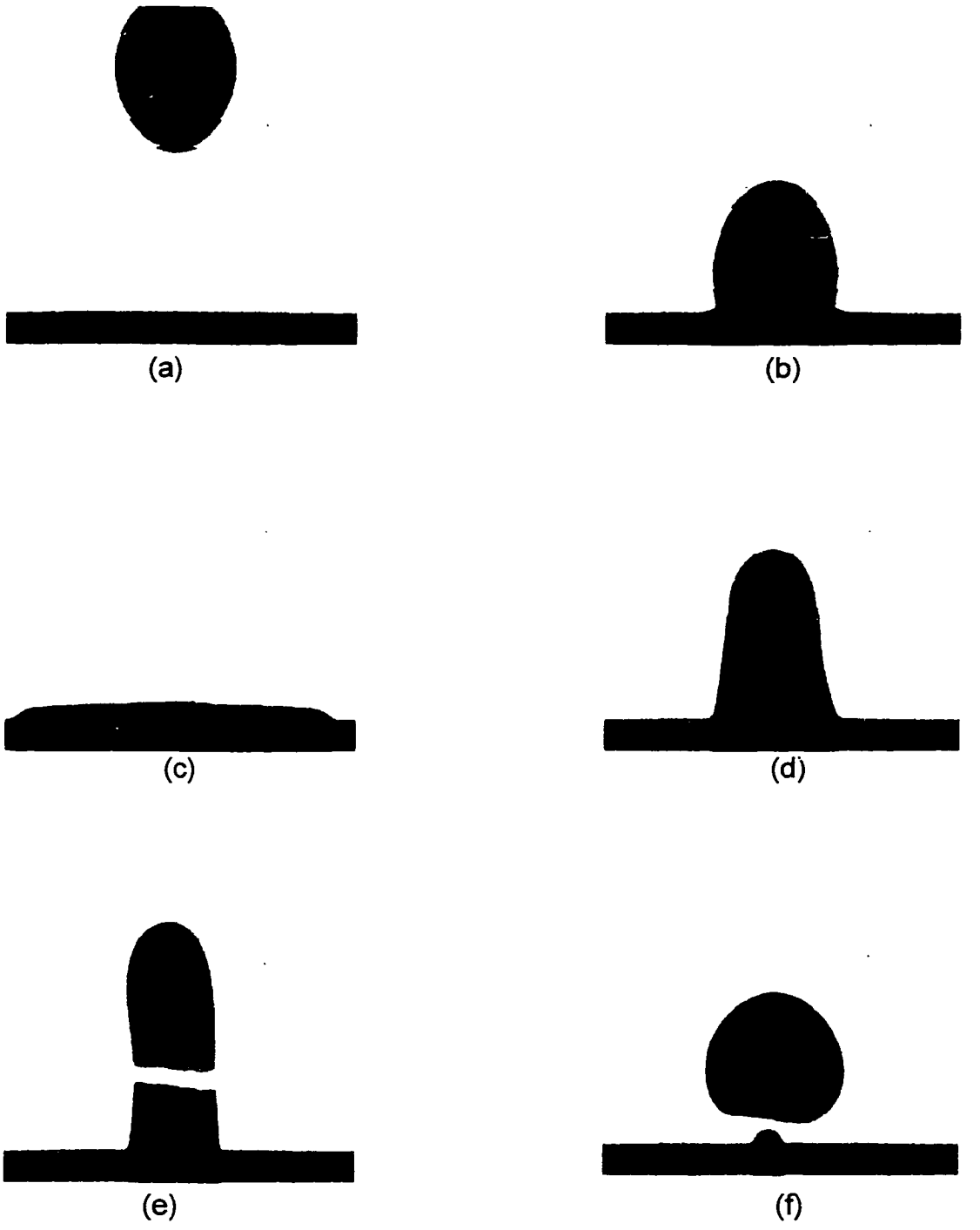

Fig. 6.4: Sequence of Images for a Water Drop Impacting on a Hydrophobic Surface-I.

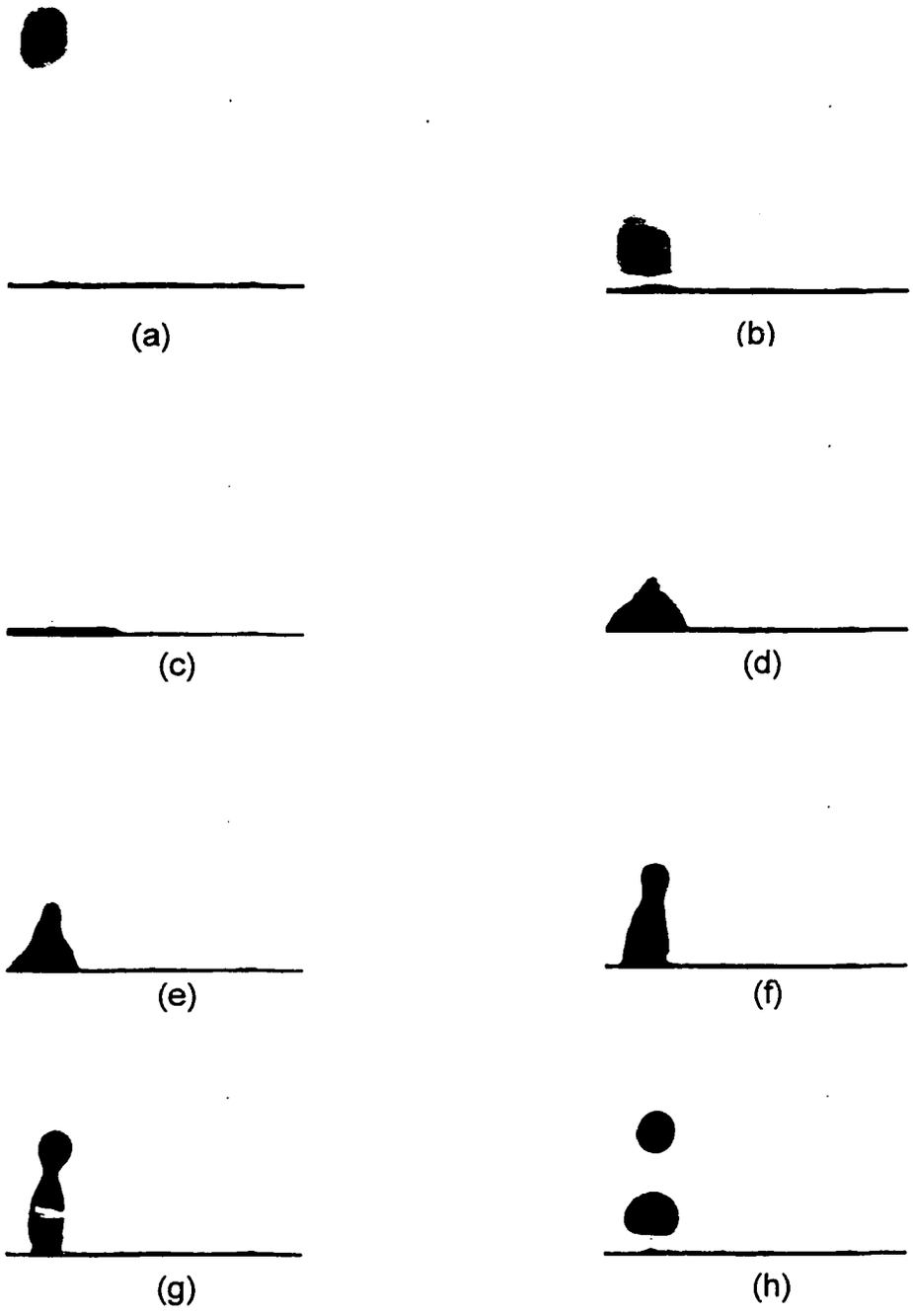

Fig. 6.5: Sequence of Images for a Water Drop Impacting on a Hydrophobic Surface-II.

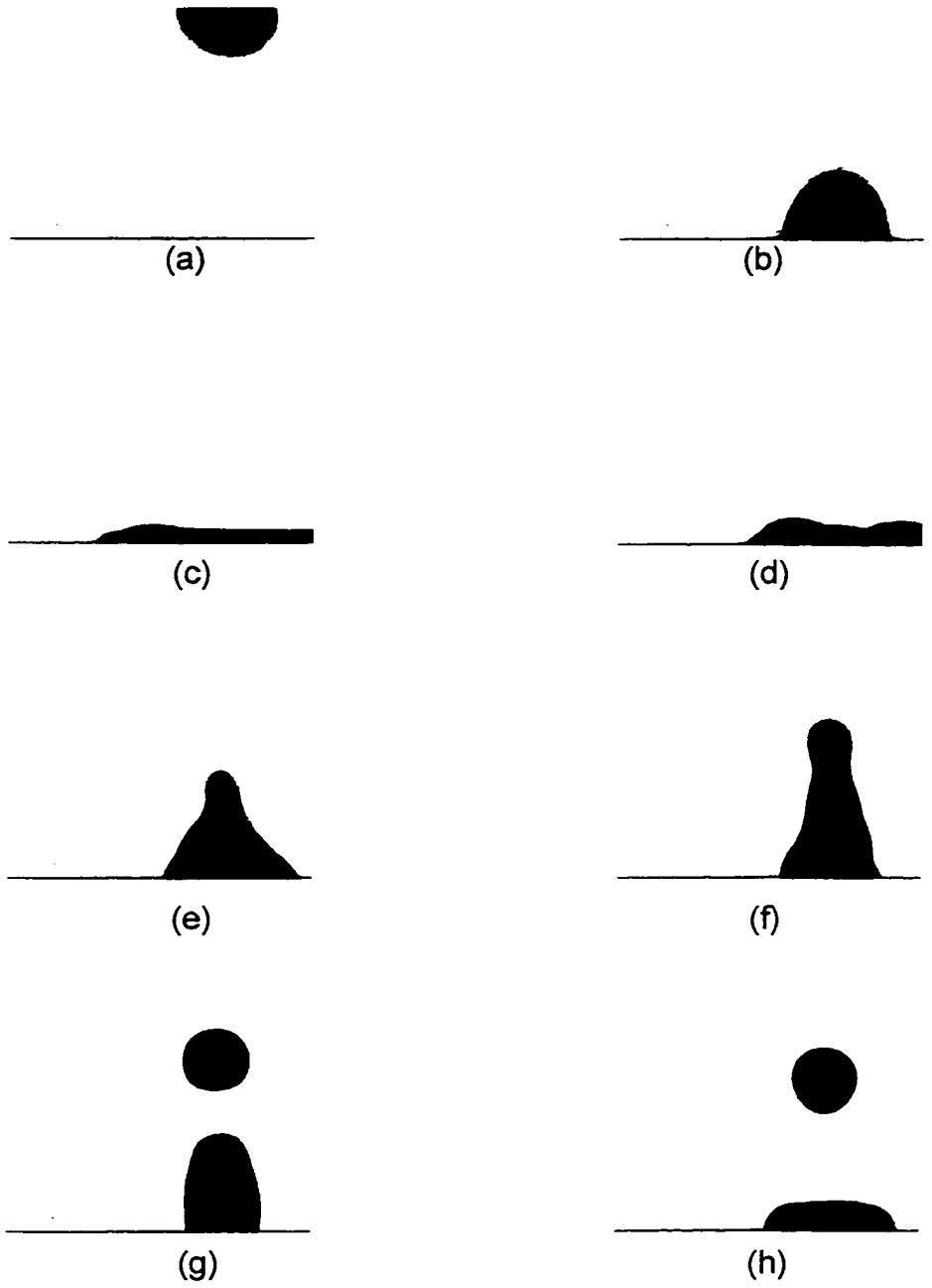

Fig. 6.6: Sequence of Images For a Water Drop With a Surfactant $C_{14}E_6$ at a Bulk Concentration of 0.0117 mol/m^3 (1.2*CMC) Impacting on a Hydrophobic Surface.

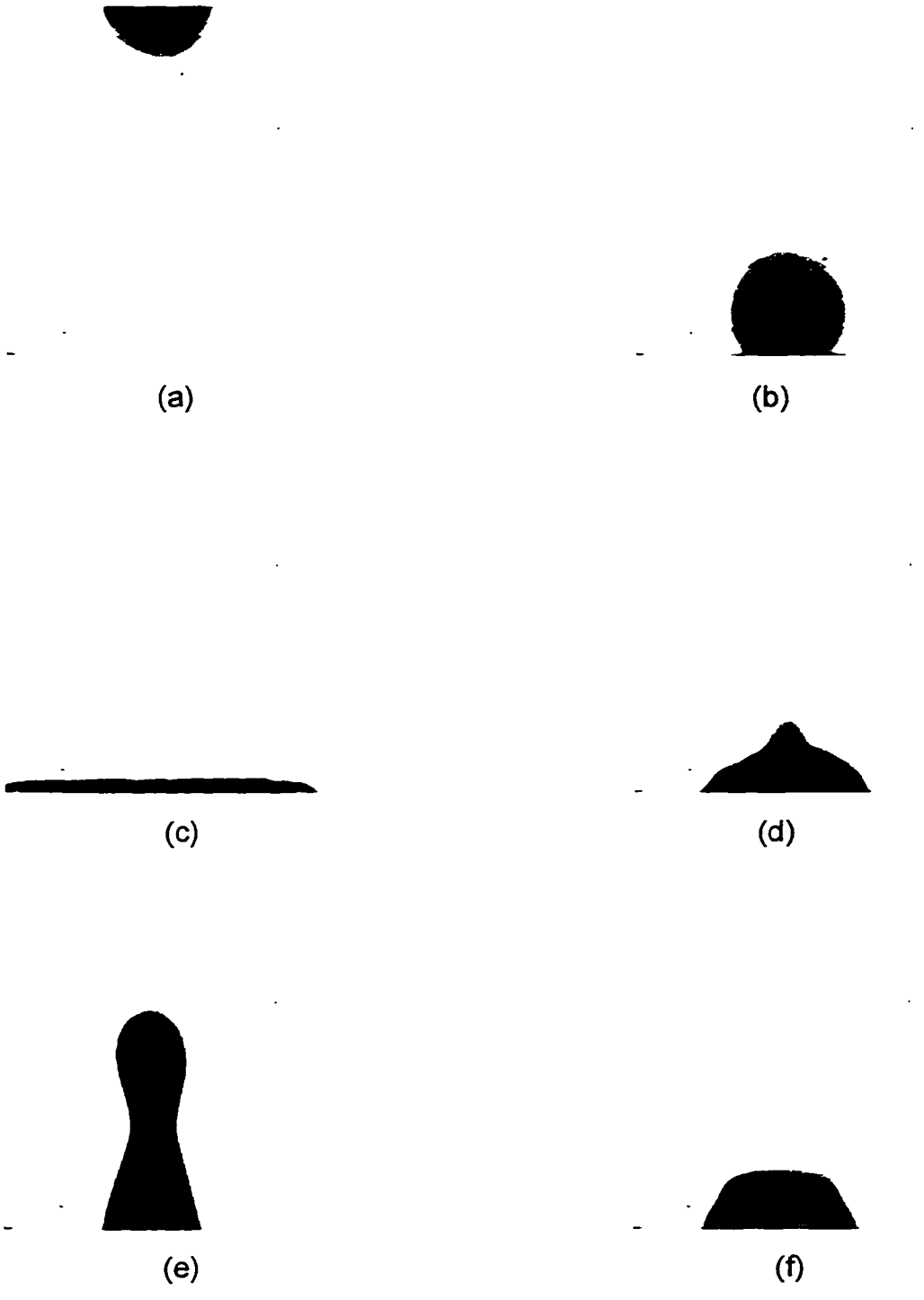

Fig. 6.7: Sequence of Images For a Water Drop With a Surfactant $C_{14}E_6$ at a Bulk Concentration of 0.0702 mol/m^3 (6*CMC) Impacting on a Hydrophobic Surface.

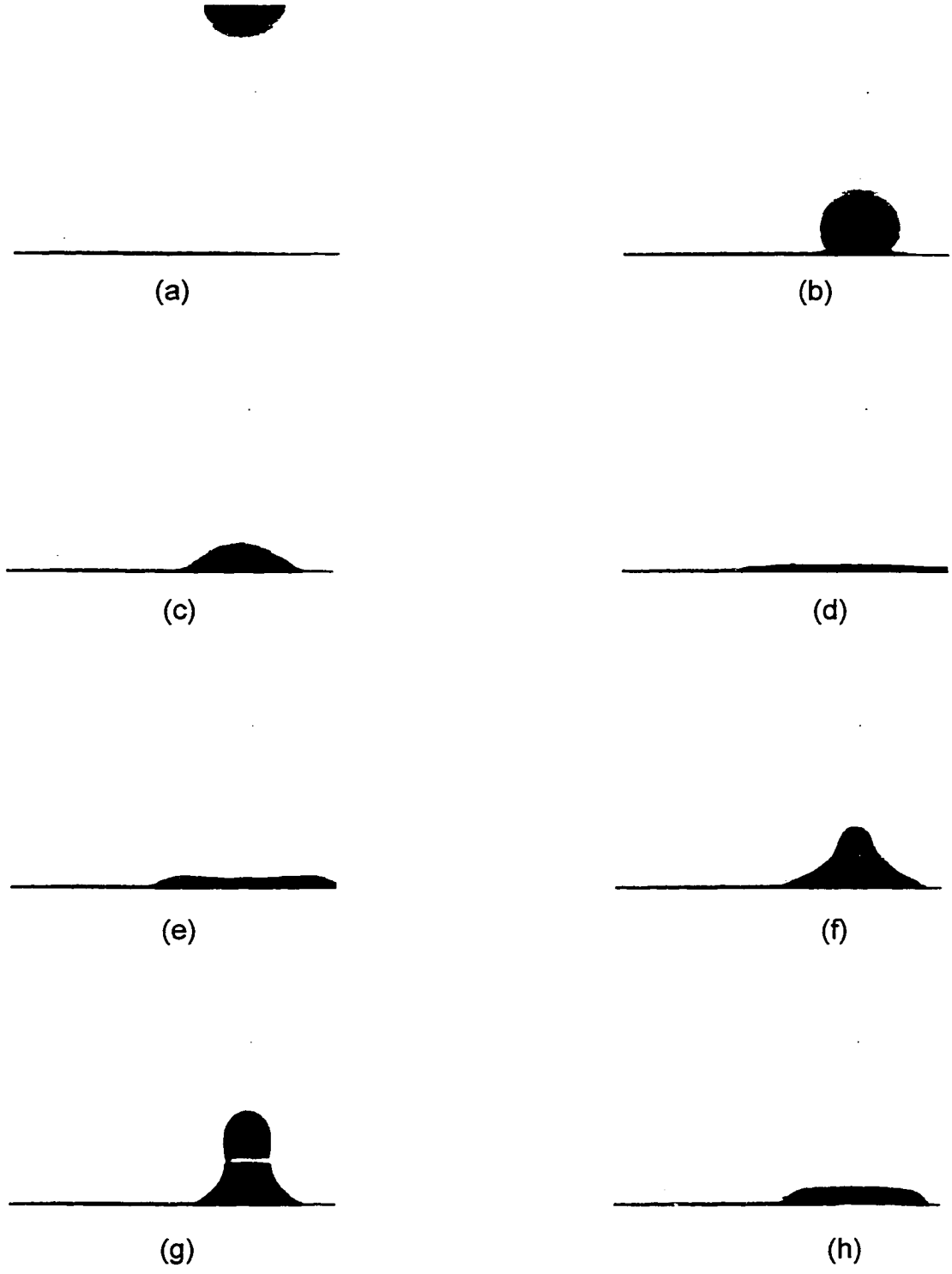

Fig. 6.8: Sequence of Images For a Water Drop With a Surfactant $C_{14}E_6$ at a Bulk Concentration of 0.482 mol/m^3 (52*CMC) Impacting on a Hydrophobic Surface.

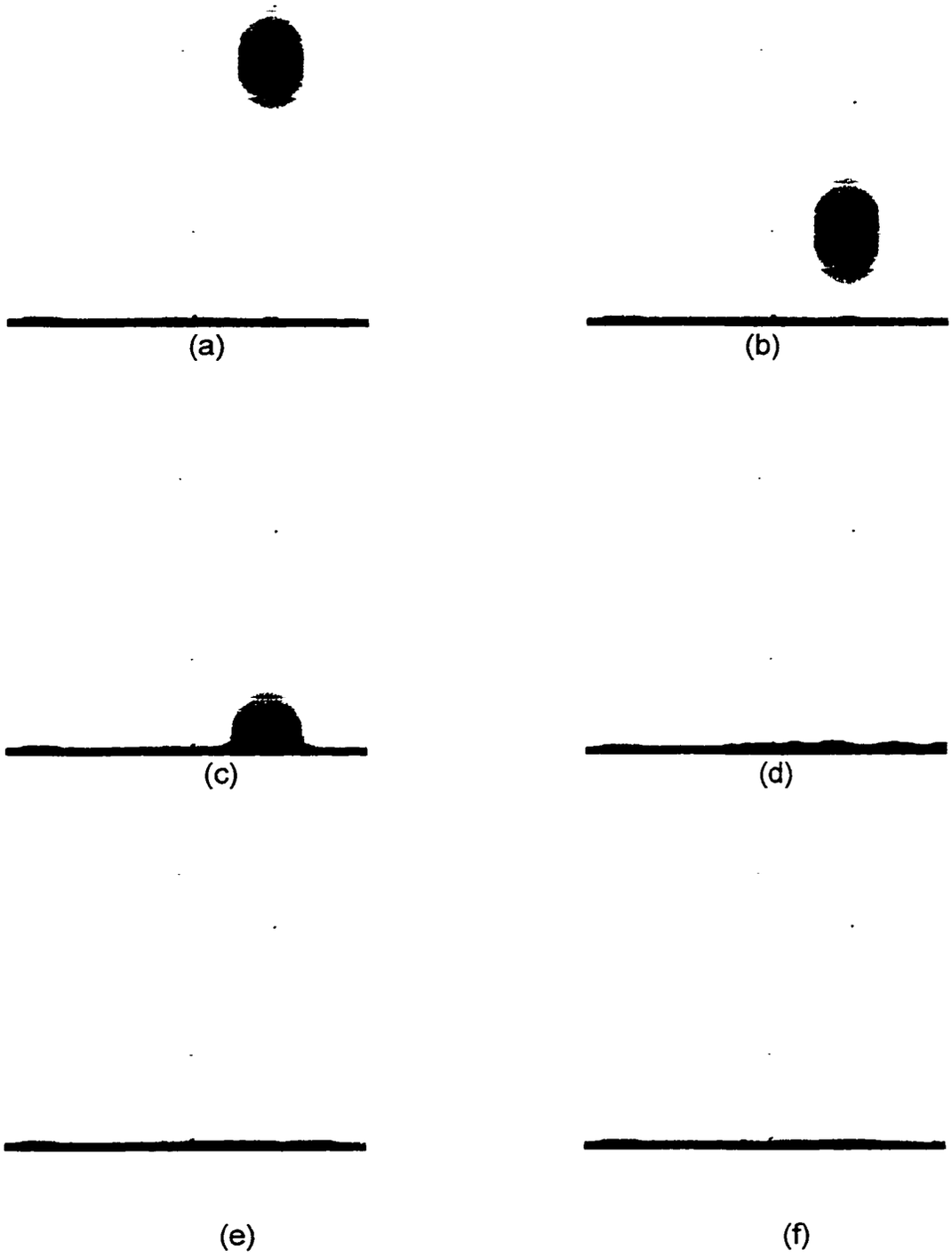

Fig. 6.9: Sequence of Images for a Water Drop With a Super-Spreader E8 at a Bulk Concentration of 1 wt% Impacting on a Hydrophobic Surface.

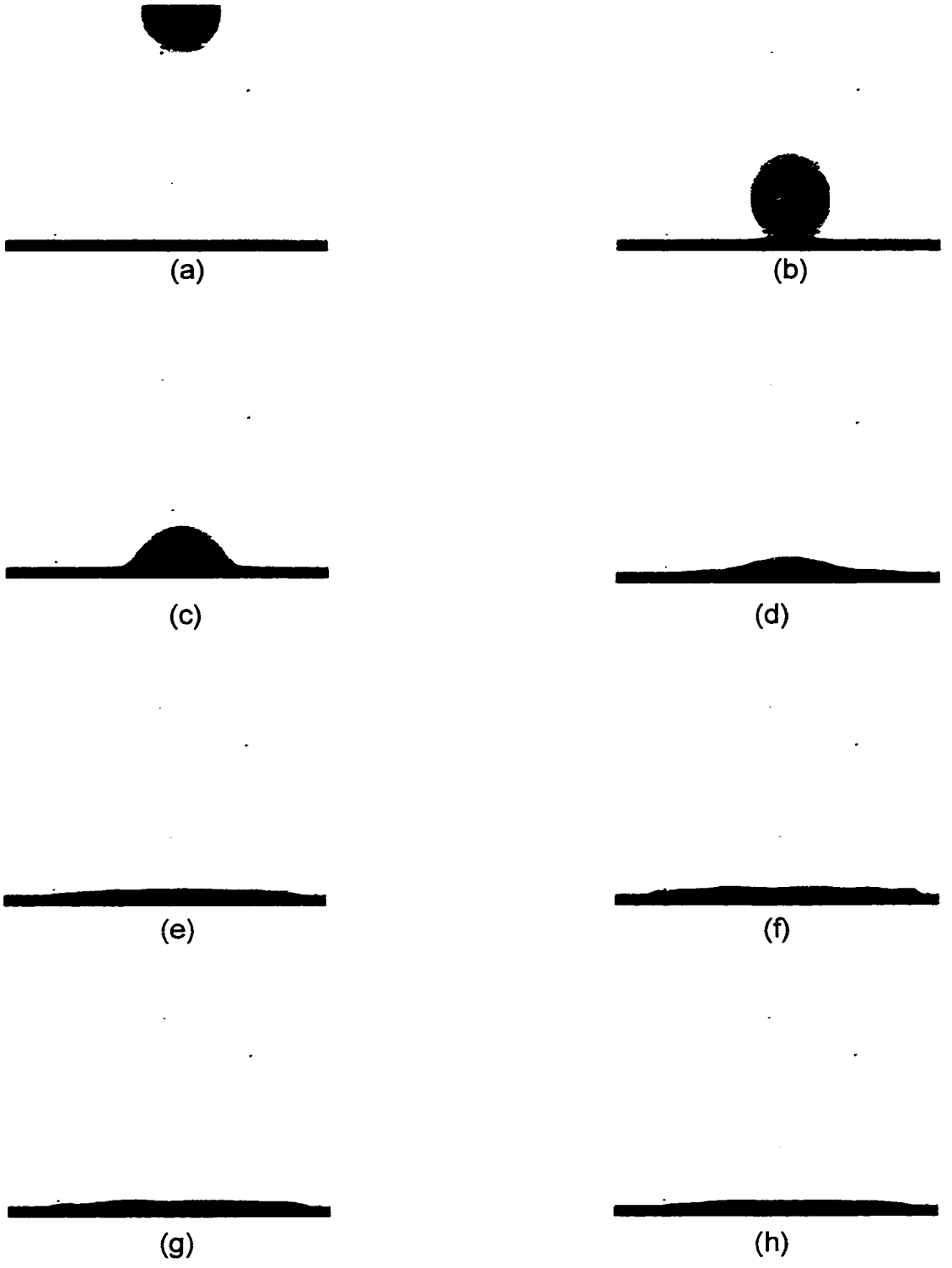

Fig. 6.10: Sequence of Images for a Water Drop with the $C_{12}E_6$/ $C_{12}E_6$ Mixture Impacting on a Hydrophobic Surface.

References

1)Oliver, J. F.; Huh, C.; Mason, S. G. *Journal of Colloid and Interface Science* **1977**, *59*, 568-580.

2)Bico, J.; Marzoiin, C.; Quere, D. *Personal Communication* **1999**.

3)Shibuichi, S.; Onda, T.; Satoh, N.; Tsuji, K. **1996**.

4)Onda, T.; Shibuichi, S.; Satoh, N.; Tsuji, K. *Langmuir* **1996**, *12*, 2125-2127.

5)Reichard, D. L.; Cooper, J. A.; Bukovac, M. J.; Fox, R. D. *Pesticide Science* **1998**, *53*, 291-299.

6)Richard, D.; Quere, D. *Personal Communication* **1999**.

7)Dussan, E. B. *Annual Reviews of Fluid Mechanics* **1979**, *11*, 371

.

8)Marmur, A. *Advances in Colloid and Interface Science* **1983**, *19*, 75.

9)DeGennes, P. *Reviews of Modern Physics* **1985**, *57*, 827.

10)Berg, J. *Marcel Dekker:New York* **1993**.

11)Mao, T.; Kuhn, D. C.; Tran, H. *AIChE Journal* **1997**, *43*, 2169.

12)Chang, C. H.; Franses, E. I. *Colloids and Surfaces A:Physicochemical and Engineering Aspects* **1995**, *100*, 1-45.

13)Stoebe, T.; Lin, Z.; Hill, R. M.; Ward, M. D.; Davis, H. T. *Langmuir* **1997**, *13*, 7270-7275.

14)Kumar, V. *PhD Thesis, City University of New York* **1997**.

15)Johal, M. S.; Usadi, E. W.; Davies, P. B. *Journal of Chemical Society:Faraday Transactions* **1996**, *92*, 573-578.

16)Bain, C. D.; Davies, P. B.; Ward, R. N. *Langmuir* **1994**, *10*, 2060-2063.

17)Krishnan, S. *PhD Thesis, City University of New York* **1999**.

18)Gun, J.; Isocovici, R.; Sagiv, J. *Journal of Colloid and Interface Science* **1984**, *101*, 201-213.

19)Sagiv, J. *Journal of American Society* **1980**, *102*, 92-98.

20)Kumar, N. *PhD Thesis, City University of New York* **2000**.

21)Lin, S.-Y.; McKeigue, K.; Maldarelli, C. *Langmuir* **1991**, *7*, 1055-1066.

22)Pan, R.; Green, J.; Maldarelli, C. *Journal of Colloid and Interface Science* **1998**, *205*, 213-230.

23)Subramanyam, R.; Pan, R.; Maldarelli, C. *Colloids and Surfaces A* **1998**, *Submitted for Publication.*

Bibliography

1)Reichard, D. L.; Cooper, J. A.; Bukovac, M. J.; Fox, R. D. *Pesticide Science* **1998**, *53*, 291-299.

2)Cox, M. F. *Journal of the American Oil Chemists Society* **1990**, *63*, 559-565.

3)Gaines, G. L. *Insoluble monolayers at liquid-gas interfaces*; Wiley-Interscience: New York, 1966.

4)McConnell, H. M.; Tamm, L. K.; Weis, R. M. *Proc. Natl. Acad. Sci. USA* **1984**, *81*, 3249-3253.

5)Knobler, C. M. *Science* **1990**, *249*, 870-874.

6)Stine, K. J. *Micros. Res. Tech.* **1994**, *27*, 439-450.

7)Hénon, S.; Meunier, J. *J. Chem. Phys.* **1991**, *68*, 936-939.

8)Hõnig, D.; Mõbius, D. *J. Phys. Chem.* **1991**, *95*, 4590-4592.

9)Vollhardt, D. *Adv. Coll. Int. Sci.* **1996**, *64*, 143-171.

10)Jacquemain, D.; Wolf, S. G.; Leveiller, F.; Deutsch, M.; Kjaer, K.; Als-Nielsen, J.; Lahav, M.; Leiserowitz, L. *Angew. Chem. Int. Ed. Engl.* **1992**, *31*, 130-152.

11)Kajiyama, T.; Oishi, Y.; Hirose, F.; Shuto, K.; Kuri, T. *Lang.* **1994**, *10*, 1297-1299.

12)Thomas, R. K.; Penfold, J. *Current Opinion in Colloid and Interface Science* **1996**, *1*, 23.

13)Als-Nielsen, J.; Jacquemain, D.; Kjaer, K.; Leveiller, F.; Lahav, M.; Leiserowitz, L. *Phys. Rep.* **1994**, *246*, 252-313.

14)Crowley, T. L.; Lee, E. M.; Simister, E. A.; Thomas, R. K.; Penfold, J.; Rennie, A. R. *Coll. Surf.* **1990**, *52*, 85-106.

15)Pallas, N. R.; Pethica, B. A. *J. Chem. Soc. Farad. Trans. I* **1987**, *83*, 585-590.

16)Winch, P. J.; Earnshaw, J. C. *J. Phys.: Condens. Matter* **1989**, *1*, 7187-7205.

17)Suresh, K. A.; Nittmann, J.; Rondelez, F. *Europhys. Lett.* **1988**, *6*.

18)Moore, B. G.; Knobler, C. M.; Akamatsu, S.; Rondelez, F. *J. Phys. Chem.* **1990**, *94*, 4588-4595.

19)Moore, B.; Knobler, C. M. *J. Chem. Soc., Faraday Trans. 2* **1986**, *82*, 1753-1761.

20)Lin, S.-Y.; McKeigue, K.; Maldarelli, C. *Langmuir* **1991**, *7*, 1055-1066.

21)Motomura, K.; Matuura, R. *J. Coll. Int. Sci.* **1969**, *29*, 617-622.

22)Motomura, K.; Matuura, R. *J. Coll. Int. Sci.* **1969**, *29*, 623-628.

23)Aratono, M.; Uryu, S.; Hayami, Y.; Motomura, K.; Matuura, R. *J. Coll. Int. Sci.* **1983**, *93*, 162-168.

24)Aratono, M.; Uryu, S.; Hayami, Y.; Motomura, K.; Matuura, R. *J. Coll. Int. Sci.* **1984**, *98*, 33-38.

25)Lunkenheimer, K.; Serrien, G.; Joos, P. *J. Coll. Int. Sci.* **1990**, *134*, 407.

26)Berge, B.; Simon, A. J.; Libchaber, A. *Phys. Rev. A* **1990**, *41*, 6893-6900.
27)Hénon, S.; Meunier, J. *J. Chem. Phys.* **1993**, *98*, 9148-9154.

28)Pollard, M.; Pan, R.; Steiner, C.; Maldarelli, C. *Langmuir* **1998**, *14*, 7222-7234.

29)Pfohl, T.; Möhwald, H.; Riegler, H. *Langmuir* **1998**, *14*, 5285-5291.

30)Takiue, T.; Uemura, A.; Ikeda, N.; Motomura, K.; Aratono, M. *Journal of Physical Chemistry B* **1998**, *102*, 3724-3729.

31)Aveyard, R.; Carr, N.; Slezok, H. *Can. J. Chem.* **1985**, *63*, 2742-2746.

32)Kim, M. W.; Cannell, D. S. *Phys. Rev. A* **1976**, *14*, 1299-1300.

33)Lin, S.-Y.; McKeigue, K.; Maldarelli, C. *AIChE J.* **1990**, *36*, 1785-1795.

34)Rosen, M. *Surfactants and Interfacial Phenomena*; Second ed.; Wiley: New York, 1989.

35)Lucassen-Reynders, E. H.; Lucassen, J.; Garett, P. R.; Giles, D.; way, F. *Advanced Chemical Ser* **1975**, *144*, 272.

36)Tempel, M. v. d.; Lucassen-Reynders, E. H. *Advances in Colloid and Interface Science* **1983**, *18*, 281.

37)Hua, X. Y.; Rosen, M. J. *Journal of Colloid and Interface Science* **1988**, *124*, 652-.

38)Joos, P.; Bleys, G. *Coll. Polym. Sci.* **1983**, *261*, 1038-1042.

39)Svitova, T. F.; Smirnova, Y. P.; Churaev, N. V.; Rusanov, A. I. *Coll. J. (Russia)* **1994**, *56*, 375-379.

40)Zhang, L. H.; Zhao, G. X. *Journal of Colloid and Interface Science* **1989**, *127*, 353.

41)Gao, T.; Rosen, M. J. *Jounal of Colloid and Interface Science* **1995**, *172*, 242-248.

42)Melzer, V.; Vollhardt, D. *Physical Review Letters* **1996**, *76*, 3770-3773.

43)Volhardt, D.; Melzer, V. *Jounal of Physical Chemistry* **1997**, *101*, 3370-3375.

44)Fainerman, V. B.; Volhardt, D.; Melzer, V. *Journal of Chemical Physics* **1997**, *107*, 243-251.

45)Melzer, V.; Vollhardt, D.; Brezesinski, G.; Mohwald, H. *Journal of Physical Chemistry B* **1998**, *102*, 591-597.

46)MacRitchie, F.; Alexander, A. E. *Journal of Colloid Science* **1963**, *18*, 458-463.

47)Joos, P.; Serrien, G. *Journal of Colloid and Interface Science* **1989**, *127*, 97-103.

48)Lin, S. Y.; McKeigue, K.; Maldarelli, C. *Langmuir* **1994**, *10*, 3442-3448.

49)Lin, S. Y.; Tsay, R.-Y.; Lin, L.-W.; Chen, S.-I. *Langmuir* **1996**, *12*, 6530-6536.

50)Pan, R.; Green, J.; Maldarelli, C. *Journal of Colloid and Interface Science* **1998**, *205*, 213-230.

51)Pan, R.; Green, J. H.; Maldarelli, C. M. *Langmuir,in press* **1999**.

52)Pan, R. *PhD Thesis,City University of New York* **1996**.

53)Subramanyam, R.; Pan, R.; Maldarelli, C. *Colloids and Surfaces A* **1998**, *Submitted for Publication.*

54)Pallas, N. R.; Pethica, B. A. *Lang.* **1993**, *9*, 361-362.

56)Hutchinson, E. *Journal of Colloid Science* **1948**, *3*, 235-250.

57)Berge, B.; Renault, A. *Europhysics Letters* **1993**, *21*, 773-777.

58)Berge, B.; Konovalov, O.; Lajzerowicz, J.; Renault, A.; Rieu, J. P.; Vallade, M. *Physical Review Letters* **1994**, *73*, 1652-1655.

59)Rieu, J. P.; Legrand, J. F.; Renault, A.; Berge, B.; Ocko, B. M.; Wu, X. Z.; Deutsch, M. *Journal of Physics II France* **1995**, *5*, 607-619.

60)Braun, R.; Casson, B. D.; Bain, C. D. *Chemical Physics Letters* **1995**, *245*, 326-334.

61)Casson, B. D.; Braun, R.; Bain, C. D. *Faraday Discussions* **1996**, *104*, 209-229.

62)Trapeznikov, A. *Acta Physicochim URSS* **1945**, *20*, 597.

63)Ross, J.; Epstein, M. B. *Journal of Physical Chemistry* **1958**, *62*, 533-535.
64)Ross, J. *Journal of Physical Chemistry* **1958**, *62*, 531-533.

65)Fainerman, V. b.; Vollhardt, D.; Melzer, V. *Journal of Chemical Physics* **1997**, *107*, 243-251.

66)Johal, M. S.; Usadi, E. W.; Davies, P. B. *Journal of Chemical Society:Faraday Transactions* **1996**, *92*, 573-578.

67)Casson, B. D.; Bain, C. D. *Journal of Physical Chemistry B* **1998**, *102*, 7434-7441.

68)Casson, B. D.; Bain, C. D. *Journal of Physical Chemistry B* **1999**, *103*, 4678-4686.

69)Bain, C. D.; Davies, P. B.; Ward, R. N. *Langmuir* **1994**, *10*, 2060-2063.

70)Brown, A. G.; Thuman, W. C.; McBain, J. W. *Jounal of Colloid Science* **1953**, *8*, 508-514.

71)Nilsson, G. *Jounal of Physical Chemistry* **1957**, *52*, 1135-1142.

72)Mysels, K. J. *Langmuir* **1986**, *2*, 423-428.

73)Mysels, K. J.; Florence, A. T. *Journal of Colloid and Interface Science* **1973**, *43*, 1973.

74)MacLeod, C. A.; Radke, C. J. *Journal of Colloid and Interface Science* **1993**, *160*, 435-.

75)Czichocki, G.; Volhardt, D.; Seibt, H. *Tenside Detergents* **1981**, *18*, 320.

76)Harkins, W. D.; Copeland, L. E. *Journal of Chemical Physics* **1942**, *10*, 272-277.
77)Motomura, K.; Iwanaga, S.; Hayami, Y.; Uryu, S.; Matuura, R. *J. Coll. Int. Sci.* **1981**, *80*, 32-38.

78)Lu, J. R.; Purcell, I. P.; Simister, E. A.; Thomas, R. K.; Rennie, A. R.; Penfold, J. *Journal of Colloid and Interface Science* **1995**, *174*, 441-455.

79)Boyd, G. E. *J Phys Chem* **1958**, *62*, 536-541.

80)Myrick, S. H.; Franses, E. I. *Langmuir* **1999**, *19*, 1556-1561.

81)Siddiqui, F. A.; Franses, E. I. *AIChE* **1997**, *43*, 1569-1578.

82)Nikas, Y. J.; Puvvada, S.; Blankschtein, D. *Langmuir* **1992**, *8*, 2680-2689.

83)Penfold, J.; Staples, E.; Thompson, L.; Tucker, I. *Colloids and Surfaces A* **1995**, *102*, 127-132.

84)Penfold, J.; Staples, E.; Thompson, L.; Tucker, I.; Hines, J.; Thomas, R. K.; Lu, J. R. *Langmuir* **1995**.

85)Staples, E.; Thompson, L.; Tucker, I.; Penfold, J.; Thomas, R. K.; Lu, J. R. *Langmuir* **1993**, *9*, 1651-1656.

86)Staples, E. J.; Thompson, L.; Tucker, I.; Penfold, J. *Langmuir* **1994**, *10*, 4136-4141.

87)Poskanzer, A. M.; Goodrich, F. C. *The Journal of Physical Chemistry* **1975**, *79*, 2122-2126.

88)Fainerman, V. B.; Miller, R. *Colloids and Surfaces A* **1995**, *97*, 65-82.

89)Oliver, J. F.; Huh, C.; Mason, S. G. *Journal of Colloid and Interface Science* **1977**, *59*, 568-580.

90)Bico, J.; Marzolin, C.; Quere, D. *Personal Communication* **1999**.

91)Shibuichi, S.; Onda, T.; Satoh, N.; Tsuji, K. **1996**.

92)Onda, T.; Shibuichi, S.; Satoh, N.; Tsuji, K. *Langmuir* **1996**, *12*, 2125-2127.
93)Richard, D.; Quere, D. *Personal Communication* **1999**.

94)Dussan, E. B. *Annual Reviews of Fluid Mechanics* **1979**, *11*, 371.

95)Marmur, A. *Advances in Colloid and Interface Science* **1983**, *19*, 75.

96)DeGennes, P. *Reviews of Modern Physics* **1985**, *57*, 827.

97)Berg, J. *Marcel Dekker:New York* **1993**.

98)Mao, T.; Kuhn, D. C.; Tran, H. *AIChE Journal* **1997**, *43*, 2169.

99)Chang, C. H.; Franses, E. I. *Colloids and Surfaces A:Physicochemical and Engineering Aspects* **1995**, *100*, 1-45.

100)Stoebe, T.; Lin, Z.; Hill, R. M.; Ward, M. D.; Davis, H. T. *Langmuir* **1997**, *13*, 7270-7275.

101)Kumar, V. *PhD Thesis, City University of New York* **1997**.

102)Krishnan, S. *PhD Thesis, City University of New York* **1999**.

103)Gun, J.; Isocovici, R.; Sagiv, J. *Journal of Colloid and Interface Science* **1984**, *101*, 201-213.

104)Sagiv, J. *Journal of American Society* **1980**, *102*, 92-98.

105)Kumar, N. *PhD Thesis, City University of New York* **2000**.